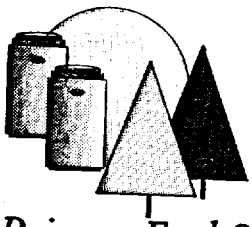

Private Fuel Storage, LLC

P.O. Box C4010, La Crosse, WI 54602-4010
John D. Parkyn, Chairman of the Board

U.S. Nuclear Regulatory Commission
ATTN: Document Control Desk
Washington, D.C. 20555-0001

December 16, 1999

LICENSE APPLICATION AMENDMENT No. 8
DOCKET NO. 72-22/TAC NO. L22462
PRIVATE FUEL STORAGE FACILITY
PRIVATE FUEL STORAGE L.L.C.

References: 1. PFS letter Donnell to U.S. NRC, Commitment Resolution Letter #22, dated November 19, 1999

2. PFS letter Donnell to U.S. NRC, Submittal of Commitment Resolution Letter #22 Information, dated November 24, 1999

The purpose of this letter is to submit Amendment 8 to the Private Fuel Storage Facility (PFSF) License Application (LA). Major changes of this amendment include:

- The ER is being revised to reflect Private Fuel Storage L.L.C. information provided in responses to NRC requests for additional information (RAIs) and commitment resolution letters that has not been previously incorporated.

- Sections of the SAR and ER dealing with geotechnical are being revised to address resolution of commitments discussed in the Reference 1 letter.

- Section 2.2 of the SAR is being revised to incorporate the latest information provided to the NRC by the Reference 2 letter.

- Appendix B of the License Application is being revised to clarify information in the Decommissioning Plan cost estimate.

This amendment impacts the PFSF Safety Analysis Report (SAR), the Environmental Report (ER), and the License Application.

1/9 DEC 20 1999

If you have any questions regarding this letter, please contact me at 608-787-1236 or Mr. J. L. Donnell, Project Director, at 303-741-7009.

Sincerely,

John D. Parkyn, Chairman
Private Fuel Storage L.L.C.

JDP:JRJ

Enclosures

PREFACE

PRIVATE FUEL STORAGE FACILITY

LICENSE APPLICATION

AMENDMENT 8

Enclosed are the following revisions to the Private Fuel Storage Facility License Application documents:

Safety Analysis Report - Revision 8

Environmental Report - Revision 6

License Application – Revision 5

The revisions are provided in the replacement page format. If a page has changed, either due to an actual text change or due to a shift in text caused by insertion of text, then the revision number of that page has been changed in the upper right hand corner. The location of text changes is noted by a side bar in the right hand margin.

DOCUMENT CONTROL

PAGE	REVISION
Document Control Tab	
a	8
b	8
c	8
d	8
e	8
f	8
g	8
h	8
i	8
j	8
k	8
l	8
m	8
n	8
o	8
p	8
q	8
r	8
s	8
t	8
u	8
v	8
w	8
x	8
Table of Contents Tab	
i	3
ii	0
iii	0
iv	0
Chapter 1 Tab	
1-i	0
1-ii	0
1.1-1	0
1.1-2	3
1.1-3	3
1.1-4	0
1.2-1	8
1.2-2	8
1.3-1	0
1.3-2	0
1.3-3	0

DOCUMENT CONTROL

PAGE	REVISION
1.3-4	0
1.4-1	4
1.4-2	4
1.5-1	5
1.5-2	0
1.6-1	0
1.6-2	0
1.7-1	0
1.7-2	0
Figure 1.1-1	3
Figure 1.1-2	2
Figure 1.2-1	3
Figure 1.3-1	0
Figure 1.3-2	0
Chapter 2 Tab	
2-i	7
2-ii	8
2-iii	7
2-iv	8
2-v	8
2-vi	6
2-vii	6
2-viii	8
2-ix	6
2-x	6
2-xi	8
2-xii	6
2.1-1	0
2.1-2	0
2.1-3	6
2.1-4	6
2.1-5	0
2.1-6	0
2.2-1	7
2.2-2	0
2.2-3	8
2.2-4	8
2.2-5	8
2.2-6	8
2.2-7	8
2.2-8	8
2.2-9	8
2.2-10	8

DOCUMENT CONTROL

PAGE	REVISION
2.2-11	8
2.2-12	8
2.2-13	8
2.2-14	8
2.2-15	8
2.2-16	8
2.3-1	0
2.3-2	0
2.3-3	0
2.3-4	0
2.3-5	0
2.3-6	0
2.3-7	0
2.3-8	0
2.3-9	0
2.3-10	0
2.3-11	0
2.3-12	0
2.3-13	0
2.3-14	0
2.3-15	0
2.3-16	0
2.3-17	0
2.3-18	0
2.3-19	0
2.3-20	0
2.4-1	0
2.4-2	0
2.4-3	3
2.4-4	3
2.4-5	6
2.4-6	3
2.4-7	3
2.4-8	3
2.4-9	3
2.4-10	3
2.4-11	3
2.4-12	3
2.4-13	3
2.4-14	3
2.5-1	0
2.5-2	3
2.5-3	3
2.5-4	3

DOCUMENT CONTROL

PAGE	REVISION
2.5-5	3
2.5-6	3
2.6-1	3
2.6-2	3
2.6-3	3
2.6-4	5
2.6-5	3
2.6-6	3
2.6-7	6
2.6-8	6
2.6-9	3
2.6-10	3
2.6-11	3
2.6-12	3
2.6-13	3
2.6-14	3
2.6-15	3
2.6-16	3
2.6-17	6
2.6-18	6
2.6-19	8
2.6-20	8
2.6-21	8
2.6-22	8
2.6-23	8
2.6-24	8
2.6-25	8
2.6-26	8
2.6.26a	8
2.6.26b	8
2.6.26c	8
2.6.26d	8
2.6-27	6
2.6-28	6
2.6-29	6
2.6-30	6
2.6-31	8
2.6-32	8
2.6-33	8
2.6-34	8
2.6-35	8
2.6-36	8
2.6-37	8
2.6-38	8

DOCUMENT CONTROL

PAGE	REVISION
2.6-39	8
2.6-40	8
2.6.40a	8
2.6.40b	8
2.6-41	8
2.6-42	8
2.6-43	8
2.6-44	8
2.6-45	8
2.6-46	8
2.6-47	8
2.6-48	8
2.6-49	8
2.6-50	8
2.6-51	8
2.6-52	8
2.6-53	8
2.6-54	8
2.6-55	8
2.6-56	8
2.6-57	8
2.6-58	8
2.6-59	8
2.6-60	8
2.6.60a	8
2.6.60b	8
2.6.60c	8
2.6.60d	8
2.6-61	6
2.6-62	6
2.6-63	6
2.6-64	6
2.6-65	6
2.6-66	6
2.6-67	6
2.6-68	6
2.6-69	6
2.6-70	6
2.6-71	6
2.6-72	6
2.6-73	6
2.6-74	6
2.6-75	6
2.6-76	6

DOCUMENT CONTROL

PAGE	REVISION
2.6-77	6
2.6-78	6
2.6-79	6
2.6-80	6
2.6-81	6
2.6-82	6
2.6-83	8
2.6-84	8
2.6-85	8
2.6-86	8
2.6-87	8
2.6-88	8
2.6-89	8
2.6-90	8
2.6-91	8
2.6-92	8
2.6-93	8
2.6-94	8
2.7-1	3
2.7-2	5
2.8-1	8
2.8-2	8
2.8-3	8
2.8-4	8
2.8-5	8
2.8-6	8
2.8-7	8
2.8-8	8
2.8-9	8
2.8-10	8
2.8-11	8
2.8-12	8
Table 2.3-1	0
Table 2.3-2	0
Table 2.3-3	0
Table 2.3-4	0
Table 2.3-5	0
Table 2.3-6	0
Table 2.3-7	0
Table 2.3-8	1
Table 2.3-9	0
Table 2.3-10	0
Table 2.6-1	6
Table 2.6-2	6

DOCUMENT CONTROL

PAGE	REVISION
Table 2.6-3	6
Table 2.6-4 (1 of 14)	0
Table 2.6-4 (2 of 14)	0
Table 2.6-4 (3 of 14)	0
Table 2.6-4 (4 of 14)	0
Table 2.6-4 (5 of 14)	0
Table 2.6-4 (6 of 14)	0
Table 2.6-4 (7 of 14)	0
Table 2.6-4 (8 of 14)	0
Table 2.6-4 (9 of 14)	0
Table 2.6-4 (10 of 14)	0
Table 2.6-4 (11 of 14)	0
Table 2.6-4 (12 of 14)	0
Table 2.6-4 (13 of 14)	0
Table 2.6-4 (14 of 14)	0
Table 2.6-5	6
Figure 2.1-1	0
Figure 2.1-2 (1 of 2)	3
Figure 2.1-2 (2 of 2)	0
Figure 2.3-1	0
Figure 2.3-2	0
Figure 2.3-3	0
Figure 2.3-4	0
Figure 2.3-5	0
Figure 2.3-6	0
Figure 2.4-1	3
Figure 2.4-2	3
Figure 2.4-3	3
Figure 2.4-4	3
Figure 2.4-5	3
Figure 2.5-1	3
Figure 2.6-1	0
Figure 2.6-2 (1 of 2)	8
Figure 2.6-2 (2 of 2)	0
Figure 2.6-3	0
Figure 2.6-4	0
Figure 2.6-5 (1 of 14)	8
Figure 2.6-5 (2 of 14)	8
Figure 2.6-5 (3 of 14)	8
Figure 2.6-5 (4 of 14)	8
Figure 2.6-5 (5 of 14)	8
Figure 2.6-5 (6 of 14)	8
Figure 2.6-5 (7 of 14)	8
Figure 2.6-5 (8 of 14)	8

DOCUMENT CONTROL

PAGE	REVISION
Figure 2.6-5 (9 of 14)	8
Figure 2.6-5 (10 of 14)	8
Figure 2.6-5 (11 of 14)	8
Figure 2.6-5 (12 of 14)	8
Figure 2.6-5 (13 of 14)	8
Figure 2.6-5 (14 of 14)	8
Figure 2.6-6	0
Figure 2.6-7	0
Figure 2.6-8	0
Figure 2.6-9	0
Figure 2.6-10	0
Figure 2.6-11	0
Figure 2.6-12	0
Figure 2.6-13A	6
Figure 2.6-13B	6
Figure 2.6-13C	6
Figure 2.6-14A	6
Figure 2.6-14B	6
Figure 2.6-14C	6
Figure 2.6-15	0
Figure 2.6-16	0
Figure 2.6-17	6
Figure 2.6-18	6
Figure 2.6-19	8
Figure 2.6-20 (1 of 2)	6
Figure 2.6-20 (2 of 2)	6
Figure 2.6-21	6
Figure 2.6-22	6
Figure 2.6-23	6
Figure 2.6-24	6
Figure 2.6-25	6
Figure 2.6-26	6
Figure 2.6-27	6
Figure 2.6-28	6
Figure 2.6-29	6
Figure 2.6-30 (1 of 6)	8
Figure 2.6-30 (2 of 6)	8
Figure 2.6-30 (3 of 6)	8
Figure 2.6-30 (4 of 6)	8
Figure 2.6-30 (5 of 6)	8
Figure 2.6-30 (6 of 6)	8

DOCUMENT CONTROL

PAGE	REVISION
Appendix 2A Tab	
Reports	8
Appendix 2B Tab	
Survey	0
Appendix 2C Tab	
Analysis	0
Appendix 2D Tab	
Deleted	3
Appendix 2E Tab	
Analysis	0
Chapter 3 Tab	
3-i	3
3-ii	3
3-iii	1
3-iv	1
3-v	0
3-vi	0
3.1-1	0
3.1-2	0
3.1-3	3
3.1-4	1
3.1-5	0
3.1-6	0
3.2-1	0
3.2-2	0
3.2-3	1
3.2-4	1
3.2-5	3
3.2-5a	4
3.2-5b	3
3.2-6	0
3.2-7	1
3.2-8	1
3.2-9	7

DOCUMENT CONTROL

PAGE	REVISION
3.2-10	5
3.2-11	5
3.2-12	3
3.2-13	3
3.2-14	3
3.2-14a	3
3.2-14b	3
3.2-15	0
3.2-16	3
3.2-17	0
3.2-18	1
3.2-19	1
3.2-20	1
3.2-21	0
3.2-22	0
3.2-23	0
3.2-24	0
3.2-25	5
3.2-26	1
3.2-27	1
3.2-28	1
3.2-29	1
3.2-30	1
3.2-31	1
3.2-32	1
3.3-1	0
3.3-2	0
3.3-3	0
3.3-4	0
3.3-5	0
3.3-6	1
3.3-7	0
3.3-8	0
3.3-9	8
3.3-10	1
3.3-11	0
3.3-12	0
3.4-1	0
3.4-2	0
3.4-3	0
3.4-4	0
3.4-5	7
3.4-6	7
3.4-7	7

DOCUMENT CONTROL

PAGE	REVISION
3.4-8	7
3.5-1	0
3.5-2	0
3.6-1	0
3.6-2	0
3.7-1	3
3.7-2	0
3.7-3	0
3.7-4	7
Table 3.1-1	0
Table 3.1-2	1
Table 3.1-3 (1 of 2)	4
Table 3.1-3 (2 of 2)	0
Table 3.2-1	0
Table 3.2-2	0
Table 3.2-3	0
Table 3.4-1	3
Table 3.6-1 (1 of 5)	7
Table 3.6-1 (2 of 5)	7
Table 3.6-1 (3 of 5)	0
Table 3.6-1 (4 of 5)	0
Table 3.6-1 (5 of 5)	0
Chapter 4 Tab	
4-i	4
4-ii	7
4-iii	8
4-iv	8
4-v	6
4-vi	3
4-vii	0
4-viii	3
4-ix	6
4-x	0
4.1-1	0
4.1-2	0
4.1-3	0
4.1-4	0
4.2-1	0
4.2-2	0
4.2-3	4
4.2-4	4
4.2-5	4
4.2-6	1

DOCUMENT CONTROL

PAGE	REVISION
4.2-7	4
4.2-8	5
4.2-9	5
4.2-10	5
4.2-11	5
4.2-12	4
4.2-13	1
4.2-14	4
4.2-15	7
4.2-16	7
4.2-16a	7
4.2-16b	7
4.2-16c	7
4.2-16d	7
4.2-17	8
4.2-18	4
4.2-19	4
4.2-20	4
4.2-21	4
4.2-22	1
4.2-23	0
4.2-24	0
4.2-25	1
4.2-26	0
4.2-27	0
4.2-28	0
4.2-29	7
4.2-30	7
4.2-31	7
4.2-32	1
4.2-33	7
4.2-34	7
4.2-34a	8
4.2-34b	7
4.2-35	0
4.2-36	0
4.2-37	0
4.2-38	0
4.2-39	7
4.2-40	7
4.2-41	6
4.2-42	3
4.2-43	3
4.2-44	6

DOCUMENT CONTROL

PAGE	REVISION
4.2-45	6
4.2-46	6
4.2-47	6
4.2-48	6
4.2-49	6
4.2-50	6
4.3-1	8
4.3-2	8
4.3-3	8
4.3-4	8
4.3-5	8
4.3-6	8
4.3-7	8
4.3-8	8
4.3-9	8
4.3-10	8
4.4-1	0
4.4-2	0
4.5-1	3
4.5-2	0
4.5-3	2
4.5-4	8
4.5-5	8
4.5-6	8
4.6-1	0
4.6-2	0
4.7-1	0
4.7-2	0
4.7-3	3
4.7-4	0
4.7-5	6
4.7-6	6
4.7-6a	6
4.7-6b	6
4.7-7	3
4.7-8	6
4.7-8a	3
4.7-8b	6
4.7-8c	6
4.7-8d	6
4.7-8e	6
4.7-8f	6
4.7-8g	6
4.7-8h	6

DOCUMENT CONTROL

PAGE	REVISION
4.7-9	3
4.7-10	2
4.7-11	3
4.7-12	2
4.7-13	6
4.7-13a	6
4.7-13b	6
4.7-13c	6
4.7-13d	6
4.7-13e	6
4.7-13f	6
4.7-13g	6
4.7-13h	6
4.7-13i	6
4.7-13j	6
4.7-14	0
4.7-15	0
4.7-16	0
4.7-17	0
4.7-18	0
4.7-19	6
4.7-20	4
4.7-21	4
4.7-22	1
4.7-23	0
4.7-24	1
4.7-25	0
4.7-26	1
4.7-27	6
4.7-28	0
4.7-29	0
4.7-30	0
4.7-31	1
4.7-32	0
4.8-1	8
4.8-2	0
4.8-3	0
4.8-4	0
4.8-5	6
4.8-6	6
4.8-7	6
4.8-8	7
Table 4.1-1 (1 of 7)	1
Table 4.1-1 (2 of 7)	1

DOCUMENT CONTROL

PAGE	REVISION
Table 4.1-1 (3 of 7)	0
Table 4.1-1 (4 of 7)	0
Table 4.1-1 (5 of 7)	0
Table 4.1-1 (6 of 7)	0
Table 4.1-1 (7 of 7)	0
Table 4.2-1	7
Table 4.2-2	8
Table 4.2-3	4
Table 4.2-4	7
Table 4.2-5	8
Table 4.2-6	0
Table 4.2-7	0
Table 4.2-8	3
Table 4.7-1	8
Table 4.7-2	4
Table 4.7-3	8
Figure 4.1-1	2
Figure 4.1-2	0
Figure 4.1-3	0
Figure 4.1-4	0
Figure 4.2-1	0
Figure 4.2-2 (1 of 3)	0
Figure 4.2-2 (2 of 3)	0
Figure 4.2-2 (3 of 3)	0
Figure 4.2-3	0
Figure 4.2-4	0
Figure 4.2-5 (1 of 4)	0
Figure 4.2-5 (2 of 4)	0
Figure 4.2-5 (3 of 4)	0
Figure 4.2-5 (4 of 4)	0
Figure 4.2-6	0
Figure 4.2-7	8
Figure 4.2-8	0
Figure 4.5-1	0
Figure 4.5-2	0
Figure 4.5-3 (1 of 2)	2
Figure 4.5-3 (2 of 2)	2
Figure 4.5-4	2
Figure 4.5-5	2
Figure 4.5-6 (1 of 4)	3
Figure 4.5-6 (2 of 4)	3
Figure 4.5-6 (3 of 4)	3
Figure 4.5-6 (4 of 4)	3
Figure 4.7-1 (1 of 3)	2

DOCUMENT CONTROL

PAGE	REVISION
Figure 4.7-1 (2 of 3)	2
Figure 4.7-1 (3 of 3)	2
Figure 4.7-2	0
Figure 4.7-3	0
Figure 4.7-4	0
Figure 4.7-5	3
Figure 4.7-6	3
Figure 4.7-7	6
Chapter 5 Tab	
5-i	0
5-ii	7
5-iii	0
5-iv	0
5-v	0
5-vi	0
5.1-1	0
5.1-2	0
5.1-3	3
5.1-4	2
5.1-5	6
5.1-6	6
5.1-7	0
5.1-8	0
5.1-9	1
5.1-10	1
5.2-1	1
5.2-2	7
5.2-3	7
5.2-4	7
5.2-5	7
5.2-6	7
5.3-1	0
5.3-2	0
5.4-1	0
5.4-2	0
5.5-1	1
5.5-2	0
5.6-1	0
5.6-2	0
5.7-1	0
5.7-2	0
Table 5.1-1 (1 of 2)	6
Table 5.1-1 (2 of 2)	6

DOCUMENT CONTROL

PAGE	REVISION
Table 5.1-2 (1 of 2)	0
Table 5.1-2 (2 of 2)	1
Figure 5.1-1	1
Figure 5.1-2	0
Figure 5.1-3	0
Figure 5.1-4	0
Figure 5.1-5	0
Chapter 6 Tab	
6-i	0
6-ii	0
6.1-1	0
6-1-2	0
6.2-1	1
6.2-2	0
6.3-1	0
6.3-2	0
6.4-1	0
6.4-2	7
6.4-3	7
6.4-4	7
6.5-1	0
6.5-2	0
6.6-1	0
6.6-2	0
Chapter 7 Tab	
7-i	0
7-ii	7
7-iii	0
7-iv	0
7-v	0
7-vi	0
7.1-1	0
7.1-2	0
7.1-3	0
7.1-4	0
7.1-5	0
7.1-6	0
7.1-7	0
7.1-8	3
7.1-9	3
7.1-10	3
7.1-11	3

DOCUMENT CONTROL

PAGE	REVISION
7.1-12	3
7.2-1	0
7.2-2	0
7.2-3	0
7.2-4	0
7.2-5	0
7.2-6	0
7.2-7	0
7.2-8	0
7.2-9	0
7.2-10	7
7.2-11	0
7.2-12	3
7.3-1	0
7.3-2	0
7.3-3	0
7.3-4	0
7.3-5	0
7.3-6	0
7.3-7	0
7.3-8	0
7.3-9	7
7.3-10	7
7.3-11	7
7.3-12	7
7.3-13	7
7.3-14	7
7.3-15	7
7.3-16	7
7.3-17	7
7.3-18	7
7.3-19	7
7.3-20	7
7.4-1	7
7.4-2	7
7.4-3	7
7.4-4	0
7.5-1	3
7.5-2	0
7.5-3	8
7.5-4	8
7.5-5	8
7.5-6	8
7.5-7	8

DOCUMENT CONTROL

PAGE	REVISION
7.5-8	8
7.6-1	0
7.6-2	0
7.6-3	0
7.6-4	0
7.7-1	0
7.7-2	0
7.7-3	7
7.7-4	0
Table 7.3-1	0
Table 7.3-2	0
Table 7.3-3	0
Table 7.3-4	0
Table 7.3-5	0
Table 7.3-6	0
Table 7.3-7	0
Table 7.3-8	0
Table 7.4-1 (1 of 4)	1
Table 7.4-1 (2 of 4)	0
Table 7.4-1 (3 of 4)	1
Table 7.4-1 (4 of 4)	1
Table 7.4-2 (1 of 4)	1
Table 7.4-2 (2 of 4)	1
Table 7.4-2 (3 of 4)	1
Table 7.4-2 (4 of 4)	1
Figure 7.3-1	0
Figure 7.3-2	0
Chapter 8 Tab	
8-i	0
8-ii	7
8-iii	7
8-iv	7
8-v	0
8-vi	0
8.1-1	0
8.1-2	0
8.1-3	0
8.1-4	0
8.1-5	0
8.1-6	0
8.1-7	7
8.1-8	0
8.1-9	0

DOCUMENT CONTROL

PAGE	REVISION
8.1-10	7
8.1-11	0
8.1-12	0
8.1-13	0
8.1-14	0
8.1-15	0
8.1-16	0
8.1-17	7
8.1-18	7
8.1-19	7
8.1-20	7
8.2-1	3
8.2-2	3
8.2-3	7
8.2-4	7
8.2-5	7
8.2-6	7
8.2-7	7
8.2-8	7
8.2-9	7
8.2-10	7
8.2-11	7
8.2-12	7
8.2-13	3
8.2-14	3
8.2-15	6
8.2-15a	6
8.2-15b	6
8.2-16	0
8.2-17	0
8.2-18	0
8.2-19	7
8.2-20	0
8.2-21	7
8.2-22	7
8.2-23	7
8.2-23a	7
8.2-23b	7
8.2-23c	7
8.2-23d	7
8.2-24	4
8.2-25	7
8.2-26	7
8.2-27	7

DOCUMENT CONTROL

PAGE	REVISION
8.2-28	4
8.2-28a	4
8.2-28b	4
8.2-28c	4
8.2-28d	4
8.2-29	4
8.2-30	5
8.2-31	5
8.2-32	5
8.2-32a	5
8.2-32b	5
8.2-33	0
8.2-34	0
8.2-35	7
8.2-36	3
8.2-37	3
8.2-38	3
8.2-39	3
8.2-40	7
8.2-41	7
8.2-42	7
8.2-43	7
8.2-44	0
8.2-45	4
8.2-46	0
8.2-47	7
8.2-48	7
8.2-49	0
8.2-50	0
8.3-1	7
8.3-2	7
8.4-1	7
8.4-2	7
8.4-3	0
8.4-4	3
8.4-5	4
8.4-6	7
8.4-7	7
8.4-8	7
Table 8.1-1	4
Table 8.1-2	4
Chapter 9 Tab	
9-i	0

DOCUMENT CONTROL

PAGE	REVISION
9-ii	1
9-iii	4
9-iv	4
9-v	0
9-vi	0
9.1-1	0
9.1-2	0
9.1-3	0
9.1-4	4
9.1-5	4
9.1-6	4
9.1-7	4
9.1-8	4
9.1-9	4
9.1-10	4
9.1-11	4
9.1-12	4
9.1-13	0
9.1-14	0
9.1-15	1
9.1-16	1
9.1-16a	1
9.1-16b	1
9.1-17	0
9.1-18	0
9.1-19	0
9.1-20	0
9.1-21	0
9.1-22	0
9.1-23	0
9.1-24	3
9.1-25	4
9.1-26	4
9.1-27	4
9.1-28	4
9.1-29	4
9.1-30	4
9.2-1	1
9.2-2	1
9.2-2a	1
9.2-2b	1
9.2-3	0
9.2-4	0
9.2-5	0

DOCUMENT CONTROL

PAGE	REVISION
9.2-6	0
9.2-7	1
9.2-8	1
9.2-8a	1
9.2-8b	1
9.3-1	4
9.3-2	4
9.3-3	4
9.3-4	4
9.3-5	4
9.3-6	4
9.3-7	4
9.3-8	4
9.4-1	3
9.4-2	4
9.4-2a	4
9.4-2b	4
9.4-3	3
9.4-4	3
9.4-5	3
9.4-6	3
9.4-7	3
9.4-8	3
9.5-1	0
9.5-2	1
9.5-3	0
9.5-4	0
9.6-1	0
9.6-2	0
9.7-1	0
9.7-2	0
9.7-3	0
9.7-4	0
Figure 9.1-1	4
Figure 9.1-2	4
Figure 9.1-3	4
Chapter 10 Tab	
10-i	0
10-ii	0
10.1-1	0
10.1-2	0
10.2-1	0
10.2-2	1

DOCUMENT CONTROL

PAGE	REVISION
10.2-3	4
10.2-4	4
10.2-5	1
10.2-6	1
10.2-6a	1
10.2-6b	1
10.2-7	0
10.2-8	0
10.2-9	0
10.2-10	0
10.2-11	1
10.2-12	0
10.2-13	0
10.2-14	0
10.2-15	0
10.2-16	0
10.2-17	1
10.2-18	0
10.2-19	0
10.2-20	0
10.2-21	0
10.2-22	0
10.2-23	0
10.2-24	0
10.3-1	0
10.3-2	0
Chapter 11 Tab	
11-i	0
11-ii	0
11.1-1	4
11.1-2	4
11.1-3	4
11.1-4	0
11.1-5	0
11.1-6	0
11.1-7	0
11.1-8	0
11.1-9	0
11.1-10	0
11.2-1	0
11.2-2	0

1.2 GENERAL DESCRIPTION OF FACILITY

The PFSF is designed to store up to 40,000 Metric Tons of Uranium [2](MTU) of spent fuel from U.S. commercial power reactors in sealed metal canisters (approximately 4,000 storage casks). A detailed description of the fuel types that can be stored is provided in Chapter 3 and 10. The canister-based spent fuel storage system selected for use at the PFSF utilizes sealed metal canisters to store multiple spent fuel assemblies. Each canister is placed inside of a concrete storage cask. The storage system is passive and relies on natural convection for cooling. The system is an integral part of the facility "Start Clean / Stay Clean" philosophy which eliminates the need to handle individual fuel assemblies at the site. The system assures there is negligible contamination or radioactive waste generated at the site and facilitates the ease of decommissioning at the end of the life of the facility. Design criteria are described in more detail in Chapter 3.

The passive nature of the storage systems results in a relatively simple facility as shown on Figure 1.2-1. The Restricted Area (RA), is approximately 99 acres and is surrounded by a chain link security fence and an outer chain link nuisance fence with an isolation zone and intrusion detection system between the two fences. The cask storage area within the RA is surfaced with compacted gravel that slopes slightly to allow for runoff of storm water. The cask storage area consists of concrete cask storage pads that support the storage casks. Each pad is designed to support up to 8 storage casks in a 2 by 4 array. The Canister Transfer Building, as well as the Security and Health Physics Building, are also located within the RA. An overhead bridge crane and a semi-gantry crane are located within the Canister Transfer Building to facilitate shipping cask load/unload operations and canister transfer operations.

[2] Metric Tons of Uranium (initial uranium). This includes the small amount of mixed oxide fuels that are anticipated to require storage.

A main gate is provided for vehicular access to the RA. Light poles are located within the RA inside the security fence. Outside the RA is an Administration Building, and an Operations and Maintenance Building. The overall site or owner controlled area (OCA) is approximately 820 acres and is bounded by a range fence. The fence will be a typical 4-strand wire range fence, which will serve to identify the limit of PFSF activities and to keep out any stray livestock. Specifications for the fence, such as wire type and spacing, and pole type and spacing will meet the requirements of the BLM Manual Handbook H-1741-1 for Fencing and/or other applicable requirements identified by the BLM and BIA. PFS will consult with the BLM and BIA prior to construction of the fence to make sure the fence meets the latest BLM/BIA requirements.

The PFSF is designed to accommodate the storage system and the transportation of spent fuel canisters to and within the facility. The amount of yard area provided within the RA is sized to limit the radiation dose outside of the RA from the storage casks to less than 2 mrem/hr per 10 CFR 20.1301(a)(2). The yard area is also sized to provide adequate space for maneuvering the onsite cask transporter used during storage cask placement. The area of the OCA is based on 10 CFR 72.104(a) requirements of maintaining the annual dose to any real individual outside the OCA during normal operations to less than 25 mrem whole body, as well as 10 CFR 72.106(b) requirements of maintaining a minimum distance of 100 meters (328 ft) from spent fuel storage and handling areas to the OCA boundary and limiting the dose to 5 rem, to the whole body or any organ, from any design basis accident.

In compliance with 10 CFR 72.122 (d), the PFSF does not share structures, systems, or components with other facilities.

CHAPTER 2

SITE CHARACTERISTICS

TABLE OF CONTENTS

TABLE OF CONTENTS (cont.)

TABLE OF CONTENTS (cont.)

TABLE OF CONTENTS (cont.)

TABLE OF CONTENTS (cont.)

TABLE OF CONTENTS (cont.)

LIST OF APPENDICES

TABLE OF CONTENTS (cont.)

LIST OF TABLES

TABLE OF CONTENTS (cont.)

LIST OF FIGURES

TABLE OF CONTENTS (cont.)

LIST OF FIGURES

THIS PAGE INTENTIONALLY BLANK

required to exceed 1 psi overpressure for detonation of explosives transported by highway.

The Tooele Army Depot facilities, where toxic gas munitions are stored and incinerated, are located west and south, respectively, of Tooele City. The North Tooele Army Depot is 17 miles east-northeast of the PFSF and the South Tooele Army Depot is 21 miles east-southeast of the PFSF. The Stansbury Mountains, with an elevation of approximately 8,000 feet, lie between the PFSF and the Tooele Army Depots. The activities and materials at the Tooele Army Depots will therefore present no credible hazard to the PFSF, because of their relative distance and the intervening Stansbury Mountains.

2.2.2 Hazards from Air Crashes

Aircraft flights in the vicinity of the PFSF take place to and from Michael Army Airfield on Dugway Proving Ground, on and around the Utah Test and Training Range (UTTR), and on federal airways J-56 and V-257. While there are no civilian airports within 25 miles of the PFSF, general aviation aircraft, while not reported, may also transit the region. The average annual probability of an aircraft crashing into the PFSF has been calculated to be less than 1 E-6 per year and qualitative factors indicate that the true probability of an aircraft impacting the PFSF is less than 1 E-7 per year. (PFS Nov. 1999) This is an extremely low probability, well below the 1 E-6 regulatory standard the NRC has promulgated for above ground facilities at geologic repositories (which are similar to ISFSIs) (61 Fed. Reg. 64,257, 64,261-62, 64,265-66 (1996)) and below the 1E-7 guideline of NUREG-0800 established for nuclear power plants. Therefore, aircraft crashes do not present a credible hazard to the PFSF and the facility does not need to be designed to withstand the impact of an aircraft crash.

2.2.2.1 Michael Army Airfield and Airway IR-420

Michael Army Air Field is located on the Dugway Proving Ground, 17 miles south-southwest of the PFSF. This military airfield has a 13,125 foot runway, and can accommodate all operative aircraft in the Department of Defense inventory, although the majority of the aircraft flying to and from Michael AAF are large cargo aircraft such as the C-5, C-17, and C-141. The airspace over the Dugway Proving Ground is restricted. Military airway IR-420 passes over the PFSF site area. The methods of NUREG-0800 Section 3.5.1.6 were used to estimate the probability of an aircraft impacting the PFSF from this airway, using the equation:

$$P = C \times N \times A / w, \quad \text{where}$$

P = probability per year of an aircraft crashing into the PFSF
C = in-flight crash rate per mile
N = number of flights per year along the airway
A = effective area of the PFSF in square miles
w = width of airway in miles

NUREG-0800 states the in-flight crash rate as 4 E-10 per mile, which is appropriate to apply to the types of aircraft flying to and from Michael AAF. (PFS Nov. 1999) Information provided by the Dugway Proving Ground states that there are approximately 414 flights annually at this airfield. The effective area of the PFSF is 0.2116 mi^2, calculated using Department of Energy (DOE) formulas. (DOE 1996) The width of the airway is 10 nautical miles (nm), or 10nm x 1.15 mile/nm = 11.5 miles. The probability of an aircraft impacting the PFSF is therefore 3.0 E-9 per year. Because of the distance from the PFSF to Michael Army Airfield, takeoff and landing operations at Michael pose a negligible hazard to the PFSF.

2.2.2.2 Utah Test and Training Range

The UTTR is an Air Force training and testing range over which the airspace is restricted to military operations. It is divided into a North Area, located on the western shore of the Great Salt Lake, north of Interstate 80, and a South Area, located to the west of the Cedar Mountains, south of Interstate 80 and northwest of Dugway Proving Ground. (PFS Nov. 1999) The airspace over the UTTR extends somewhat beyond the range's land boundaries and is divided into military operating areas (MOAs) and restricted areas. The MOAs on the UTTR are located on the edges of the range, adjacent to the restricted areas. The PFSF site is located over 18 statute miles east of the eastern land boundary of the UTTR South Area and 8.5 statute miles northeast of the northeastern boundary of Dugway Proving Ground. The site lies within the Sevier B MOA, two statute miles to the east of the edge of restricted airspace. (PFS Nov. 1999)

Military aircraft flying in or around the UTTR South Area comprise three groups: 1) F-16 fighter aircraft flying from Hill Air Force Base (AFB), near Ogden, Utah, down Skull Valley en route to the range (Section 2.2.2.2.1); 2) aircraft conducting training in the restricted airspace on the range (Section 2.2.2.2.2); and 3) aircraft departing the range via the Moser Recovery to return to Hill AFB (Section 2.2.2.2.3). Aircraft flying in or around the UTTR North Area pose no credible hazard to the PFSF because of the distance from the facility.

2.2.2.2.1 F-16s Transiting Skull Valley

F-16 fighter aircraft fly north to south down Skull Valley, within Sevier B MOA, en route from Hill AFB to the UTTR South Area. The F-16s use the eastern side of Skull Valley as their predominant route of travel and typically pass approximately five miles to the east of the PFSF site. The U.S. Air Force has indicated that the F-16s typically fly

between 3,000 and 4,000 ft. above ground level (AGL), with a minimum altitude of 1,000 ft AGL. In 1998, 3,871 such flights passed through Skull Valley.

Because the predominant route of travel for the F-16s is down the eastern side of Skull Valley, away from the PFSF; because the likely nature of an F-16 crash in Skull Valley would be such that a crashing aircraft would not pose a hazard to the PFSF unless it was pointed directly at the site at the time of the event leading to the crash; and because Air Force pilots are instructed to avoid ground facilities in the event of a mishap in which the pilot retained control of the direction of the aircraft, it is not credible that a crashing F-16 would impact the PFSF. Nevertheless, an impact probability was calculated, using the methodology of NUREG-0800, in which it was conservatively assumed that the F-16 flights are uniformly distributed within the Sevier B MOA airspace in the vicinity of the PFSF. (PFS Nov. 1999)

To calculate the F-16 impact probability using the NUREG-0800 method, the Sevier B MOA airspace in the vicinity of the PFSF was treated as an airway with a width of 10 miles. Given the flight characteristics of the F-16, the PFSF has an effective area of 0.1337 mi^2, assuming a facility at full capacity with 4,000 spent fuel storage casks on site. The number of flights through the valley was taken to be 3,871 per year. The crash rate for the F-16 was calculated from Air Force data to be 2.736 E-8 per mile. It was also determined from Air Force data that over 95 percent of the F-16 crashes in the normal phase of flight (the phase of flight in which the F-16s transit Skull Valley) are attributable to engine failure. Furthermore, because of the training Air Force pilots receive in responding to engine failures, the flight characteristics of the F-16, the absence of other built up areas in Skull Valley, and the small effort required for the pilot to avoid the PFSF site in the event of a crash caused by an engine failure, the pilot would be able to direct the aircraft away from the PFSF at least 95 percent of the time in which an engine failure caused a crash in Skull Valley. Accordingly, 90.25 percent

(95% x 95%) of the crashing F-16s would be able to avoid the PFSF and hence the calculated crash impact hazard to the PFSF would be reduced by this fraction. Thus, the annual crash impact probability for the F-16s in Skull Valley (assuming a fully loaded facility) was calculated to be 1.38 E-7. (PFS Nov. 1999)

PFS also calculated the probability that ordnance jettisoned from a crashing F-16 in Skull Valley would impact the PFSF. (PFS Nov. 1999) Some of the F-16 flights through Skull Valley carry ordnance (live or inert) and in the event of an incident leading to a crash in which the pilot would have time to respond before ejecting from the aircraft (e.g., an engine failure), one of the pilot's first actions would be to jettison any ordnance carried by the aircraft. PFS used an approach similar to that of NUREG-0800 to calculate the probability that such ordnance would impact the PFSF. The fraction of the 3,871 F-16s transiting Skull Valley per year that would be carrying ordnance was determined from Air Force data to be 11.8 percent. Thus the number of aircraft carrying ordnance through Skull Valley per year, N, would be 457. The crash rate for the F-16s, C, was taken to be 2.736 E-8 per mile, as above. Nonetheless, the pilot was assumed to jettison ordnance in only 95 percent of all crashes, the fraction of the crashes, e, assumed to be attributable to engine failure (in crashes attributable to other causes it was assumed that the pilot would eject quickly and would not jettison ordnance). Skull Valley was treated as an airway with a width, w, of 10 miles. As with the calculation for F-16s transiting Skull Valley, PFS conservatively assumed that the F-16s are uniformly distributed across the 10 miles, despite the fact that their predominant route of flight is down the eastern side of the valley and that, according to the Air Force, aircraft carrying live ordnance avoid flying over populated areas to the maximum extent possible. The area of the PFSF, from the perspective of a piece of ordnance jettisoned from an aircraft flying from north to south over the site, A, was taken to be the product of the width and the depth of the cask storage area (assuming a full facility with 4,000 casks) plus the product of the width and depth of the canister transfer building, in that the

pieces of ordnance are small relative to an aircraft and impact the ground at a steep angle. Thus, the area of the PFSF was calculated to be 0.08763 mi^2. The probability that the ordnance would impact the PFSF is given by P = N x C x e x A/w, or:

P = 457 x 2.736 E-8 x 0.95 x 0.08763 / 10 = 1.04 E-7

2.2.2.2.2 Aircraft Training on the UTTR

According to the Air Force, 8,284 sorties were flown over the UTTR South Area in 1998. (PFS Nov. 1999) Those aircraft conducted a variety of activities, including air-to-air combat training, air-to-ground attack training, air-refueling training, and transportation to and from Michael Army Airfield (which is located beneath UTTR airspace). Hazards posed by aircraft flying to and from Michael Army Airfield are addressed in Section 2.2.2.1 above. Of the remaining aircraft, only fighter aircraft conducting air-to-air training represent a potential hazard to the PFSF, in that aircraft conducting air-to-ground attack training do so over targets that are located more than 20 miles from the PFSF site and aircraft conducting air refueling training do so on the far western side of the UTTR, over 50 miles from the site. The Air Force indicated 6,360 fighter sorties were flown on the UTTR South Area in 1998 and one-third, or approximately 2,120, involved fighter aircraft conducting air-to-air training.

The crash impact probability for fighter aircraft conducting air-to-air training on the UTTR was calculated as follows:

$P = C_a \times A_c \times A/A_p \times R$, where

P = annual crash impact probability

C_a = total air-to-air training crash rate per square mile on the UTTR

A_c = the area of the UTTR from which aircraft could credibly impact the PFSF in the event of a crash

A = effective area of the PFSF in square miles

A_p = the footprint area, in which a disabled aircraft could possibly hit the ground in the event of a crash

R = the probability that the pilot of a crashing aircraft would be able to take action to avoid hitting the PFSF

The total air-to-air training crash rate per square mile on the UTTR, C_a, was calculated from the total number of hours flown in air-to-air training on the UTTR South Area (2,468), the crash rate per hour for fighter aircraft (the F-16) in combat training (3.96 E-5), the distribution of air operations over the sectors of the UTTR nearest the PFSF, and the ground areas of those sectors. (PFS Nov. 1999) As with the F-16s transiting Skull Valley, 95 percent of the crashes on the UTTR attributable to engine failure were determined not to pose a hazard to the PFSF, in that the pilot would retain control of the aircraft and would be able to avoid the site. Based on Air Force data, 44 percent of all F-16 crashes occurring during combat training are attributable to engine failure; thus the factor R in the equation above was set equal to 0.582 (1-(44% x 95%)). The area from which an aircraft could credibly impact the PFSF in the event of a crash, A_c, was taken to be the portion of the UTTR within 10 miles of the PFSF, in that a crashing aircraft more than 10 miles from the site would have to be under control of the pilot in order to glide and reach the site, and the pilot would guide any such aircraft away from the site, which is outside the land boundaries and the restricted airspace of the UTTR. The site effective area, A, was determined as in Section 2.2.2.2.1 above for a facility at a full capacity of 4,000 storage casks. The footprint area, A_p, was calculated by assuming that a crashing aircraft could glide in any direction up to a distance equal to the product of its starting altitude above ground and its glide ratio. Accordingly, the aircraft conducting air-to-air training over the UTTR were divided into altitude bands and

an impact probability calculated for each band. Aircraft too low to glide to the PFSF in the event of a mishap were calculated not to contribute to the crash impact hazard, in that they would have no chance of reaching the site. The maximum annual air crash impact probability for aircraft conducting air-to-air training on the UTTR South Area was calculated from the sum of impact probabilities of the altitude bands to be 2.02 E-7.

2.2.2.2.3 Aircraft Using the Moser Recovery

Most of the F-16s returning to Hill AFB from the UTTR South Area exit the northern edge of the range (away from the PFSF) in coordination with air traffic control. However, some aircraft returning to Hill from the UTTR South Area may use the Moser recovery route, which runs from the southwest to the northeast, approximately two miles from the PFSF site. (PFS Nov. 1999) The Moser route is only used during marginal weather conditions or at night under specific wind conditions which require the use of Runway 32 at Hill AFB. Based on information from local air traffic controllers, conservatively estimated, the Moser recovery is used by less than five percent of the aircraft returning to Hill. According to the Air Force, 5,726 F-16 sorties were flown on the UTTR South Area, almost all of which flew from Hill AFB (not all aircraft transit Skull Valley en route to the South Area); thus fewer than 286 aircraft per year (5% x 5,726) would use the Moser recovery on their return flights.

The average annual crash impact probability for aircraft flying the Moser recovery was calculated using the NUREG-0800 method. The Moser recovery is defined as an airway with a width, w, of 10 nautical miles (11.5 statute miles) (equal to the width of military airway IR-420). The number of aircraft, N, is conservatively taken to be 286; the crash probability, C, is equal to 2.736 E-8 per mile; the effective area of the site is 0.1337 mi^2; and it is calculated that 90.25 percent of all crashes would be those attributable to engine failure in which the pilot could direct the aircraft away from the

PFSF (see Section 2.2.2.2.1). Thus, the annual crash impact probability is conservatively estimated to be 8.87 E-9.

2.2.2.3 Aircraft Flying Federal Airways

Federal airway J-56 runs east-northeast to west-southwest at a distance (from the airway centerline) of 11.5 miles north of the PFSF. (PFS Nov. 1999) Local air traffic controllers have indicated that fewer than 12 aircraft per day use the airway. The crash impact probability for aircraft on the airway was calculated for the PFSF using the method of NUREG-0800. Using the standard width for federal airways, J-56 is 8 nautical miles (9.2 statute miles) wide and the closest edge of J-56 is 6.9 miles from the PFSF. For facilities outside an airway, the effective width of the airway, w, is equal to the actual width plus twice the distance from the facility to the closest edge. Thus, J-56 has an effective width of 23 miles. The number of aircraft, N, is conservatively taken to be 12 per day, the crash rate, C, from NUREG-0800 is 4 E-10 per mile, and the effective area of the PFSF for commercial airliners (the most common aircraft on the airway) is 0.2615 mi^2, assuming a full facility with 4,000 casks. Accordingly, the maximum annual crash impact probability is 1.9 E-8. (PFS Nov. 1999)

Federal airway V-257 runs north and south at a distance (from the airway centerline) of 19.5 miles east of the PFSF. (PFS June 1999) Local air traffic controllers have indicated that fewer than 12 aircraft per day use the airway. The crash impact probability for aircraft on the airway was calculated for the PFSF using the method of NUREG-0800. V-257 is 12 nautical miles (13.2 statute miles) wide and its closest edge is 12.6 miles from the PFSF. Thus, V-257 has an effective width of 39 miles. The number of aircraft, N, is conservatively taken to be 12 per day, the crash rate, C, is 4 E-10 per mile, and the effective area of the PFSF is 0.2615 mi^2. Accordingly, the annual crash impact probability is 1.2 E-8. (PFS Nov. 1999)

2.2.2.4 General Aviation

There are no civilian airports within 25 miles of the PFSF, the PFSF is located in a sparsely populated area, and the PFSF is located inside a military operating area (MOA) in which flight by civilian aircraft is restricted while the MOA is being used by the Air Force (and which is avoided by general aviation pilots because of the difficulty of getting clearance through it). Thus, the general aviation traffic over Skull Valley is negligible; in fact F-16 pilots who have flown from Hill AFB through Skull Valley indicate never having seen general aviation traffic there. Therefore, it is highly unlikely that a general aviation aircraft would crash into the PFSF. (PFS Nov. 1999) Nevertheless, a conservative upper bound on the crash impact probability for general aviation aircraft was calculated using National Transportation Safety Board (NTSB) crash data and the population of general aviation aircraft in the state of Utah. (PFS Nov. 1999) The crash impact probability is equal to $C_a \times A$, where C_a is the crash rate per square mile and A is the effective area of the PFSF. In 1995, the 184,434 general aviation aircraft in the United States suffered 412 fatal accidents. There are 1,218 general aviation aircraft in the state of Utah, which covers an area of 84,094 mi^2. NTSB crash data indicate, however, that only 15 percent of all general aviation crashes occur during the cruise mode of flight, which, because there are no airports nearby, is the mode in which general aviation aircraft would be flying near the PFSF. Furthermore, business jets experience 7.85 percent of all general aviation fatal crashes and they can be excluded from this calculation, in that they fly mostly on federal airways. The effective area of the PFSF with respect to general aviation aircraft crashes is 0.1173 mi^2 (assuming a fully loaded facility with 4,000 casks). Accordingly, the average annual crash impact probability for general aviation aircraft is 5.19 E-7. (PFS Nov. 1999)

The crash impact hazard to the PFSF, however, would be reduced below the calculated impact probability, in that the spent fuel storage casks would be able to withstand the

crash impact of most general aviation aircraft. Fifty-five percent of all general aviation aircraft are single-engine piston types weighing less than 3,500 lbs. (PFS Nov. 1999) Such aircraft typically fly at speeds under 100 knots (114 mph). Therefore, the impact of such aircraft at the PFSF would be bounded by the design basis tornado missile impact for the PFSF, an automobile weighing 1800 kg (3,968 lbs.) moving at a speed of 126 mph. (p. 8.2-17) Thus, the impact of such light general aviation aircraft would not cause a radioactive release from a storage cask. Therefore, the calculated general aviation crash impact hazard to the PFSF can be reduced by 55 percent to 2.34 E-7.

2.2.2.5 Cumulative Air Crash Impact Probability

The cumulative maximum air crash impact probability is given in the table below.

Aircraft Crash Impact Probabilities	
Aircraft	**Maximum Annual Probability**
Skull Valley F-16s	1.38 E-7
Aircraft Using the Moser Recovery	8.9 E-9
UTTR Aircraft	2.02 E-7
Aircraft on Airway J-56	1.9 E-8
Aircraft on Airway V-257	1.2 E-8
General Aviation Aircraft	2.34 E-7
Aircraft on Airway IR-420	3.0 E-9
Cumulative Crash Probability	6.17 E-7
Jettisoned Military Ordnance	1.04 E-7
Cumulative Hazard	7.21 E-7

The table shows that the cumulative air crash impact probability is less than 1 E-6 for the PFSF. Qualitative factors discussed below show further that the true impact probability for both facilities is less than 1 E-7. Thus, air crash impact does not pose a credible hazard to the PFSF and the PFSF does not need to be designed to withstand the effects of air crash impacts.

2.2.2.6 Projected Growth in Air Traffic

The Federal Aviation Administration projects that the number of commercial aviation flights in the United States will increase by approximately 66 percent between 1998 and 2025, that the number of general aviation flights will increase by approximately 14 percent over the same period, and that the number of military flights will not increase during this period. (FAA 1999) Because most of the air traffic near the PFSF site is military, the growth in commercial and general aviation projected by the FAA will have no material effect on the air crash impact probability calculated for the facility.

2.2.2.7 Conservatism in the PFSF Air Crash Impact Probabilities

While the calculated cumulative hazard for the PFSF is 7.21 E-7, qualitative factors indicate that the true probability of an aircraft or jettisoned ordnance impacting the site is significantly lower, less than 1 E-7 per year. With respect to the F-16s transiting down Skull Valley en route to the UTTR South Area (and jettisoned military ordnance), these factors include the fact that, according to the U.S. Air force, the predominant route of choice for the F-16s is the east side of the Valley, approximately five miles from the site. Thus, the uniform distribution assumed in calculations in Section 2.2.2.2.1 is highly conservative, especially considering the fact that the only aircraft that pose a real hazard to the site are those that are pointed directly toward it at the time of the incident leading to a crash. In addition. the Skull Valley F-16 calculations assume that F-16s will

crash at the 10-year average rate rather than the more recent and lower 5-year average rate.

The calculations of the crash impact hazard posed by other aircraft are conservative as well. The calculations assume that the density of flight operations involving air-to-air training near the edge of the UTTR (near the PFSF) is the same as it is near the center of the range, when in fact it is much lower. They also assume that an aircraft could glide up to 10 miles to impact the PFSF in a crash in which the pilot could not retain control over the aircraft, when in fact such aircraft would most likely fall to the ground without flying a significant distance. The calculation of the general aviation aircraft crash hazard assumes that the density of aircraft over Skull Valley is equal to the average density over the State of Utah, when in fact it is much lower. Therefore, the true crash hazard from those aircraft is significantly lower than the calculated value and in fact is insignificant.

Furthermore, the cumulative hazard calculated above is also conservative in two other major respects. First, the calculated probability is for a fully loaded, 4,000 cask facility, which would be the case for only a short period in the life of the PFSF. The average area of the PFSF site, and hence the average annual probability that an aircraft or jettisoned ordnance would impact the site, is 55 percent of that of the full facility. Thus, the average annual impact probability is roughly 4 E-7. Second, no credit was taken for the resistance to the effects of an air crash impact provided by the concrete storage casks in which the spent fuel canisters will be located (other than resistance to impacts of light general aviation aircraft). The cask construction is robust enough that a significant fraction of the potential air crash impacts at the PFSF would not cause a release of radioactivity. (Davis et al. 1998) The casks could withstand the direct impact of a jet fighter or commercial airliner at a speed of over 370 knots, which is significantly greater than typical air crash impact velocities, and the casks could withstand the

impact of the great majority of general aviation aircraft altogether. (PFS Nov. 1999) This resistance of the casks to penetration further reduces significantly the calculated risk to the PFSF from aircraft crashes or jettisoned ordnance.

2.2.3 The Use of Ordnance on the UTTR

As discussed in Section 2.2.2.2, military aircraft conduct air-to-ground attack training using air-delivered ordnance on the UTTR South Area. Military aircraft also conduct weapons testing, including the testing of cruise missiles. (PFS Nov. 1999) The use of air-delivered ordnance on the UTTR does not pose a significant hazard to the PFSF (the hazard posed by jettisoned ordnance in Skull Valley was calculated in Section 2.2.2.2.1 above). The PFSF site is located 18 miles to the east of the easternmost land boundary of the range. Aircraft flying over Skull Valley are not permitted to have their armament switches in a release capable mode, and all switches are "safe" until the aircraft are inside DOD land boundaries. Weapons use on the UTTR is strictly controlled and the UTTR has never experienced an unanticipated munitions release outside of designated launch/release areas. Furthermore, the targets on the UTTR are all over 20 miles from the PFSF site and no run-in headings for weapons delivery cross Skull Valley. Any aircraft with hung ordnance are directed to Michael Army Airfield on a flight path that is not near Skull Valley. In addition, weapon systems that have a capability of exceeding range boundaries, such as cruise missiles, are required to have a Flight Termination System (FTS) installed prior to testing on the UTTR. FTSs are designed to destruct the weapons and terminate the weapons' flight paths in the event of an anomaly. The UTTR has never experienced an FTS failure. Therefore, weapons use on the UTTR does not pose a credible hazard to the PFSF and the facility does not need to be designed to withstand a weapon impact.

2.6.1.5 Facility Plot Plan and Geologic Investigations

Figure 2.6-2 is a plot plan showing the locations of the major structures of the PFSF, the locations of the 1996 geotechnical borings and geophysical survey lines, and the location of foundation profiles through the pad emplacement area. Plate 1 of Geomatrix Consultants, Inc. (1999a), indicates the locations of both the 1996 and 1998 investigations, exclusive of the geotechnical borings for the Canister Transfer Building. Figure 2.6-18 shows the locations of the geotechnical borings that were drilled in the vicinity of the Canister Transfer Building in 1998, along with the locations of the CTB foundation profiles.

Geotechnical boring programs were conducted in 1996 and 1998. The borings drilled in October 1996 were located in the pad emplacement area and along the access road corridor, as shown in Figure 2.6-2. The borings drilled in October and December of 1998 were located in the Canister Transfer Building area, as shown in Figure 2.6-18. The soil samples obtained from these borings were sent to the Stone & Webster Geotechnical Laboratory in Boston for testing. The results of the boring programs and laboratory testing are found in Appendix 2A.

In April 1999, ConeTec, Inc performed cone penetration tests (CPT) and dilatometer tests (DMT) in the pad emplacement area and the Canister Transfer Building area. The locations of these CPTs and DMTs are presented in Figure 2.6-19. The results from this subsurface investigation are presented in ConeTec (1999). The primary goal of this investigation was to develop profiles of the relative strength and compressibility of the soils within the depth interval of 10 ft to ~25 ft in the pad emplacement area. As stated in ConeTec (1999), the other interpretations are presented only as a guide for geotechnical use and should be carefully scrutinized for consideration in any geotechnical design.

This program included performing 36 cone penetration tests (CPT) to develop continuous profiles of the strength of the soils in the upper layer (from the surface down to ~25 ft) within the pad emplacement area and 2 under the CTB. Sixteen of these were performed using a seismic CPT to measure down-hole P and S-wave velocities, and the two CPTs performed in the CTB included resistivity measurements. The cone penetration testing program also included performing dilatometer tests (DMT) to develop profiles of the variation of compressibility of the in situ soils. These were located, primarily, in areas where the preliminary tip resistance profiles from the CPT tests indicated that the in situ soils had the lowest strengths and the highest compressibilities.

Phase 1 of this program included performing 36 CPTs, located on a grid pattern of ~300 ft within the entire pad emplacement area. This layout provided nine CPTs in each of the four quadrants of the pad emplacement area. Several of these CPTs were located in close proximity to the borings that were drilled previously at the site, permitting correlations between the previous boring and laboratory data to be utilized in the interpretation of the CPT and DMT data. Additional CPTs and DMTs were performed in the vicinity of Borings CTB-4, CTB-5(OW), and C-1, to obtain data for correlating the CPT data with the laboratory testing that was performed on samples from these borings, as well.

The results of the Phase 1 CPTs included measuring continuous profiles of tip resistance and sleeve friction stress, which were used to identify the extent and thickness of the lower blow count soils within the upper layer. The plots of corrected tip resistance, Q_t, vs depth, presented in Appendix E of ConeTec (1999), document the relative strength and compressibility of the soils within the profile. The results are consistent with the results of the borings that were drilled previously at the site; i.e., Q_t increases from grade to a depth of about 15 to 17 ft. Below this depth, it drops slightly

or remains constant with depth, down to a depth of about 23 ft, at which point it increases markedly, as did the Standard Penetration Test blow counts in most of the borings in the pad emplacement area.

These data were interpreted to provide profiles of the variation of strength, which are plotted in Appendix D and listed in tabular form in Appendix F of ConeTec (1999). A review of the plots of the undrained shear strength, s_u, vs depth indicates that s_u measured in the CPTs increases with depth, and it generally exceeds 1 tsf. Note, this value corresponds with the lower bound of the values of s_u measured in the CU and UU tests. These plots indicate that s_u remains fairly constant in the depth range from ~15 ft to ~23 ft, and normally exceeds 2 tsf. Therefore, the lower blow count zone at approximately 20 ft has undrained shear strengths that are at least twice those used in the analyses of the stability of the cask storage pads.

In Phase 2 of the cone penetration testing program, dilatometer tests were performed to measure, in situ, the variation of compressibility of the soils vs depth at the locations identified in Phase 1 where the softer soils exist. The compressibility is reported as the constrained modulus, M, in the plots and tables included in Appendices G and H of ConeTec (1999).

The plots of M vs depth in Appendix G of ConeTec (1999) show that M generally is lowest near the surface of the site, increases with increasing depth to about 4 to 5m (13 to 16 ft), at which point it decreases, generally remaining fairly constant at a value that is equal to or greater than that near the top of the profile. This trend is evident on the plots of DMT-1, 2, 3, 4, 8, 9 (excluding the high modulus values above 2.5m), 11, 12, 14, 15, 16, 17, and 18. Although DMT-6 found a slight decrease in M from ~5.5m to 7m, the resulting values were higher than in the other DMTs in this depth range. DMT-

5, 7, and 13 show only slight increases in M with depth to ~4 to 5m, followed by slight drop in modulus to ~7.5 to 8m.

In general, DMT-10 had the lowest constrained modulus (i.e., highest compressibility) for the entire profile. DMT-10 is anomalous in that M remains fairly constant throughout the entire depth range of ~2m to 7.8m, with a minimum value of 130 bars (135.7 tsf). This DMT was located about half-way between Borings B-1 and C-1 at the northern edge of the pad emplacement area. Note, the consolidation tests reported in Attachment 2 of Appendix 2A of the SAR were performed on samples obtained at a depth of 10 ft in Boring C-1 and C-2, which were near this location.

See Section 2.1.12.1 for discussion of incorporation of these CPT results in the bearing capacity and settlement analyses.

Geophysical surveys were conducted at the site and are discussed in Section 2.6.1.10.

2.6.1.6 Relationship of Major Foundations to Subsurface Materials

Figure 2.6-5, Sheets 1 through 14, present foundation profiles in the pad emplacement area, showing the locations of the proposed structures in relationship to the subsurface materials encountered in the borings. Based on the borings and laboratory test data, the generalized subsurface profile consists of three layers. The uppermost layer extends to a depth of between 25 and 35 ft below existing grade and is mainly interlayered silt, silty clay, and clayey silt. Standard Penetration Test (SPT) N-values for this layer are mostly between 8 and 20 blows per ft, with an average value of 16 blows per ft and a median value of 14 blows per ft, indicating that these are "stiff" or "medium dense" materials. The casks and the Canister Transfer Building will be placed

on mat foundations and the other proposed structures will be constructed on strip and spread footings founded on this layer.

The value of standard penetration resistance, N, was determined to be approximately 15 blows/ft for the top 25 to 30-ft soil layer based on the data obtained in Borings A-1 through A-4, B-1 through B-4, C-1 through C-4, and D-1 through D-4. This set of borings represents all of the borings that were drilled over the entire proposed pad emplacement area, as shown in Figure 2.6-2. The blow count data are summarized in Table 2.6-5. As indicated in this table, the average blow count is 15.7 blows/ft, and the median value is 14.0 blows/ft. These two values were combined to obtain the value of ~15 blows/ft.

These blow count data are plotted versus elevation in Figure 2.6-27. The average blow count for each 5-ft elevation interval is plotted using an open circle, whereas the median value is plotted as an open square. Also shown, by the heavy dash-dot line, is the average value of all SPT blow counts in the upper 25 to 30-ft layer of silt, silty clay, and clayey silt, at N = 15.

A distinct change in material occurs at about 25 to 35 ft, where refusal (N>100 blows per 6 inches) conditions are often encountered. The following 25 to 30 ft consists of very dense, dry, fine sand. Thin layers of fine gravel and coarse sand also are evident. A few clayey zones were encountered, but they had no apparent effect on the blow counts. The borings that were drilled to a depth of 100 ft or more (Borings A-1, D-4, CTB-1, and CTB-5) indicate that this layer is mainly underlain by very dense silt, silty sand, and sandy silt with occasional layers of clayey silt. Several layers of volcanic ash were also encountered in these borings.

A groundwater observation well was installed in Boring CTB-5(OW) in early 1999 in the vicinity of the Canister Transfer Building. Initial readings from this well indicate the groundwater table is about 125 ft below ground surface, approximate elevation 4,350 ft. Seismic refraction results (Appendix 2B) in the vicinity of the Storage Facility (see Figure 2.6-2, Seismic Lines 1 & 2) indicate the compression wave (P-wave) velocity changes from approximately 2,780 ft/sec to approximately 5,525 ft/sec at depths of between 90 and 131 ft below grade, which corroborates the depth to the water table measured in CTB-5(OW).

As indicated in Section 2.6.1.5, cone penetration tests were performed to further investigate the properties of the upper 25 to 30-ft thick layer at the site. There are some differences between the results of the cone penetration testing and the borings in regard to descriptions of the types of soils encountered, mostly in the 10 to 20-ft depth range. The CPTs indicated that the soils between approximately 10 ft and 20 ft below existing grade at the site ***behave as though they are silty sands and sandy silts.*** This finding was not corroborated by the descriptions of the soils obtained from that zone in the borings, many of which are confirmed by laboratory test results.

The soil behavior type data presented in the CPT report (ConeTec, 1999) were determined using empirical correlations derived primarily from data collected from testing saturated and uncemented soils. Experience has shown that, typically, the cone penetration tip resistance is high in sands and low in clays and the friction ratio ($R_f = F_s/Q_t$) is low in sands and high in clays. This observation is incorporated in several soil classification charts. The correlations used to interpret the data measured in the CPTs performed at the site were developed by Robertson and Campanella (1988) and are presented in Figure 5, "Soil Behavior Type Classification Chart," of ConeTec (1999).

The soil descriptions shown in the CPT test results in ConeTec (1999) are based on the soil behavior type zones defined by the cone tip resistance and friction ratio values. The SBTs indicate that the soils within the 10 to 20-ft depth range generally behave like sandy silts or silty sand/sand, while the boring logs show the soils to be primarily a slightly to highly plastic silt. This difference is believed due to the partially saturated and weakly cemented soils encountered at the site. Many of the samples in this depth range had water contents near to or below the plastic limit. It is believed that, because of the low water contents and partial saturation effect, the slightly to highly plastic silts have low or no dynamic pore pressure response, which results in low measured sleeve friction values when penetrated by the cone. The cementation effect results in higher cone tip resistance values when penetrated by the cone and, likely, lower sleeve friction values. The higher tip resistance, in combination with measured sleeve friction values that are lower than they would otherwise be if they were saturated and uncemented, results in the interpretation that these soils behave like sandy soils when the SBT classification chart developed by Robertson and Campanella (1988) is used. However, as observed in the borings and confirmed by the laboratory test results, most of these soils are clayey silts to silty clays.

As stated on page 51 of Robertson Campanella (1988),

> *"... CPT classification charts cannot be expected to provide accurate predictions of soil type based on grain size distribution but provide a guide to soil behaviour type. The CPT data provide a repeatable index of the aggregate behavior of the in situ soil in the immediate area of the probe."*

As indicated on page 8 of ConeTec (1999),

> *"It should be noted that it is not always possible to clearly identify a soil type based on Qc, Fs and Ud."*

Factors such as changes in stress history, *in situ* stresses, sensitivity, stiffness, macrofabric, mineralogy, and void ratio will also influence the classification. As indicated on page 8 of ConeTec (1998),

> *"... the chart is global in nature and provides only a guide to soil behaviour type (SBT). Overlap in some zones should be expected and the zones should be adjusted somewhat based on local experience.*
>
> *If no prior CPT experience exists in a given geologic environment it is advisable to obtain samples from appropriate locations to verify the classification and soil behaviour type."*

To appropriately use the cone penetration test results for soil classification at this site, the soil behavior type chart developed based on saturated uncemented soils must be recalibrated for the partially saturated and cemented soils encountered at the site. This was done by plotting the results of the soil classifications determined based on the borings and laboratory tests alongside plots of the soil behavior types from the CPT results. The borings and CPTs selected for this comparison were those that were performed within ~50 ft of each other, which included the following:

Boring	CPT	Distance Between (Ft)
CTB-4	CPT-37	4.2
CTB-5(OW)	CPT-38	4.2
C-1	CPT-39	5.5
A-2	CPT-34	15.0
B-3	CPT-20	29.8
A-3	CPT-32	50.9

Figure 2.6-30, Sheets 1 through 6, present these plots. The boring data are plotted vs elevation to indicate the locations of the samples, the Standard Penetration Test N-values, the USC Codes, and the sample descriptions. Also indicated are the SBT values appropriate for the samples obtained in the borings. The soil behavior type values from the CPTs are listed and plotted along the right side of the figures to facilitate comparison. The differences shown under the column labeled ΔSBT represent the SBT zoning shift required to more correctly characterize these soils as a result of the effects of partial saturation and cementation, as discussed above. Evaluation of these ΔSBT values leads to the conclusion that the soil behavior type values reported in ConeTec (1999) that are greater than 5 (i.e., sandier soils), as well as some of those equal to 5 (i.e., clayey silts), typically should be adjusted downward one or two zones to more accurately reflect the soil classifications that were determined based on the borings and confirmed by the laboratory tests performed specifically for the purpose of classifying the soil types.

To more accurately reflect the actual soil classification at the site, the SBT values reported by ConeTec (1999) were adjusted downward by 1 zone for those whose SBT values were greater than 5. Based on the results of this recalibration, the soil behavior type data from ConeTec (1999) are replotted, as shown in Figure 2.6-5, Sheets 2 through 14, along with the data from the soil borings, to generate the generalized soil profiles at the pad emplacement area.

As shown in Figure 2.6-2, Borings AR-1 through AR-5 were drilled along the proposed corridor for the access road, which extends easterly from the area in the vicinity of the proposed Operations & Maintenance (O&M) Building and the Administration Building to Skull Valley Road. These borings indicate that the near-surface soils are similar to the uppermost layer described above; i.e., silt, silty clay, and clayey silt, although the layer is somewhat thinner. Sands were encountered at depths of 5 and 10 ft in Boring AR-1

and from a depth of 5 ft to 20 ft in Boring AR-2. These sands are likely the subsurface continuation of the surficial beach ridges identified by Currey (Appendix 2C) and shown on Figure 1-3 of Geomatrix Consultants, Inc. (1999a). Silty or sandy gravels were encountered at a depth of 30 ft in Boring AR-3, 20 ft in Boring AR-4, and 6 ft in Boring AR-5.

These borings did not encounter bedrock. Interpretation of the seismic reflection survey data (Appendix 2B) indicates that the depth to bedrock is between 520 ft and 820 ft below the surface at the site in the vicinity of the storage pads and that it drops off towards the east, dipping from an estimated depth of 740 ft at Station 700 on Seismic Line 3 (shown on Figure 2.6-2) to approximately 1,020 ft at the eastern end of this seismic line. This is consistent with the interpretation that the Tertiary half-graben basin beneath Skull Valley is tilted down to the east along the East fault (Geomatrix Consultants, Inc., 1999a).

The original subsurface investigation, performed during the latter part of 1996, determined the suitability of the soil at the site for the proposed facility. The boring data indicated that the subsurface profile (Figure 2.6-5) was fairly consistent across the storage pad area. The results of the seismic survey performed in the storage pad area (Appendix 2B, Figures 4.1 & 4.3, primary wave refraction sections for Seismic Lines 1 & 2), corroborated the generalized subsurface profile developed based on the borings. Additional subsurface work has been performed in response to PFSF SAR RAI No.1, dated April 1, 1998, including field work that was performed at the site (Geomatrix, 1999a) in response to PFSF SAR RAI No. 1, Question 2-5. This program focused on defining the presence and capability of all faults beneath the site area, and it included borings, trenching, and high resolution seismic reflection surveys. Additional laboratory (Atterberg limits) testing was performed and is reported in Attachment 2 of Appendix 2A. These data are also included on Figure 2.6-20. The detailed stratigraphy

developed from this program corroborated the conclusions drawn from the previous work.

The boring and trench data reported by Geomatrix (1999a) are stratigraphically very consistent across the storage pad area with the original boring data presented in Appendix 2A, both in the north-to-south and the east-to-west directions. The upper 30-ft (approximately) layer of soil is comprised of mixtures of silt, silty clay, clayey silt, and some sandy silt, that can be interpreted to represent stages in the cyclic history of Lake Bonneville (Geomatrix, 1999a). These stages are, from oldest to youngest, a Stansbury deepwater facies, a post-Stansbury transgressive and regressive facies, and the Provo and Bonneville deepwater facies.

These site materials are consistent with what would be expected for deposits of a lacustrine environment, away from the direct influence of range-front alluvial fans. These deposits are overlain at the surface by thin, post-Provo eolian silt and recent playa deposits. They lie upon a uniform, fine sand that forms a nearly horizontal surface across the site at about elevation 4,440 ± 5 ft. This sand is the Stansbury transgressive facies, representing a series of shorelines and deltas that developed as Lake Bonneville initially occupied the area and rose to the deepwater Stansbury level. At the base of the sand unit is an unconformity marked by the Promontory soil that developed on pre-Bonneville subaerial deposits. This gravelly layer occurs in the borings drilled in the storage pad area at a depth of about 45 to 50 ft (at about elevation 4410 to 4430 ft).

As shown in the pad emplacement area foundation profiles (Figure 2.6-5, Sheets 1 through 14), the cask storage pads will be founded in the surficial eolian silt layer. The eolian silt, in its in situ loose state, is not suitable for founding the cask storage pads. Instead of excavating the eolian silt and replacing it with suitable structural fill, the

eolian silt will be mixed with sufficient portland cement and water and compacted to form a strong soil-cement subgrade to support the cask storage pads. The engineering characteristics of the soil-cement can be easily engineered during detailed design to meet the necessary strength requirements. For the purpose of safety analysis of this facility, it is conservatively assumed that the strength of the eolian silt soil-cement will be at least equal to or better than the strength and compressibility characteristics of the underlying silty clay/clayey silt layer. Therefore, the strength and compressibility characteristics of the underlying silty clay/clayey silt layer are used in the geotechnical analyses described in the sections below.

Refer to Sections 2.6.1.11 and 2.6.2.1 for a discussion of the engineering characteristics of these soils.

void ratio of these soils. Therefore, it is not unexpected that the shear wave velocities would change within this zone.

A review of the shear wave velocities vs depth presented in Appendix C of ConeTec (1999) indicates that they do not level off with depth. The general trend in the data is to increase with respect to depth; however this trend is masked by the presence of the marked increase in the shear wave velocities in the "harder" zone that exists generally within the depth range of about 13 feet to about 20 feet. If the shear wave velocities associated with this harder zone are excluded, all of the plots of shear wave velocities show a general increase with respect to depth. This general increase in velocity with increasing depth is more readily observed in Figure 2.6-28.

2.6.1.11 Static and Dynamic Soil and Rock Properties at the Site

Geotechnical laboratory tests were performed on samples obtained from the borings. The results of these tests are included in Appendix 2A and are summarized below. Figure 2.6-20 presents plots of the SPT blow counts vs depth in the pad emplacement area, on a row-by-row basis. This figure also presents the index properties that were measured for these soils, along with the results of triaxial testing. Comparison of these plots indicates that the soil properties are fairly consistent across the site.

For the soils in the pad emplacement area, consisting of silt, clayey silt, and silty clay, as shown in Figure 2.6-5 above the dense sand layer that exists at a depth of approximately 25 to 30 ft:

Index Property:	Minimum	Maximum	Average
Water Content, %	8	58	32
Liquid Limit	25	77	44
Plastic Limit	20	46	30

Plasticity Index	0.5	38	14
Moist Unit Weight, pcf	64	91	78
Dry Unit Weight, pcf	40	71	56
Void Ratio	1.4	3.2	2.1
Saturation, %	28	64	53

Specific Gravity =2.72

Consolidation parameters:	**Low**	**High**	**Average**
Maximum past pressure, ksf:	5.6	7.2	6.2
Virgin compression ratio, CR:	0.25	0.34	0.29
Recompression ratio, RR:	0.008	0.017	0.012

Rate of secondary compression is shown by the dashed curve in Figure 2.6-6.

Total-stress strength parameters are $\phi = 24.9°$ and c = 1.22 ksf, based on direct shear tests that are included in Attachments 7 and 8 of Appendix 2A. Total strength parameters are $\phi = 21.8°$ and c = 1.4 ksf, based on consolidated-undrained triaxial tests that are included in Attachments 5 and 8 of Appendix 2A. These strength parameters are derived from consolidated-undrained (CU) tests to simulate conditions that will exist during the earthquake loading. For the partially saturated cohesive soils at the site, the undrained strength of the soil is dependent on its apparent cohesion, friction angle, as well as the consolidation pressure. The strain rates are very high during the seismic event; therefore, the partially saturated cohesive soils will be stressed essentially under undrained conditions. The effect of the pore pressure response, if any, during such tests, either positive or negative, will be manifested directly in the shear strength value measured. Because the strain rate of the laboratory tests is at least one order of magnitude slower than the rate associated with the design basis ground motion, the strength measured in the laboratory is a lower bound estimate

of the strength that will be available to resist the dynamic loadings during the seismic event. See the section titled "Dynamic Strength of Soils", presented below, for additional details.

The undrained shear strength of the partially saturated cohesive soils was measured in the laboratory by consolidating the samples to the confining pressure that will exist prior to the seismic loading and then shearing them rapidly to simulate undrained conditions. The original triaxial tests (results reported in Appendix 2A, Attachments 2, 4, and 5) were performed at confining stresses that represent the static conditions that will exist under the fully loaded pads. To demonstrate the cohesive nature of these soils, an additional consolidated-undrained triaxial compression test was performed at a confining stress of 1 ksf, which is representative of the minimum confining stresses expected to exist under the fully loaded pads when the maximum uplift forces due to the design basis ground motion occurs, and one test was performed at a confining stress of 0, which is essentially an unconfined compression test. The results of these tests are included in the total strength parameters reported above, and details of these tests are included in Attachment 8 of Appendix 2A.

For the silt, clayey silt, and silty clay soils in the Canister Transfer Building area, above the dense sand layer located at approximately 30 ft depth:

Index Property:	Minimum	Maximum	Average
Water Content, %	7	86	40
Liquid Limit	28	83	51
Plastic Limit	18	48	30
Plasticity Index	4	38	20
Moist Unit Weight, pcf	73	118	92
Dry Unit Weight, pcf	40	98	65
Void Ratio	0.7	3.3	1.8

Saturation, %	40	88	71
Specific Gravity	2.71	2.73	2.72

Consolidation parameters:	**Low**	**High**	**Average**
Maximum past pressure, ksf:	6	26	13
Virgin compression ratio, CR:	0.13	0.37	0.31
Recompression ratio, RR:	0.014	0.020	0.018

Total-stress strength parameters are $\phi = 21.1°$ and $c = 1.13$ ksf, based on direct shear tests that are included in Attachments 7 and 8 of Appendix 2A.

For the sand or sandy soils layer in the Canister Transfer Building area found in some of the borings located at a depth of 8 to 20 ft:

Index Property	**Minimum**	**Maximum**	**Average**
Water Content, %	3	15	6
Moist Unit Weight, pcf	85	105	98
Dry Unit Weight, pcf	77	102	93
Void Ratio	0.64	1.2	0.83
Saturation, %	11	32	19
% Fines	9	38	23
Specific Gravity = 2.69			

Effective-stress strength parameters are estimated to be $\phi = 30°$ and $c = 0$, based on the plasticity index of the silts and clays. These values are very conservative for the sandy soils, which are characterized as dense based on their SPT N-values and the CPT Q_t data. Note, Appendix D of ConeTec (1999) indicates that ϕ based on the CPTs generally exceeds 35 to 40°.

The recommended coefficients of earth pressure for the silts and clays are as follows:

- At-rest, K_o, is 0.5
- Active, K_a, is 0.33
- Passive, K_p, is 3.0.

The recommended value of the coefficient of vertical subgrade reaction of the silt, silty clay, clayey silt for a 1 ft x 1 ft square is 100 kips/ft^3 for the clayey soils. Where the near-surface soils are cohesionless silts, this value should be 120 kips/ft^3. This value should be reduced for footing widths greater than 1 ft by applying a reduction factor, RF, calculated as follows:

For clayey soils: $RF = 1/B$

For cohesionless soils, $RF = [(B+1) / 2B]^2$

where B is the effective width of the footing.

This value should also be reduced for rectangular footings by $(1 + 0.5 \times B / L) / 1.5$, where L is the effective length of the footing.

The recommended value of the coefficient of vertical subgrade reaction of the in situ clayey soils for use in design of the storage pads is 2.75 kips/ft^3, and for the cohesionless soils is 26 kips/ft^3.

The recommended value of the coefficient of horizontal subgrade reaction of the in situ clayey soils for use in the design of drilled caissons is 67 / B kips/ft^3. For cohesionless soils, the recommended value of the coefficient of horizontal subgrade reaction is $20 \cdot z / B$ kips/ft^3.

Soil compressibility parameters and values of undrained shear strength were obtained from a number of tests to provide conservative results that were applicable for the

upper 25 to 30 feet over the storage pad area because of the consistency of the subsurface conditions encountered in these borings. In addition, these results are considered to be conservative for the soils in the upper layer because they were obtained from testing specimens from the upper 25 to 30 feet where the Standard Penetration Test (SPT) blow count was less than or equal to the average value of all samples obtained in this layer, as indicated in Figure 2.6-27. Note, the SPT blow count is directly related to the density and strength of soils and inversely related to compressibility of soils.

Figure 54.4 of Terzaghi and Peck (1967) illustrates this for cohesionless soils. This figure presents the relationship between SPT blow counts (values of "N" in the figure), density, and compressibility of sands. It indicates that the density increases as the N-value increases. It also illustrates that a footing of a given width has a higher allowable soil pressure for a given settlement (1" in this chart) as the SPT blow count increases. Therefore, as the blow count increases, the strength of cohesionless soil increases and its compressibility decreases.

Table 45.2 of Terzaghi and Peck (1967) presents the relationship between consistency, SPT blow count, and strength of clay. This table indicates that the consistency increases from very soft to hard for blow counts ranging from less than 2 blows/ft to greater than 30 blows/ft, respectively. Table 2 of Terzaghi (1955) indicates that the coefficient of subgrade reaction, defined as the ratio between the pressure at a given point of the surface of contact and the settlement produced by that load, increases as the consistency of clay increases. Therefore, as the SPT blow count increases, the consistency of clay increases, and the compressibility (and, hence, settlement) decreases.

This has been demonstrated by the laboratory testing that was performed on samples obtained at greater depths in the Canister Transfer Building area. Additional laboratory tests were performed on samples of the soils from deeper within the profile than those that were tested (from depths of about 10 to 11 ft) in 1996. These tests, reported in Attachments 4 and 6 of Appendix 2A, indicate that the strengths of these deeper soils are higher than those tested in 1996 and their compressibilities are lower.

The depths of the specimens tested for strength and compressibility in Attachment 2 of Appendix 2A were selected to investigate conditions at a depth of about 10 feet below grade, which represents a depth of approximately ½ the width of the loaded area below the foundation due to the loading from the storage cask. It is generally acknowledged in geotechnical engineering that the zone of influence of loads on foundations spread out below the footing (e.g., Section 8.3 of Lambe and Whitman, 1969). The stress increase is greatest at the base of the footing, and it dissipates to an insignificant value at a depth of twice the width of the foundation. It is common practice to place a greater emphasis on the depth below the foundation equal to the width of the load. Testing the soils at ½ of this depth provides parameters that reflect the average performance of the soils within the depth equal to the width of the loaded area.

As indicated in Figure 2.6-27, the average and median values of the SPT blow counts, plotted for each 5-ft elevation interval versus elevation, illustrate that the blow counts increase with depth from grade. This figure also indicates that the locations of the specimens tested for strength and compressibility fall within the zone where the average and median blow counts for each 5-ft elevation interval were less than or equal to the average value for the entire layer (15 blows/ft). Since the strength of these soils is directly related to the blow count, testing soils whose blow count is less than the average provides a conservative estimate of the strength of the soil. In addition, since the compressibility of these soils is inversely related to their blow count, testing soils

whose blow count is less than the average provides a conservative estimate of their compressibility and, hence, result in conservative (i.e., higher) estimates of settlements that the cask storage pads will experience.

Figure 2.6-20 plots all of the N-values vs depth for each of the borings drilled in the proposed emplacement area. The borings are plotted by row in the four sets of plots according to their locations in the field, as shown in Figure 2.6-2. That is, the top row of plots on Sheet 1 of Figure 2.6-20 includes the data from the northernmost row of borings, the next row down the sheet represents the next row of borings, moving south on the site, etc. The N-value plots in Figure 2.6-20 illustrate that the soils in the upper 25 to 30-ft thick layer of the profile do not vary significantly across the site.

Additional field work, performed at the site in 1998, is described in Geomatrix Consultants, Inc, (1999a) and included detailed lithostratigraphic soils mapping in test pits and trenches, as well as logging of continuous split-barrel samples in closely spaced boreholes. The results of these studies reaffirm the consistency of the upper layer of the subsurface profile across the site.

Subsurface profiles and stratigraphic descriptions are presented in Plates 3 and 4 in Geomatrix Consultants, Inc (1999a), and they illustrate convincingly that the subsurface conditions are very uniform. They identify a thin (<2.5 ft) surface layer of eolian silt and playa deposits with a poorly developed soil structure. This layer corresponds to the first SPT sample in the borings that were drilled in late 1996 (Attachment 1 of Appendix 2A) in the proposed pad emplacement area. This layer is underlain by a sequence of typical lacustrine sediments associated with several stages of Lake Bonneville, an inland sea that covered the area from about 30,000 to 10,000 years before present (B.P.). These sediments are, by and large, the fine-grained end members of a ternary diagram consisting of silt, clay, and sand. Samples are consistently described as silt,

silty clay, clayey silt, or sandy silt. Geomatrix used the term marl or marly as an additional component of these descriptions, which refers to a high calcium carbonate content clay or silt deposited in a fresh-water environment (deep-water facies of Bonneville alloformation).

Geomatrix was able to subdivide the lacustrine sequence into several lake stages based on sedimentary relationships and physical characteristics exposed in continuous wall exposures in trenches and test pits. Their subdivisions of the Bonneville alloformation, presented in their Plate 3, "Map of North Wall Trench T-2", are as follows:

- Bonneville Deep-Water Blocky,
- Bonneville Deep-Water Laminated,
- Post-Stansbury Transgressive, and
- Stansbury Regressive.

This sequence extends to a depth of about 25 to 30 ft, where a continuous, nearly horizontal layer of dense, fine sand is encountered. This layer is the "Stansbury Transgressive", and it represents the oldest deposit of the Bonneville Cycle. The base of this unit occurs at a depth of about 45 to 50 ft and is believed to be an unconformity represented by the Promontory soil. This boundary is an apparent seismic velocity contrast that is recognizable on the recent seismic reflection profiles as a continuous, nearly horizontal layer, the Qp reflector (Geomatrix Consultants, Inc, 1999a).

Dynamic Strength of Soils

It has been recognized in the past that the strength of cohesive soil increases as the rate of loading increases. For example, Casagrande and Shannon (1948) conducted soil dynamics investigations in 1948 with research efforts directed at finding the effects of rate of loading on soils common to the Panama Canal zone, i.e., clays, muck, shales, and dense dry sand. A "strain-rate" effect, defined as the ratio of maximum dynamic strength to the maximum static strength, was observed in all soils tested,

except for the dry sand. Tests performed on Cambridge Clay (Cambridge, MA), showed that, tested at a rapid rate of loading (0.02 sec), the strength of the clay was approximately 1.9 times greater than that measured at a slow rate of loading (465 sec). This is illustrated in Figure 2.6-24.

Schimming et al (1966) studied the effects of loading rate on the strength of various soil types and defined the "apparent cohesion (c_a)" ratio to compare the dynamic and static failure envelopes of soil. Two different strain-rate strength tests were used in the study. For "dynamic" tests, the maximum shear force in soil specimens was attained within a period of 1 to 5 milliseconds after imposition of the initial force. Conversely, for "rapid static" tests, times to failure ranged from 30 seconds to nearly 50 seconds.

The c_a ratio is defined as: c_a = c (dynamic) ÷ c (rapid static).

Strength and index properties of the silty clay at the PFSF site are very similar to a soil studied by Schimming et al (i.e., Jordan Buff Clay). Average values of the index properties for both soils are as follows:

	PFSF Silty Clay	Jordan Buff Clay
Dry density (pcf)	65 (35)	86 (2)
Water content (%)	39 (117)	32 (2)
Liquid limit (LL)	51 (42)	54 (2)
Plastic limit (PL)	29 (42)	26 (2)
Plasticity index (PI)	21 (42)	28 (2)
Cohesion (psf)	1,100 (2)	1,124 (2)

Note: numbers in parentheses above indicate number of tests.

They report that the c_a ratio for this clay ranged from approximately 1.8 to 2.0, as shown in Figure 2.6-25.

Direct shear tests were performed on samples of the silty clay obtained from Elevation 4,468.4 to 4,469.4 in the Canister Transfer Building area, which is near the bottom of the foundation mat (Elevation 4,470). The results of these tests are included in Attachments 7 and 8 of Appendix 2A and they indicate that the average cohesion of these soils is ~1.1 ksf. The rate of loading used in these tests is slower than the "rapid static" tests performed by Schimming et al (1966). The rate of loading due to the design basis ground motion approximates those used for the "dynamic" tests performed by Schimming et al. To estimate the cohesion that will be available to resist these dynamic forces, the cohesion measured in the direct shear tests are multiplied by an estimated c_a ratio, which Schimming et al indicated varied between 1.8 and 2.1 for similar soils. Therefore, the cohesion available to resist forces caused by the design basis ground motion is estimated to be at least 1.5 to 2 times those measured in the direct shear tests. Stone & Webster (1995) used a similar approach for determining the dynamic strength of clays available to resist uplift loads on H-piles for Category I structures at the TVA's Sequoyah Nuclear Power Plant, Units 1 and 2.

Analyses of resistance to sliding of the Canister Transfer Building due to dynamic forces from the design basis ground motion, discussed in Section 2.6.1.12.2, are performed using a value of cohesion that is conservatively specified using c_a based on the lower bound of this range; i.e., only a 50% increase:

$$c_{dynamic} = 1.1 \text{ ksf} \times 1.5\ (c_a) = 1.65 \text{ ksf}.$$

The dynamic foundation parameters in support of the soil-structure interaction analyses are discussed in Section 2.6.2.1.

THIS PAGE INTENTIONALLY LEFT BLANK

2.6.1.12 Stability of Foundations for Structures and Embankments

All exterior footings will be founded at a depth of no less than 30 inches below finished grade to provide protection against frost, in accordance with local code requirements. Interior footings in heated areas may be founded at shallower depths, if desired.

The minimum factor of safety against a bearing capacity failure due to static loads (dead load plus maximum live loads) is 3.0.

In accordance with the requirements of NUREG-75/087, Section 3.8.5, "Foundations," Section II.5, "Structural Acceptance Criteria," the recommended minimum factor of safety against overturning or sliding failure from static loads (dead load plus maximum live loads) is 1.5 and due to static loads plus loads from extreme environmental conditions, such as the design basis ground motion, is 1.1. In addition, it is recommended that a factor of safety of 1.1 be used to design footings against a bearing capacity failure from static loads plus loads due to the design basis ground motion.

If the factor of safety against sliding is less than 1 due to the design basis ground motion, additional analyses of the displacements the structure may experience are calculated using the method proposed by Newmark (1965) for estimating displacements of dams and embankments during earthquakes to demonstrate that such displacements, if they did occur, would not have an adverse impact on the performance of the important-to-safety structures.

Recommended design earth pressure distributions are presented in Figure 2.6-7. Lateral earth pressures for determining driving forces shall be based on K_o, the at-rest earth pressure coefficient. These can be reduced to "active" earth pressures if the yield ratio exceeds 0.1%, where yield ratio, S/H, is defined as shown for the active case in Figure 2.6-8. In determining "passive" pressures resisting lateral movement, assume

the lateral earth pressure coefficient varies from K_o at a yield ratio of 0% to a maximum of K_p at a yield ratio of 2%, where yield ratio, S/H, is defined as shown for the passive case in Figure 2.6-8. Compaction-induced lateral stresses are determined as shown in Figure 2.6-9.

2.6.1.12.1 Stability and Settlement Analyses—Cask Storage Pads

The gross allowable bearing pressure for the cask storage pads to obtain a factor of safety of 3.0 against a shear failure from static loads is 4 ksf. However, loading the storage pads to this value may result in undesirable settlements. This minimum allowable value was obtained in analyses that conservatively assume $\phi = 0°$ and c = 2.2 ksf, as measured in the UU tests that are reported in Attachment 2 of Appendix 2A. Using the estimated effective-stress strength of $\phi = 30°$ or the total stress strength parameters of $\phi = 21.1°$ and c = 1.13 ksf, as measured in the direct shear tests (Attachments 7 and 8 of Appendix 2A), results in higher allowable bearing pressures. Triaxial test results included in Attachments 4 and 6 of Appendix 2A indicate that 2.2 ksf is a reasonable lower-bound value to use for bearing capacity analyses. These triaxial tests were performed at confining pressures comparable to the estimated final stresses under the fully loaded pads and, thus, provide a realistic estimation of the minimum strength that will be available for resisting a bearing capacity failure.

As indicated in Section 2.6.1.6, based on the CPT program, most of the soils underlying the pad emplacement area are mischaracterized as soils that behave as "sandy" soils, rather than as cohesive soils. These soils were found to be mostly cohesive soils in the borings that were drilled in 1996, as indicated in Attachment 1 of Appendix 2A. The soil behavior types reported in ConeTec (1999) were determined based on correlations developed from testing saturated, uncemented soils. The soils at the site are partially saturated and cemented; thus, the soil behavior types determined from the cone penetration test data must be recalibrated to agree with the soil classifications

determined based on samples obtained in the borings and tested in the laboratory. Figure 2.6-30, Sheets 1 through 6, present comparisons of the boring and laboratory soil classifications plotted vs elevation alongside the soil behavior type data from nearby cone penetration tests. The differences shown under the column labeled ΔSBT represent the SBT zoning shift required to more correctly characterize these soils as a result of the effects of partial saturation and cementation, as discussed above. Evaluation of these ΔSBT values leads to the conclusion that the soil behavior type values reported in ConeTec (1999) that are greater than 5 (i.e., sandier soils), as well as some of those equal to 5 (i.e., clayey silts), typically should be adjusted downward one or two zones to more accurately reflect the soil classifications that were determined based on the borings and confirmed by the laboratory tests performed specifically for the purpose of classifying the soil types. Conservatively adjusting these data by subtracting 1 from the SBTs that were reported to be greater than 5 (i.e., "sandy" soils), as discussed in Section 2.6.1.6, results in the SBTs presented on the foundation profiles, Sheets 2 through 14 of Figure 2.6-5. As shown on these figures, the subsurface soils that were reported in ConeTec (1999) as being silty sands/sand and sands; are more correctly described as silts with some sandy silts. The following discussion is included to demonstrate that even if these soils are cohesionless soils, the factor of safety against a bearing capacity failure is much greater than that reported above for the clayey soils identified in the borings.

Whereas the bearing capacity of cohesive soils is a function of the strength of the soil, that of cohesionless soils is also a function of the width of the foundation. The foundations in question for this project have widths that are greater than 30 ft. Such large foundations, supported by soils having Standard Penetration Test blow counts that were measured for these soils, have much greater bearing capacities if they are founded on cohesionless soils than if supported by cohesive soils. Therefore,

characterizing the soils in the upper layer as cohesive even though some of these may be cohesionless provides a conservative estimate of the bearing capacity.

Analyses of bearing capacity were made in Calculation 05996.02-G(B)-4, (SWEC, 1999e), based on the assumption that the entire upper layer, approximately 25 to 30-ft thick, was comprised of cohesive soils similar to those tested at depths of 10 to 12 ft. In these analyses, the strength of the soils in the entire upper layer (~25 to 30-ft thick) was set equal to that measured in the UU tests (s_u > 2.2 ksf) that were performed at depths of approximately 10 to 12 feet. As indicated on page 9 of that calculation, the factor of safety of the cask storage pad foundation is 6.3 using this undrained strength for the cohesive soils. Page 10 of that calculation illustrates that the factor of safety against a bearing capacity failure increases to greater than 13 when a drained strength of $\phi = 30°$ is used. Both of these cases result in factors of safety against a bearing capacity that exceed the minimum allowable value of 3 for static loads.

The friction angle used in the drained analyses discussed above is less than the friction angle shown for the soils that behave as sandy soils (SBT>5) based on the CPT data presented in Appendix D of ConeTec (1999). These plots illustrate that most of the "Phi" values are between 35° and 40° for these soils, with very few values that are slightly less than 35°. Therefore, assuming that all of the soils underlying the cask storage pads are cohesionless, as represented by the preponderance of soils that behave as "sandy" soils based on the uncorrected CPT SBT data, the factor of safety against a bearing capacity failure will be much greater than 13.

Analyses were performed to estimate the settlement of the storage pads as a result of the weight of the pad and the weight of eight, fully loaded, Holtec HI-STORM casks (356.5 K vs. 310 K for the SNC cask) in Calculation 05996.02-G(B)-3 (SWEC, 1999f). The actual bearing pressure for this case was about 1.9 ksf, and the estimated total settlement of the pad was determined to be about 3.3 inches.

The total settlement consists of the following three components:

• Elastic settlement	0.5 inch
• Primary consolidation settlement	1.7 inches
• Secondary compression	1.1 inches
• Total estimated settlement	3.3 inches

In order to accommodate the total estimated settlement, the storage pads will be constructed 3.5 inches above adjacent finished grade. Exposed edges of the pads will be chamfered and the compacted aggregate surface material will be feathered to meet the edges of the raised pads for transporter access, as shown in Figure 4.2-7.

This settlement represents an upper-bound estimate of the total compression, because it was developed assuming that the consolidation characteristics that were measured for the clayey soils at a depth of about 10 ft are applicable for the entire upper layer. The SPT data from the borings and the CPT results indicate that the soils become stiffer within the 10 to 20 ft depth zone. Additional consolidation tests performed on samples obtained from depths of about 25 ft in the Canister Transfer Building area, reported in Attachment 6 of Appendix 2A, indicate that the soils at that depth are less compressible than those used to estimate the settlements presented above. Further, based on the CPT program, most of the soils underlying the pad emplacement area are characterized as soils that ***behave*** as "sandy" soils, rather than as cohesive soils. Such soils are much less compressible than the clayey soils described above. Therefore, assuming that the entire upper layer at the site was comprised of soils whose compressibilities are similar to those measured at a depth of 10 to 12 ft conservatively overestimates the expected settlements.

As discussed above, the soil behavior types determined from the cone penetration test data and reported in ConeTec (1999) must be recalibrated to agree with the soil classifications determined based on samples obtained in the borings and tested in the laboratory. Figure 2.6-30, Sheets 1 through 6, present comparisons of the boring and laboratory soil classifications plotted vs elevation alongside the soil behavior type data from nearby cone penetration tests. These figures illustrate that the soil behavior type values reported in ConeTec (1999) that are greater than 5 (i.e., sandier soils), as well as some of those equal to 5 (i.e., clayey silts), typically should be adjusted downward one or two zones to more accurately reflect the soil classifications that were determined based on the borings and confirmed by the laboratory tests performed specifically for the purpose of classifying the soil types. The following discussion is included to demonstrate that even if these soils are cohesionless soils, the estimated settlements will be much less than those reported above assuming that the entire upper layer at the site was comprised of soils whose compressibilities are similar to those measured in consolidation tests performed on samples obtained at a depth of 10 to 12 ft.

A review of the CPT data (ConeTec, 1999) indicates that most of the soil behavior type (SBT) values represent soils whose behavior is similar to that of "sandy" soils. As indicated in Figure 5 of ConeTec (1999), these include SBT values that are greater than 5. A map was produced to show the thickness of those soils for which the soil behavior type values are greater than 5. The purpose of this map is to readily identify those areas where the subsurface profile differs from the assumption that the soils in the upper layer (~25 to 30 ft) are predominantly cohesive soils.

This map, titled "Contour Map Showing Thickness of Soils with CPT Soil Behavior Type > 5 (Sandy)", is included as Figure 2.6-29. The thickness of the soils beneath the cask storage pads that behave as "sandy" soils based on the CPT data are posted under the CPT identifiers shown on this plan view of the site. These values were calculated by

subtracting the top three feet, to account for the proposed depth of the pads, as well as the total thickness of all zones where the SBT values were found to be less than 6, from the total depth of the CPT. The thicknesses were contoured to facilitate interpretation of the SBT > 5 data obtained in the CPT program. As indicated in the figure, the thickness of the soils that behave as sandy soils (SBT>5) based on the CPT data ranges from 13.8 feet at CPT-15, near the center of the pad emplacement area, to a high of 26.4 feet at CPT-33 near the center of the western edge of the pad emplacement area. The thicknesses are generally about 20 to 25 feet.

Stone & Webster (1999f) incorporated the calculation of settlements for the soils whose behavior is similar to that of "sandy" soils based on the CPT data. In this analysis, settlements are calculated based on Equation 6-17 of Lunne, Robertson, and Powell (1997), which was developed by Schmertmann (1970, 1978). This method is applicable for estimating settlements of foundations over sand using CPT data. The Schmertmann method takes into account the depth of footing, time of loading (40 years was used in the analysis), shape of the footing, and strain influence factor, which varies with depth. The equivalent Young's modulus, which appears in the equation, is related to the cone penetration resistance by a factor, α, which is related to the degree of loading, soil density, stress history, cementation, age, grain shape, and mineralogy of the deposit. In this analysis, α was assumed to be 5, which equals the middle of the range recommended in ConeTec (1998) for aged (>1,000 years) normally consolidated sands.

Two sets of estimated settlements were calculated and are summarized in the table presented on Page 44 of the calculation. Because of the preponderance of soils whose behavior is similar to that of "sandy" soils when the CPT data are interpreted using the SBT classification chart developed by Robertson and Campanella (1988) based primarily on saturated, uncemented soils, settlements were calculated assuming that

the Schmertmann method is applicable to the entire upper layer. As indicated by the left-hand column of settlements reported on Page 44 of the calculation, the estimated settlements for this case varied from 0.34 inches at CPT-26 to 0.56 inches at CPT-38.

The analyses were repeated, excluding those soils whose behavior is not similar to "sandy" soils, since the Schmertmann method is applicable only for cohesionless soils. In this analysis, cohesionless soils were defined as those with SBT values greater than 5, which includes silts, sandy silts, silty sands, and sands. The estimated settlements for this case are presented in the right-hand column on Page 44 of the calculation and range from 0.24 inches at CPT-31 to 0.50 inches at CPT-10.

These results are posted on the map showing the locations of the CPTs on Page 46 of the calculation. As indicated, the differential settlements between CPT locations average less than 0.1 inches. The maximum difference between two adjacent (diagonally) CPTs is 0.19 inches, CPT-34 to CPT-29. Total and differential settlements of this magnitude are not significant in the design of the cask storage pads. These analyses confirm that if the soils are actually "sandy" soils, as indicated by the uncorrected SBTs from the cone penetration testing (ConeTec, 1999), then the estimated settlements will be much less than those reported above assuming that the entire upper layer at the site was comprised of soils whose compressibilities are similar to those measured in consolidation tests performed on samples obtained at a depth of 10 to 12 ft.

Dynamic Stability Analyses

The allowable bearing pressure for the storage pads for dynamic loads from the design basis ground motion was determined based on the assumption that the horizontal inertia of the casks due to the earthquake may exceed the frictional resistance available

between the cask and the top of the pad. If this were to occur, the horizontal force that would be imparted to the pad from the casks would equal $\mu \cdot F_v$, where:

μ = the coefficient of friction between the steel bottom of the cask and the top of the concrete storage pad.
F_v = weight of the casks + the vertical inertial force of the casks as result of the design basis ground motion.

These analyses were performed for various values of μ and the lowest allowable bearing pressure was 4.30 ksf. This case corresponds to the upper-bound friction case discussed in Section 4.2.3.5.1B, which results in an upper-bound estimate of the cask dynamic forces acting on the pad. For the lower-bound friction case discussed in Section 4.2.3.5.1B, wherein μ between the steel bottom of the cask and the top of the concrete storage pad = 0.2, the allowable bearing pressure was 7.30 ksf.

Because of the nature of the subsurface materials, dynamic settlements due to the design basis ground motion are not expected to occur. See Section 2.6.4.7 for more details.

Sliding Stability of the Cask Storage Pads

The sliding stability analyses of the cask storage pads are presented in Calculation G(B)-4 (SWEC, 1999e). In these analyses, the factor of safety (FS) against sliding is defined as:

FS = resisting force ÷ driving force

The resisting force, or tangential (T) shear force, below the base of the pad is defined as:

$$T = [N \tan(\phi)] + [cBL]$$

where: N = normal force,

$\phi = 24.9°$,

c = 1.22 ksf, and

B and L are the dimensions of the pad.

The values of ϕ and c are based on the results of the direct shear tests that were performed on specimens obtained from a depth of 5 to 6.3 ft from Sample U-1 in Boring C-2, which was drilled in the pad emplacement area. These test results are consistent with the results obtained from the direct shear tests that were performed on samples obtained from within the Canister Transfer Building area (Borings CTB-6 and CTB-S). All of these direct shear test results are reported in Attachments 7 and 8of Appendix 2A. Minimum sliding resistance exists when the dynamic forces due to the vertical component of the earthquake act in an upward direction. In determining the resisting forces in these analyses, no credit is taken for passive resistance acting on the embedded pad.

The horizontal driving forces used in these analyses were obtained from Attachment B of Calculation G(B)-4 (SWEC, 1999e) and are based on the higher ground accelerations associated with the PFSF deterministic design basis ground motion (0.67g horizontal and 0.69g vertical). To be conservative, credit was not taken for the lower ground accelerations (0.53g) applicable for the 2,000-yr return period design basis ground motion.

The driving force in these analyses includes the inertial forces of the casks and the pad, due to the horizontal component of the earthquake. The dynamic loads due to soil pressures acting on the embedded pad were also included, calculated based on

the Mononobe-Okabe method, as described in Seed and Whitman (1970). The driving forces were calculated based on the peak vertical and peak horizontal accelerations; i.e., no credit was taken for the fact that these peaks are not expected to occur at different times.

These analyses indicate that the factor of safety against sliding of the pads supported directly on the in situ clayey soils is ~1.2, which provides an adequate margin against sliding. As indicated above, these analyses are very conservative for a number of reasons. The horizontal driving forces used in this analysis are based on the higher ground accelerations (0.67g horizontal and 0.69g vertical) due to the PFSF deterministic design basis ground motion, rather than those (0.53g) for the 2,000-yr return period earthquake from the probabilistic seismic hazard analysis. In addition, this analysis combines the maximum horizontal and vertical forces of the earthquake, rather than using reduced values to account for the fact that the peaks in these motions are not expected to occur at the same time. They also conservatively use the shear strength parameters as measured in the static direct shear tests — no credit is taken for the increase in this strength that is applicable for dynamic loadings, as discussed in Section 2.6.1.11 under "Dynamic Strength of Soils." Therefore, it is assumed that these forces yield lower-bound factors of safety against sliding where the pads are supported on clayey soils.

Sliding Stability of the Cask Storage Pads on Cohesionless Soils

The storage pads founded on clayey soils have an adequate factor of safety against sliding due to forces associated with the PFSF deterministic design basis ground motion. The majority of the shearing resistance along the base of the pads in this case comes from the cohesive portion of the shear strength of the clayey silt/silty clay layer, which is not affected by upward acting earthquake loads. The frictional portion

of the shear strength, however, is directly related to the normal stress. During an earthquake, the vertical component of earthquake motions results in upward forces that reduce the normal stress and, consequently, the shearing resistance available to resist sliding due to the frictional portion of the shear strength. Factors of safety against sliding for cohesionless soils can be low if the maximum components of the ground motion are combined.

The CPT results (ConeTec, 1999) indicate the presence of a layer of soils that behave like silty sands and sands under the clayey layer at a depth of about 10 ft. Note, however, that recalibrating the SBTs as discussed in Section 2.6.1.6 results in most of these silty sands and sands being more correctly identified as clayey silt/silt with some sandy silt, as shown in Sheets 2 through 14 of Figure 2.6-5. The plots included in Appendix D of ConeTec, 1999) indicate that s_u, the undrained shear strength, or the cohesion, drops to 0 and that ϕ is generally greater than 35 to 40° for these soils. If the cohesion available to resist sliding drops to 0 and cementation effects are ignored, the shearing resistance of this layer is directly related to the normal stress.

Analyses were performed to address the possibility that sliding may occur along a deep slip plane at the clayey soil/sandy soil interface as a result of the earthquake forces. To simplify the analysis, it was assumed that cohesionless soils extend above the 10 ft depth and, thus, the pads are founded directly on cohesionless materials. Conservatively assuming that ϕ = 30°, which is more reasonable for nonplastic silts and sandy silts than the values of 35 to 40° measured in the CPTs, the resistance to sliding is calculated as N tan 30°, or 0.58 N, where N is the normal force. Because of the magnitude of the peak ground accelerations (0.53g) due to the design basis ground motion at this site, the frictional resistance available when N is reduced due to the uplift from the inertial forces applicable for the vertical component of the design basis ground motion is not sufficient to resist sliding. However, analyses were

performed to estimate the amount of displacement that might occur due to the design basis ground motion for this case. These analyses, based on Newmark's method as described below, indicate that even if these soils are cohesionless and even if they are conservatively located directly at the base of the pads, because this is a horizontal ground site, the estimated displacements would be less than ¾ inch. Whereas there are no connections between the ground and these pads or between the pads and other structures, displacements of this magnitude will not adversely affect the performance of these structures.

Where the factor of safety against sliding is less than 1, the displacements the pads may experience were calculated using the method proposed by Newmark (1965) for estimating displacements of dams and embankments during earthquakes. In these analyses, it was conservatively assumed that cohesionless soils extend above the 10 ft depth and, thus, the pads are founded directly on cohesionless materials. For motion to occur on a slip surface in the deeper cohesionless layer, the slip surface must pass through the overlying clayey soils. This simplification, therefore, results in some conservatism. A friction angle of 30° was used for the cohesionless layer, hypothetically located directly at the base of the pads, and the cohesion was assumed to be 0. The deeper layers, identified as silty sands and sands in ConeTec (1999), are medium dense to dense with higher friction angles, as evidenced by the CPT tip resistance values and the ϕ vs depth data presented in Appendix D of ConeTec (1999). Therefore, assuming $\phi = 30°$ for these soils provides for additional conservatism in these analyses.

Additional conservatism is provided in these analyses by the use of the peak ground accelerations from the PFSF deterministic design basis ground motion, 0.67g horizontal and 0.69g vertical, rather than the 0.53g associated with the PSHA 2,000-yr return period design basis ground motion. Maximum ground velocities were estimated

for the pads using the maximum horizontal velocities of the mat in the Canister Transfer Building and scaling them based on the ratio of the maximum accelerations.

The seismic displacements were calculated, combining the maximum earthquake ground motions in the vertical, north-south (N-S), and east-west (E-W) directions. Because the peak motions of the three components are not expected to occur at the same time, their effects are accounted for by combining 100% of the maximum motion in one direction with 40% of the maximum motions in the other two directions. The following ground motions result from the three possible combinations.

- Load Combination 1: 100% Vertical, 40% N-S, 40% E-W (Load #1)
- Load Combination 2: 40% Vertical, 100% N-S, 40% E-W (Load #2)
- Load Combination 3: 40% Vertical, 40% N-S, 100% E-W (Load #3)

Newmark's Method of Estimating Displacements Due to Earthquakes

Newmark (1965) defines N W as the steady force applied at the center of gravity of the sliding mass in the direction in which the force can have its lowest value to just overcome the stabilizing forces and keep the mass moving. For a block sliding on a horizontal surface, N W = T, where T is the shearing resistance between the base of the block on the sliding surface.

Shearing resistance, $T = \tau \times \text{Area}$

where: $\tau = \sigma_n \tan \phi$

σ_n = Normal Stress

ϕ = Friction angle of cohesionless layer

σ_n = (Net Vertical Force) / Area = $(F_v - F_{v(Eqk)})$ / Area

$$\therefore \quad T = (F_v - F_{v(Eqk)}) \tan \phi$$

$$N W = T$$

$$\therefore \quad N = [(F_v - F_{v(Eqk)}) \tan \phi] / W$$

Maximum relative displacement of the pad relative to the ground, u_m, is calculated as

$$u_m = [V^2 (1- N/A)] / (2gN)$$

The above expression for the relative displacement is an upper bound for all the data points for N/A less than 0.15 and greater than 0.5, as shown in Figure 2.6-26, which is a copy of Figure 21 of Newmark (1965). Within the range of 0.5 to 0.15 the following expression gives an upper bound for all data.

$$u_m = V^2 /(2gN)$$

The following table presents the results (from Calculation G(B)-4, SWEC, 1999e) of estimating the displacements of the cask storage pads assuming that they are supported on cohesionless soils with $\phi = 30°$.

LOAD COMBINATION	DISPLACEMENT
1. 100% Vertical, 40% N-S, 40% E-W	0.4 to 0.7 inches
2. 40% Vertical, 100% N-S, 40% E-W	0.5 inches
3. 40% Vertical, 40% N-S, 100% E-W	0.5 inches

The estimated relative displacement of the pads ranges from 0.4 inches to 0.7 inches. The higher displacement corresponds to the load combination where the maximum upward earthquake force reduces the normal stress and, hence, the shearing resistance of the cohesionless layer, postulated to exist directly beneath the pads. For the pads to slide, a surface of sliding must be established between the horizontal sliding surface in the silty sand/sandy silt layer and the overlying clayey layer. The contribution

of this surface of sliding to the dynamic resistance to sliding is ignored in the simplified model used to estimate these displacements.

The procedure used to estimate relative displacements has several measures of conservatism, as discussed above, and, thus, the estimated displacements represent upper-bound values. Motions of this magnitude, occurring at the depth of the sandy silt layer, would likely not even be evident at the ground surface. Further, movements of this amount as a result of the earthquake are much less than those applicable for the casks (Section 8.2.1.2) and, thus, would not adversely affect the performance of the cask storage system. It is likely, that should such slippage occur within the soils underlying the pads if they were cohesionless, it would minimize the level of the accelerations that would be transmitted through the soil and into the structure. In this manner, these soils would act as a built-in base-shear isolation system. Any decrease in these accelerations as a result of this would increase the factor of safety against sliding, which would decrease the estimated displacements as well.

2.6.1.12.2 Stability and Settlement Analyses—Canister Transfer Building

The Canister Transfer Building is a large and massive building consisting of exterior reinforced concrete walls 2'-0" thick, a reinforced concrete roof 1'-0" thick, and a solid reinforced concrete mat foundation 5'-0" thick. The interior partitions that make up the low level waste holding area will be constructed of concrete or concrete masonry. The equipment and office areas on the east side of the building will utilize steel-framed partition walls covered with gypsum board. The total weight (static load) of the building and foundation is approximately 75,000 kips (Calculation 05996.02-SC-5, SWEC, 1999h) or 37,500 tons.

In addition to the finite element, soil-structure interaction analysis described in Chapter 4, conventional static and dynamic stability analyses of the building mat foundation were performed. These included bearing capacity, overturning, and sliding stability analyses. These analyses, performed in Calculation 05996.02-G(B)-13 (SWEC, 1999g), are discussed below. These analyses indicate that the building is stable and the performance of the structure will not be adversely affected by the estimated settlements or seismic displacements.

Bearing Capacity of the Canister Transfer Building

The bearing capacity analyses were performed for the mat founded on a layered soil medium using both 'effective stress' and 'total stress' soil parameters for the various soil layers identified in the PFSF Storage Facility Design Criteria. Several load cases were considered, which consisted of combinations of vertical static, vertical seismic in upward and downward directions, and horizontal seismic in E-W and N-S directions. Loads developed in Calculation 05996.02-SC-5 (SWEC, 1999h) were used in these analyses. As in the structural analyses discussed in Section 4.7.1.5.3., "Structural Analysis," seismic loads used were based on 100% of the enveloped ZPA acceleration in one direction, combined with 40% of the enveloped ZPA accelerations in each of the other two directions. For the static load case, a factor of safety in excess of 10 was obtained, exceeding the minimum required factor of safety of 3 by a wide margin. For seismic loadings, the load combination of full static, 40% seismic uplift, and 100% horizontal seismic in E-W, and 40% horizontal seismic in N-S direction was the most critical load case. This load case resulted in an actual soil bearing pressure of 2.5 kips per square foot (ksf), compared with an ultimate bearing capacity of 4.3 ksf. The resulting factor of safety against a bearing capacity failure for this load case is 1.7, compared with the minimum allowable factor of safety for seismic loading cases of 1.1.

described in Section 2.6.1.12.1. In this case, the strength of the clayey soils at the bottom of the CTB mat were based on the average of the two sets of direct shear tests performed on samples of soils obtained from beneath the CTB at the elevation proposed for founding the mat. The results of these tests are included in Attachment 7 of Appendix 2A.

The results of the sliding stability analysis of the Canister Transfer Building are presented in Table 2 of Calculation G(B)-13 (p9-6 of SWEC, 1999g), and indicate that for all load combinations examined, the factors of safety were >1.1. The lowest factor of safety was 1.27, which applies for the case where 100% of the dynamic earthquake forces acts in the east-west direction and 40% acts in the other two directions. Table 3 of that calculation indicates that if credit is not taken for the increase in strength applicable for the "dynamic" rates of shearing applicable for earthquakes, the factor of safety for this case drops to 0.94. This case is less critical, however, than the case described below, which postulates that the soils at the base of the foundation are cohesionless.

Sliding Stability of the Canister Transfer Building on Cohesionless Soils

The Canister Transfer Building will be founded on clayey soils that have an adequate amount of cohesion to resist sliding due to the dynamic forces from the design basis ground motion. As shown in Figures 2.6-21 through 2.6-23, however, some of the soils underlying the building may be cohesionless within the depth zone of about 10 to 20 ft, especially near the southern portion of the building. Analyses were performed to address the possibility that sliding may occur along a deeper slip plane at the clayey soil/sandy soil interface as a result of the earthquake forces. To simplify the analysis, it was assumed that the cohesionless soils extend above the depth of 10 ft and the

structure is founded directly on the cohesionless materials. These analyses conservatively assumed that $\phi = 30°$ and $c = 0$ for these soils.

Because of the magnitude of the dynamic forces resulting from the soil-structure interaction analyses, the factor of safety against sliding of this building would be less than 1 if it were founded on cohesionless soils. Where the factor of safety against sliding is less than 1, the displacements the building may experience were calculated using the method proposed by Newmark (1965) for estimating displacements of dams and embankments during earthquakes. Refer to the discussion regarding Newmark's method of analyzing displacements due to earthquakes presented above in Section 2.6.1.12.1 for the storage pads for more information about this analysis.

The maximum ground accelerations and velocities of the Canister Transfer Building due to the design basis ground motion, which were developed in Calculation SC-5 (SWEC, 1999h, p. 37), were used in this analysis of displacements. The displacements were calculated, combining the maximum earthquake ground motions in the vertical, north-south (N-S), and east-west (E-W) directions. Because the peak motions of the three components are not expected to occur at the same time, their effects are accounted for by combining 100% of the maximum motion in one direction with 40% of the maximum motions in the other two directions. The following ground motions result from the three possible combinations.

- Load Combination 1: 100% Vertical, 40% N-S, 40% E-W (Load #1)
- Load Combination 2: 40% Vertical, 100% N-S, 40% E-W (Load #2)
- Load Combination 3: 40% Vertical, 40% N-S, 100% E-W (Load #3)

The following table presents a summary of the evaluation of sliding of the Canister Transfer Building, assuming it is founded directly on cohesionless soils.

LOAD COMBINATION	DISPLACEMENT
1. 100% Vertical, 40% N-S, 40% E-W	0.8 to 1.2 inches
2. 40% Vertical, 100% N-S, 40% E-W	0.6 inches
3. 40% Vertical, 40% N-S, 100% E-W	0.5 inches

In these analyses, several conservative assumptions were made, and even with this high level of conservatism, the estimated relative displacement of the building ranged from 0.5 inches to 1.2 inches. Motions of this magnitude, occurring at the depth of the silty sand/sandy silt layer, would likely not even be evident at the ground surface. For the building to slide, a surface of sliding must be established between the horizontal sliding surface in the silty sand/sandy silt layer and through the overlying clayey layer. In the simplified model used to estimate these displacements, the contribution of this surface of sliding through the overlying clayey layer to the dynamic resistance to sliding motion is ignored, as is the passive resistance that would act on the embedded portion of the building foundation and the block of soil that is postulated to be moving with it. It is likely, that should such slippage occur within the cohesionless soils underlying the building, it would minimize the level of the accelerations that would be transmitted through the soil and into the structure. In this manner, the cohesionless soils would act as a built-in base-shear isolation system. Any decrease in these accelerations as a result of this would increase the factor of safety against sliding, which would decrease the estimated displacements as well. Further, since there are no Important to Safety systems that would be severed or otherwise impacted by movements of this small amount as a result of the earthquake, such movements do not adversely affect the performance of the Canister Transfer Building.

2.6.1.12.3 Allowable Bearing Capacity—Other Structures

Other structures at the PFSF include the Administration Building, Operating and Maintenance Building, and Security and Health Physics Building. These structures will be founded on strip and spread footings. The allowable bearing capacity of these footings is limited by shear failure of the soil underlying the footing and by footing settlement.

Bearing capacity analyses were performed for a variety of footing widths and depths for both strip footings and square footings, for vertical loads, and for loads inclined 10 and 20 degrees from the vertical. These analyses were performed using effective-stress strength parameters to investigate long-term conditions, which are applicable for static loads. For these analyses, the allowable bearing pressure was determined using a factor of safety of 3. Bearing capacity analyses were also performed using total-stress strength parameters, which are applicable for earthquake loads. The static analyses yielded the minimum allowable bearing pressures, primarily due to the higher factor of safety required for static loadings.

To limit the expected differential settlements to tolerable values, wall footings of all structures should be designed such that the maximum estimated settlement at the center of the wall along the minimum width of the building is less than or equal to 2 inches. Spread footings supporting column loads spaced approximately 16 ft to 24 ft should be designed such that the maximum estimated settlement at the center of the footing is less than or equal to 1.5 inches. These criteria are based on Table 14.1, "Allowable Settlement," of Lambe & Whitman (1969).

The gross allowable bearing pressure of these footings is presented as a function of the minimum effective footing width and depth in Figure 2.6-10 for strip footings and Figure

2.6-11 for square footings. In these figures, the straight lines represent the allowable bearing pressure that will provide the required factor of safety against a shear failure and the curves represent the bearing pressure that will result in a given amount of settlement. As indicated, the bearing pressure based on shear failure increases with increasing depth (and, typically, increasing width) of footing. Footing settlement increases as the load increases; therefore, for a given bearing pressure, as the width of the footing increases, there comes a point at which the amount of settlement exceeds the allowable settlement. Thus, as the footing width increases beyond this point, the allowable bearing pressure must decrease as shown by the curves in Figures 2.6-10 and 2.6-11, in order to limit the settlement to a tolerable value.

The design curves in these figures are for vertical loads applied at the center of the footings. For inclined or eccentrically applied loads, the allowable bearing pressures must be reduced. For loadings inclined at 10 degrees from the vertical, these allowables must be reduced by 25%, and for loadings inclined at 20 degrees from the vertical, these allowables must be reduced by 50%. Eccentric loads are addressed using the concept of "effective footing width", where the effective width (and length, if appropriate) of the footing is determined as shown in Figures 2.6-10 and 2.6-11.

THIS PAGE INTENTIONALLY LEFT BLANK

a depth of 125 ft are similarly only partially saturated and they are very dense. The standard penetration test N-values for these soils typically exceed 100 blows per ft, and they increase with depth. The presence of this greater than 90-ft thick, very dense layer overlying the saturated soils is expected to preclude any surface manifestation of liquefaction (e.g., sand boils) of the saturated soils below the groundwater table, if it were possible for them to liquefy. Below the groundwater table, liquefaction is considered unlikely, however, because the density of the soils encountered in the borings increases with depth, as evidenced by the SPT N-values down to a depth of 226 ft in Boring CTB-1 and the high P-wave velocities (5,100 ft/sec to 5,900 ft/sec) measured for the soils below the groundwater table, reported by Geosphere Midwest, Inc. (Appendix 2B).

2.6.4.9 Design Basis Ground Motion

The design basis ground motion was determined by a probabilistic seismic hazard analysis and is defined as having a peak horizontal ground acceleration of 0.53g and a peak vertical ground acceleration of 0.53g. The development of the design basis ground motion is described in Geomatrix Consultants, Inc. (1999a and 1999b). The site specific response spectra are presented in Table 1 and Figure 5 of Geomatrix Consultants, Inc. (1999b).

2.6.4.10 Static Analyses

Refer to Section 2.6.1.12 for a detailed discussion of static analyses in the stability of foundations for structures.

2.6.4.11 Techniques to Improve Subsurface Conditions

Discussions presented in Section 2.6.1.12, above, indicate that the soils underlying the eolian silt layer at the surface of the PFSF site are suitable for support of the proposed structures; therefore, no special construction techniques are required for improving the

subsurface conditions below the eolian silt. The eolian silt, in its *in situ* loose state, is not suitable for founding the structures at the site. The Canister Transfer Building will be founded on the silty clay/clayey silt layer beneath the eolian silt. It was originally intended that the cask storage pads also would be founded on the silty clay/clayey silt layer. However, instead of excavating the eolian silt from the pad emplacement area and replacing it with suitable structural fill, it will be mixed with sufficient portland cement and water and compacted to form a strong soil-cement subgrade to support the cask storage pads. The required engineering characteristics of the soil cement can be easily engineered during detailed design to meet the necessary strength requirements.

The surficial layer of eolian silt, existing across the entire site as shown in the pad emplacement area foundation profiles (Figure 2.6-5, Sheets 1 through 14), is a major factor in the earthwork required for construction of the facility. This layer consists of a nonplastic to slightly plastic silt, and it has an average thickness of approximately 3 feet across the pad emplacement area. This layer was expected to be removed prior to construction of the storage pads. However, based on evaluation of the earthwork associated with site grading requirements for flood protection and the environmental impacts of truck trips required to import fill to replace this material, PFS will stabilize this soil with cement and use it as base material beneath the storage pads and adjacent driveways.

Section 2.6.1.12 indicates that there is ample margin in the factor of safety against a bearing capacity failure of the silty clay/clayey silt underlying the site and that the settlements are acceptable for these structures. They indicate that the critical design factor with respect to stability of these structures is the resistance to sliding due to loadings from the design basis ground motion. As discussed in that section, the silty clay/clayey silt layer has sufficient strength to resist these dynamic loadings; therefore, adequate sliding resistance can be provided by constructing the structures directly on

the silty clay/clayey silt layer. The soil cement will be designed to provide shear strength that exceeds the strength of the silty clay/clayey silt. Therefore, the resistance to sliding due to loadings from the design basis ground motion will be enhanced by constructing the cask storage pads on a properly designed and installed soil-cement subgrade.

Using soil cement to stabilize the eolian silt will reduce the amount of spoil materials generated, create a stable and level base for pad construction, and substantially improve the sliding resistance of the storage pads. The soil cement will be placed above the *in situ* silty clay/clayey silt layer and will be designed to improve the strength of the eolian silt so that it will be stronger than the clayey soils that were originally intended for use as the founding medium for the pads. The soil cement will also be used to replace the compacted structural fill that the original plan included between the rows of pads. This continuous layer of soil cement, existing under and between the pads, will spread the loads from the pads beyond the footprint of the pads, resulting in decreased total and differential settlements of the pads. The layer of soil cement above the base of the pads and the bond and friction of the pad foundation with the underlying soil-cement layer will greatly increase the sliding resistance of the pad.

Soil cement has been used extensively in the United States and around the world since the 1940's. It was first used in the United States in 1915 for constructing roads. It also has been used at nuclear power plants in the United States and in South Africa. The largest soil-cement project worldwide involved construction of soil-cement slope protection for a 7,000-acre cooling-water reservoir at the South Texas Nuclear Power Plant near Houston, TX. Soil cement also was used to replace an ~18-ft thick layer of potentially liquefiable sandy soils under the foundations of two 900-MW nuclear power plants in Koeberg, South Africa (Dupas and Pecker, 1979).

The strength of soils can be improved markedly by the addition of cement. The eolian silt at the site is similar to the soils identified as Soil A-4 in Nussbaum and Colley (1971), Soils 7 and 8 in Balmer (1958), and Soil 4 in Felt and Abrams (1957). As indicated for Soil A-4 in Table 5 of Nussbaum and Colley (1971), the addition of just 2.5% cement by weight to the silt increased the cohesion from 5 psi (720 psf) to 30 psi (4,320 psf). The cohesion for Soils 7 and 8 also were increased significantly by the addition of low percentages of cement, as shown on Tables VI and VII of Balmer (1958). Figure 10 in Felt and Abrams (1957) illustrates the continued strength increase over time for these soil-cement mixtures. Other examples of soil-cement strength increases over time are presented in Figure 4.3 of ACI (1998), Table 6 of Nussbaum and Colley (1971), and Figures 6 and 7 of Dupas and Pecker (1979). Therefore, the soil cement will be much stronger than the underlying silty clay/clayey silt and the strength will increase with time, providing an improved foundation material. This will provide additional margin against sliding compared to the original plan to construct the pads directly on the silty clay/clayey silt layer.

The minimum shear strength required at the base of the pad foundation and within the underlying soils to provide a factor of safety against sliding that is greater than 1.1 for the seismic load cases is approximately 10.7 psi (1.54 ksf), based on the driving forces identified on pages 12 and 13 of Calculation 05996.02-G(B)-04, Rev 4. This value is calculated as follows:

F_A = 69.1 K (Combined static and dynamic active earth pressure from p 12 of Calculation 05996.02-G(B)-04-4).

EQh_{pad} = 579 K (= 0.67 x 3' x 64' x 30' x 0.15 K/ft^3)

Eqh_{casks} = 2,030 K (based on deterministic earthquake horizontal ground acceleration of 0.67g).

$$\tau_{reqd} = \frac{(69.1\ K + 579\ K + 2{,}030\ K) \times 1.1 \times 1{,}000\ lbs/K}{30' \times 64' \times 144\ in.^2/ft^2} = 10.7\ psi$$

Note, these values of EQh_{pad} and Eqh_{casks} were obtained from Attachment B of Calculation 05996.02-G(B)-04, Rev 4 (i.e., P_I and F_{HT}) and are based on the original, deterministic earthquake horizontal ground acceleration of 0.67g, rather than the horizontal ground acceleration for the revised design basis ground motion based on the probabilistic seismic hazard analysis, which is 0.53g, as indicated in Section 2.6.4.9. When Rev 4 of Calculation 05996.02-G(B)-04 was being prepared, the value of Eqh_{casks} applicable for the revised design basis ground motion was not available. Since the revised horizontal ground acceleration (0.53g) is lower than the horizontal ground acceleration (0.67g) of the original deterministic earthquake, Eqh_{casks} was conservatively assumed to equal the value applicable for the original deterministic earthquake. The maximum value of Eqh_{casks} subsequently was developed and is shown as Qxd = 1,855 K in the bottom row of the rightmost column of Table D-1(a) on Sheet 238 of Calculation 05996.02-G(PO17)-2, Rev 0.

Revising the above calculation of to reflect these changes results in

EQh_{pad} = 458 K (= 0.53 x 3' x 64' x 30' x 0.15 K/ft^3)

Eqh_{casks} = 1,855 K

$$\tau_{reqd} = \frac{(69.1\ K + 458\ K + 1{,}855\ K) \times 1.1 \times 1{,}000\ lbs/K}{30' \times 64' \times 144\ in.^2/ft^2} = 9.5\ psi$$

The minimum normal load acts at the base of the pad when the inertial force of the design basis ground motion acts upward. Page 14 of Calculation 05996.02-G(B)-04 indicates that this minimum normal force is 1,735 K. Conservatively assuming that the

friction angle of the soil cement is equal to that of the silty clay/clayey silt, $\phi = 24.9°$. The lower-bound value of the frictional portion of the sliding resistance is calculated as:

$$T_f = N \times \tan \phi = 1{,}735 \text{ K} \times \tan 24.9° = 805 \text{ K}$$

Therefore, the portion of the shear strength attributed to frictional resistance is 805 K / (30' x 64'), or 0.42 ksf, which equals 2.91 psi. The remaining shear strength, which equals 9.5 – 2.9 = 6.6 psi (0.95 ksf), can be easily provided by the cohesion of the soil cement. This also is less than the cohesion of the silty clay/clayey silt layer.

As shown by the calculations presented above, the shear resistance required at the base of the pads will be provided primarily by the bond between the pad foundation and soil-cement contact and the cohesive strength of the soil cement. Shear resistance will be transferred through the approximately 3-ft thick soil-cement layer and into the underlying silty clay/clayey silt subgrade. Additional resistance will be provided by the continuous layer of soil cement under and between the pads; therefore, shear resistance requirements within the silty clay/clayey silt layer will be less with the soil-cement layer compared to the original plan to construct the pads directly on the silty clay/clayey silt without the proposed soil-cement layer.

DeGroot (1976) indicates that this bond strength can be easily obtained between layers of soil cement. He performed nearly 300 laboratory direct shear tests to determine the effect of numerous variables on the bond between layers of soil cement. These variables included the length of time between placement of successive layers of soil cement, the frequency of watering while curing soil cement, the surface moisture condition prior to construction of the next lift, the surface texture prior to construction of the next lift, and various surface treatments and additives

His results demonstrate that, with the exception of treating the surface of the lifts with asphalt emulsion, asphalt cutback, and chlorinated rubber compounds, the bond strength always exceeds this required cohesion value. The minimum bond strength he reports, other than for the asphalt and chlorinated rubber surface treatments identified above, is 8.7 psi. This value applied for two tests that were performed on samples that had time delays of 24 hours and did not have a cement surface treatment along the lift line. He reports that nearly all of the specimens that used a cement surface treatment broke along planes other than along the lift lines, indicating that the bond between the layers of soil cement was stronger than the remainder of the specimens. Excluding the specimens that had 24-hr delays between lift placements and which did not use the cement surface treatment, the minimum bond strength was 10.7 psi and there were only two others that had bond strengths that were less than 20 psi. Even these minimum values for the group of specimens that did not use a cement surface treatment exceed the required cohesive strength, and all of the rest were much greater, generally more than an order of magnitude greater than the 6.6 psi required to obtain an adequate factor of safety against sliding.

DeGroot reached the following conclusions:

1. Increasing the time delay between lifts decreases bond.
2. High frequency of watering the lift line decreases the bond.
3. Moist curing conditions between lift placements increases the bond.
4. Removing the smooth compaction plane increases the bond.
5. Set retardants decreased the bond at 4-hr time delay.
6. Asphalt and chlorinated rubber curing compounds decreased the bond.
7. Small amounts of cement placed on the lift line bonded the layers together.

DeGroot (1976) noted that increasing the time delay between placement of subsequent lifts decreases the bond strength. The nature of construction of soil cement is such that

there will be occasions when the time delay will be greater than the time required for the soil cement to set. This will clearly be the case for construction of the concrete storage pads on top of the soil-cement surface, because it will take some period of time to form the pad, build the steel reinforcement, and pour the concrete. He noted that several techniques can be used to enhance the bond between these lifts to overcome this decrease in bond due to time delay. In these cases, more than sufficient bond can be obtained between layers of soil cement and between the set soil-cement surface and the underside of the cask storage pads by simply using a cement surface treatment.

DeGroot's direct shear test results demonstrate that the specimens having a cement surface treatment all had bond strengths that ranged from 47.7 psi to 198.5 psi, with the average bond strength of 132.5 psi. Even the minimum value of this range is nearly an order of magnitude greater than the cohesion required to obtain a factor of safety against sliding of 1.1. Therefore, when required, due to unavoidable time delays, the techniques DeGroot describes for enhancing bond strength will be used between the top of the soil cement and succeeding lifts or the concrete cask storage pads, to assure that the bond at the interfaces are greater than the minimum required value. These techniques will include roughening and cleaning the surface of the underlying soil cement, proper moisture conditioning, and using a cement surface treatment.

PFS has discussed the change to use of soil cement beneath the storage pads with the project consultants who have analyses in-place that are based on the storage pads resting on the silty clay/clayey silt. The consultants contacted were Geomatrix (development of seismic criteria and soil dynamic properties), Holtec International (cask stability analysis), and International Civil engineering Consultants (pad design). Each has indicated their analyses would not be adversely affected by this proposed change.

The design, placement, testing, and performance of soil cement is a well-established technology. The "State-of-the-Art Report on Soil Cement" (ACI, 1998) provides information about soil cement, including applications, materials, properties, mix proportioning, design, construction, and quality-control inspection and testing techniques. PFS will develop site-specific procedures to implement the recommendations presented in ACI (1998) regarding mix proportioning, testing, construction, and quality control. The following describes the processes that will be used to develop a proper soil-cement mix design and establish adequate sliding resistance at each material interface in the storage pad and soil system:

- Soil-Cement Mix and Procedure Development – The sliding forces due to the design basis ground motion will be resisted primarily by bond between the foundation and soil cement. The soil-cement mix will be designed and constructed to exceed the minimum shear resistance requirements. During the soil-cement design phase, direct shear testing will be conducted along manufactured soil-cement lift contacts and concrete contacts that represent anticipated field conditions. The direct shear testing, along with other standard soil-cement testing, will be used to confirm that adequate shear resistance and other strength requirements will be provided by the final soil-cement mix design. Procedures required for placement and treatment of the soil cement, lift surfaces, and foundation contact will be established in accordance with the recommendations of ACI (1998) during the mix design and testing process. Specific construction techniques and field quality control requirements will be identified in the construction specifications developed by PFS during this detailed design phase of the project.

- Soil-Cement Lift and Concrete Interface – The soil cement will be constructed in lifts approximately 6-in thick (compacted thickness) as described in ACI (1998). Construction techniques will be used to ensure that the interface between the soil-

cement layers will be adequately bonded to transmit shear stresses. Techniques described in Section 6.2.2.5 of ACI (1998) will include, but will not be limited to: minimizing the time between placement of successive layers of soil cement, moisture conditioning required for proper curing of the soil cement, producing a roughened surface on the soil cement prior to placement of additional lifts or concrete foundations, and using a dry cement or cement slurry to enhance the bonding of concrete or new soil cement layers to underlying layers that have already set. In addition to conventional quality control testing performed for soil-cement projects, direct shear testing will be performed on representative samples obtained from placed lift contacts to confirm design requirements are obtained. Sacrificial soil-cement lifts may be used to protect the soil-cement subgrade in the pad foundation areas.

- Soil Cement and *In Situ* Clay Interface – The soil cement and *in situ* clay interface will be constructed such that a good bond will be established between the two materials. Construction techniques will be utilized that will ensure that the integrity of the upper surface of the clay is maintained and that a good interface bond between the two materials is obtained. Specific construction techniques and field quality control requirements will be identified in the construction specifications developed by PFS during the detailed design phase of the project.

An additional benefit of incorporating the soil cement into the design is that it will minimize the environmental impacts of constructing the facility. Using on-site materials to construct the soil cement, rather than excavating and spoiling those materials, will reduce environmental impacts of the project. In addition, replacement of some of the structural fill layer between the rows of pads with soil cement, as shown in SAR Figure 4.2-7, will result in reduced trucking requirements associated with transporting those materials to the site.

2.6.4.12 Criteria and Design Methods

The allowable bearing capacity of footings is limited by shear failure of the underlying soil and by footing settlement. The minimum factor of safety against a bearing capacity failure from static loads (dead load plus maximum live loads) is 3.0 and from static loads plus loads due to extreme environmental conditions, such as design basis ground motion, is 1.1. Allowable settlements are determined based on Table 14.1, "Allowable Settlement," of Lambe & Whitman (1969) and assume that the differential settlement will be 3/4 of the maximum settlement. Section 2.6.1.12 provides more details.

In order to comply with the requirements of NUREG-75/087, Section 3.8.5, "Foundations," Section II.5, "Structural Acceptance Criteria," the recommended minimum factor of safety against overturning or sliding failure from static loads (dead load plus maximum live loads) is 1.5 and from static loads plus loads due to extreme environmental conditions, such as design basis ground motion, is 1.1. Where the factor of safety against sliding is less than 1 due to the design basis ground motion, the displacements the structure may experience are calculated using the method proposed by Newmark (1965) for estimating displacements of dams and embankments during earthquakes. The magnitude of these displacements are evaluated to assess the impact on the performance of the structure. See Section 2.6.1.12 for details about these analyses.

2.6.5 Slope Stability

There are no slopes close enough to the proposed important to safety facilities that their failure could adversely affect the operation of these facilities.

THIS PAGE INTENTIONALLY LEFT BLANK

2.8 REFERENCES

ACI, 1998, "State-of-the Art Report on Soil Cement," reported by ACI Committee 230, ACI 230-1R-90 (Reapproved 1997), American Concrete Institute, Detroit, MI.

American National Standards Institute, 1982, American national standard minimum design loads for buildings and other structures: ANSI A58.1-1982, published by the American National Standards Institute, Inc., New York, New York.

Anderson, J.G., Wesnousky, S.G., and Stirling, M.W., 1996, Earthquake size as a function of fault slip rate: Bulletin of the Seismological Society of America, v. 86, No. 3, p. 683-690.

Anderson, R.E., 1989, Tectonic evolution of the Intermontane system; Basin and Range, Colorado Plateau, and High Lava Plains, in Pakiser, L.C., and Mooney, W.D., eds., Geophysical framework of the continental United States: Geological Society of America Memoir 172, pp. 163-176.

Arabasz, W.J., Pechmann, J.C., and Brown, E.D., 1987, Evaluation of seismicity relevant to the proposed siting of a Superconducting Supercollider (SSC) in Tooele County, Utah: Technical report for the Dames and Moore Utah SSC Proposal Team, June 1987, 107 pp.

Arabasz, W.J., Pechmann, J.C., and Brown, E.D., 1992, Observational seismology and the evaluation of earthquake hazards and risk in the Wasatch Front area, Utah, in Gori, P.L., and Hays, W.W., eds., Assessment of regional earthquake hazards and risk along the Wasatch Front, Utah: U.S. Geological Survey Professional Paper 1500-A-J, pp. D1-D36.

Arabasz, W.J., Smith, R.B., and Richins, W.D., 1980, Earthquake studies along the Wasatch Front, Utah: Network monitoring, seismicity, and seismic hazards: Bulletin of Seismological Society of America, vol. 70, pp. 1479-1499.

Ashcroft, G.L., D.T. Jensen and J. L. Brown, 1992, Utah climate: Logan, UT, Utah Climate Center, Utah State University, 127 p.

Atwood, G., and Mabey, D.R., 1995, Flooding hazards associated with Great Salt Lake, in Lund, W.R., ed., Environmental and engineering geology of the Wasatch Front Region: Utah Geological Assoc. Pub. 24, pp. 483-493.

Baer, J.L. and Bensen, A.K., 1987, Results of gravity survey, Skull Valley - Ripple Valley, Tooele County, Utah, in Dames and Moore, The Ralph M. Parsons Company, and Roger Foott Associates, Inc. (preparers), Site Proposal for the Superconducting Super Collider, Geotechnical Report, v. 2, pages E1-E8.

Balmer, G.G., 1958, "Shear Strength and Elastic Properties of Soil-cement Mixtures Under Triaxial Loading", Portland Cement Association, Bulletin No. D 32.

Barnhard, T.P. and Dodge, R.L., 1988, Map of fault scarps formed on unconsolidated sediments, Tooele 1° x 2° quadrangle, northwestern Utah: U.S. Geological Survey Miscellaneous Field Studies Map MF-1990, scale 1:250,000.

Bay Geophysical Associates, Inc., 1999, High-resolution seismic shear-wave reflection profiling for the identification of faults at the Private Fuel Storage Facility, Skull Valley, Utah-final report, prepared for Stone and Webster Engineering Corp., Denver, CO, 16 pp.

BLM, 1985, Skull Valley Allotment Management Plan. Salt Lake District, BLM, US Department of the Interior, Salt Lake City, UT. August, 1985.

BLM, 1986, South Skull Valley Allotment Management Plan. Salt Lake District, BLM, US Department of the Interior, Salt Lake City, UT. January, 1986.

BLM, 1988, Bureau of Land Management, Draft Pony Express Resource Management Plan and Environmental Impact Statement. Salt Lake District, BLM, US Department of the Interior, Salt Lake City, UT. May 1988.

BLM, 1992, Horseshoe Springs Habitat Management Plan. UT-020-WHA-T-7. Salt Lake District, BLM, US Department of the Interior, Salt Lake City, UT. February 26, 1992

Casagrande, A. and W.L. Shannon, 1948. Strength of Soils under Dynamic Loads. Proceedings, ASCE, Vol. 74, No.4, April, pp. 591-608.

Christie-Blick, N., 1983, Structural geology of the southern Sheeprock Mountains, Utah: regional significance, in Miller, D.M., Todd, V.R., and Howard, K.A., editors, Tectonic and stratigraphic studies in the eastern Great Basin: Geological Society of America Memoir 157, pp. 101-124.

Coffman, J.L. and von Hake, C.A., 1973, Earthquake history of the United States, revised edition (through 1970): U.S. Dept. of Commerce - NOAA Publication 41-1, 208 pp.

ConeTec, 1998, "Cone Penetration Testing - Geotechnical Applications Guide", October, 1998.

ConeTec, 1999, Cone penetration testing report, Private Fuel Storage Facility, prepared for Stone and Webster Engineering Corp., Denver, CO, 2 volumes.

Cook, K.L., Bankey, V., Mabey, D.R., and DePangher, M., 1989, Complete Bougher gravity anomaly map of Utah: Utah Geological and Mineral Survey Map 122, scale 1:500,000.

Currey, D.R., 1990, Quaternary paleolakes in the evolution of semi-desert basins, with special emphasis on Lake Bonneville and the Great Basin, U.S.A.: Paleogeography, Paleoclimatology, and Paleoecology, vol. 76, pp. 189-214.

Davis, P.R., et al., 1998, Accident Analysis for Continued Storage, Oct. 1998, cited in Department of Energy, Draft Environmental Impact Statement for a Geologic Repository for the Disposal of Spent Nuclear Fuel and High-Level Radioactive Waste at Yucca Mountain, Nye County, Nevada, July 1999, p. 7-31.

DeGroot, G., 1976, "Bonding Study on Layered Soil Cement", REC-ERC-76-16, U.S. Bureau of Reclamation, Denver, CO, September 1976.

Department of Energy (DOE), 1996, DOE Standard, Accident Analysis for Aircraft Crash into Hazardous Facilities, DOE-STD-3014-96, Oct. 1996, Appendix B.

dePolo, C.M., 1994, The maximum background earthquake for the Basin and Range Province, western North America: Bulletin of the Seismological Society of America, v. 84, pp. 466-472.

dePolo, C.M., Clark, D.G., Slemmons, D.B., and Aymard, W.G., 1989, Historical Basin and Range Province surface faulting and fault segmentation, in Schwartz, D.P., and Sibson, R.H., editors, Fault segmentation and controls of rupture initiation and termination--proceedings of conference XLV: U.S. Geological Survey Open-file Report 89-315, pp. 131-162.

Dupas, J., and Pecker, A., 1979, "Static and Dynamic Properties of Sand-Cement," *Proceedings ASCE*, JGED, Vol. 105, GT 3, March 1979, pp 419-436.

Everitt, B.L. and Kaliser, B.N., 1980, Geology for assessment of seismic risk in the Tooele and Rush Valleys, Tooele County, Utah: Utah Geological and Mineral Survey Special Study 51, 33 pp.

Federal Aviation Administration, Office of Aviation Policy and Plans (FAA), 1999, FAA Long-Range Forecasts, Fiscal Years 2015, 2020 and 2025, FAA-APO-99-5, June 1999.

Federal Highway Administration (FHWA), 1977, Runoff Estimate for Small Rural Watersheds and Development of a Sound Design Method, 248 pp.

Felt, E.J. and Abrams, M.S., 1957, "Strength and Elastic Properties of Compacted Soil-Cement Mixtures, Portland Cement Association, Bulletin No. D 16.

Everitt, B.L. and Kaliser, B.N., 1980, Geology for assessment of seismic risk in the Tooele and Rush Valleys, Tooele County, Utah: Utah Geological and Mineral Survey Special Study 51, 33 pp.

Geomatrix Consultants, Inc, 1997, PFSF Calculation 05996.01-G(PO5)-1, "Development of Soil and Foundation Parameters in Support of Dynamic Soil-Structure Interaction Analyses," San Francisco, CA, March (73 pp).

Geomatrix Consultants, Inc., 1999a, Fault evaluation study and seismic hazard assessment study-final report, prepared for Stone and Webster Engineering Corp., Denver, CO, 3 volumes.

Geomatrix Consultants, Inc., 1999b, Development of design ground motions for the Private Fuel Storage Facility, prepared for Stone and Webster Engineering Corp., Denver, CO, 19 pp.

Geomatrix Consultants, Inc., 1999c, PFSF Calculation 05996.02-G(PO18)-2, Rev 0, Soil and Foundation Parameters for Dynamic Soil-Structure Interaction Analyses, 2,000-Year Return Period Design Ground Motions, prepared for Stone and Webster Engineering Corp., Denver, CO, 53 pp.

Geomatrix Consultants, Inc., 1999d, PFSF Calculation 05996.02-G(PO18)-1, Rev 1, Soil and Foundation Parameters for Dynamic Soil-Structure Interaction Analyses, prepared for Stone and Webster Engineering Corp., Denver, CO, 125 pp.

Gibbs, H. J., and W. G. Holtz, 1957, "Research on Determining the Density of Sands by Spoon Penetration Testing," *Proceedings of the 4th International Conference on Soil Mechanics and Foundation Engineering* (London), Vol I, 35-39.

Gilbert, G.K., 1890, Lake Bonneville, U.S. Geological Survey Monograph 1, 428 pp.

Goter, S.K., compiler, 1990, Earthquakes in Utah, 1884-1989: U.S. Geological Survey, National Earthquake Information Center, scale 1:500,000.

Grazulis, Thomas P., 1993, Significant tornadoes 1680 - 1991: Published by The Tornado Project of Environmental Films, St. Johnsbury, Vermont.

Hecker, Suzanne, 1993, Quaternary tectonics of Utah with emphasis on earthquake-hazard characterization: Utah Geological Survey Bulletin 127, Salt Lake City, UT, 156 pp.

Helm, J.M., 1994, Structure and tectonic geomorphology of the Stansbury fault zone, Tooele County, Utah, and the effect of crustal structure on Cenozoic faulting patterns, M.S. thesis, Univ. of Utah, Salt Lake City, Utah, 128 pp.

Helm, J.M., 1995, Quaternary faulting in the Stansbury fault zone, Tooele County, Utah, in Lund, W.R., editor, Environmental and engineering geology of the Wasatch Front Region: Utah Geological Association Publication 24, pp. 31-44.

Hintze, L.H. (compiler), 1980, Geologic Map of Utah, Utah Geological and Mineral Survey, Salt Lake City, UT, scale 1:500,000.

Holzworth, G.C., 1972, Mixing heights, wind speeds, and potential for urban air pollution throughout the contiguous United States: Environmental Protection Agency, Office of Air Programs, Research Triangle Park, North Carolina.

Holzworth, G.C., 1974, Meteorological episodes of slowest dilution in contiguous United States: National Environmental Research Center, Research Triangle Park, North Carolina, Report No. EPA-650/4-74-002.

Hood,J.W., and Waddell,K.M., 1968, Hydrologic reconnaissance of Skull Valley, Tooele County, Utah, DNR Tech Pub. No. 18, 57 pp.

Hosler, Charles R., 1961, Low-level inversion frequency in the contiguous United States: Monthly Weather Review, pp. 319-339.

Howard, K.A. editors, Tectonic and stratigraphic studies in the eastern Great Basin: Geological Society of America Memoir 157, pp. 61-73.

Huschke, R. E., ed., 1959, Glossary of meteorology: Published by the American Meteorological Society, Boston, Massachusetts.

Johnson, J.B., and Cook, K.L., 1957, Regional gravity survey of parts of Tooele, Juab, and Millard Counties, Utah: Geophysics, vol. 22, pp. 48-61.

Lambe, T.W., and R.V. Whitman, 1969, Soil Mechanics, John Wiley & Sons, Inc., N.Y., 553 pp.

Lund, W.R., Christenson, G.E., Harty, K.M., Hecker, S., Atwood, G., Case, W.F., Gill, H.E., Gwynn, J.W., Klauk, R.H., Mabey, D.R., Mulvey, W.E., Sprinkel, D.A., Tripp, B.T., Black, W.D., and Nelson, C.V., 1990, Geology of Salt Lake City, Utah, U.S.A.: Assoc. of Engineering Geologists Bull., vol. XXVII, pp. 391-478.

Lunne, T., Robertson, P. K., and Powell, J. J. M., (1997), Cone Penetration Testing in Geotechnical Practice, Blackie Academeic & Professional, London, 1997.

Machette, M.N., and Scott, W.E., 1988, Field trip introduction-A brief review of research on lake cycles and neotectonics of the eastern Basin and Range province: Utah Geological and Mineral Survey Misc. Publ. 88-1, p. 7-14.

Malde, H.E., 1968, The catastrophic late Pleistocene Bonneville flood in the Snake River plain, Idaho: U.S. Geological Survey Professional Paper 596, 52 pp.

Moore, W.J., and McKee, E.H., 1983, Phanerozoic magmatism and mineralization in the Tooele 1° x 2° quadrangle, Utah, in Miller, D.M., Todd, V.R., and Howard, K.A., eds., Tectonic and stratigraphic studies in the eastern Great Basin: Geological Society of America Memoir 157, pp. 183-190.

Moore, W.J., and Sorensen, M.L., 1979, Geologic map of the Tooele 1° x 2° quadrangle: U.S. Geological Survey Miscellaneous Investigations Series Map I-1132, scale 1:250,000.

National Oceanic and Atmospheric Administration, National Environmental Satellite, Data, and Information Service, National Climatic Data Center, 1960, Climatography of the United States No. 60, Climate of Utah.

National Oceanic and Atmospheric Administration, National Environmental Satellite, Data, and Information Service, National Climatic Data Center, 1992, Local climatological data, annual summary with comparative data for 1991: Salt Lake City, Utah.

National Oceanic and Atmospheric Administration, National Environmental Satellite, Data, and Information Service, National Climatic Data Center, 1975-1995, Storm data and unusual weather phenomena with late reports and corrections.

Newmark, N. M., 1965, Effects of earthquakes on dams and embankments, Fifth Rankine Lecture, Geotechnique, Institution of Civil Engineers, London, 15(2), pp139-60.

Newmark, N. M., and Rosenblueth, E., 1971, Fundamentals of Earthquake Engineering, Prentice-Hall, Englewood Cliffs, NJ.

Nussbaum, P. J., and Colley, B. E., 1971, *Dam Construction and Facing with Soil-Cement*, Portland Cement Association Publication RD010.01W.

Oaks, S.D., 1987, Effects of six damaging earthquakes in Salt Lake City, Utah, in Gori. P.L., and Hays, W.W., editors, Assessment of regional earthquake hazards and risk along the Wasatch Front, Utah: U.S. Geological Survey Open-file Report 87-585, vol. 2, pp. P-1-95.

Oviatt, C.G., Currey, D.R., and Miller, D.M., 1990, Age and paleoclimatic significance of the Stansbury shoreline of Lake Bonneville, northwestern Great Basin: Quaternary Research, vol. 33, pp. 291-305.

Pacific Gas and Electric Company, 1988, Final Report of the Diablo Canyon Long Term Seismic Program, Docket Nos. 50-275 and 50-323, July 31, 1988.

Pasquill, F., 1961, The estimation of the dispersion of windborne material: Meteorol. Mag., 90, 1063, 33-49.

Pechmann, J.C. and Arabasz, W.J., 1995, The problem of the random earthquake in seismic hazard analysis: Wasatch Front region, Utah, in Lund, W.R., editor, Environmental and engineering geology of the Wasatch Front region: Utah Geological Association Publication 24, pp. 77-93.

PFS Letter, Parkyn to Delligatti (NRC), Request for Exemption to 10 CFR 72.102(f)(1), dated April 2, 1999.

PFS Letter, Parkyn to U.S. NRC Document Control Desk, Request for Exemption to 10 CFR 72.102(f)(1), dated August 24, 1999.

PFS Nov. 1999, "Report to Nuclear Regulatory Commission, Aircraft Crash Impact Hazard at the Private Fuel Storage Facility," Nov. 24, 1999.

Pyke, R., H. B. Seed, and C. K. Chan, 1975, "Settlement of Sands Under Multidirectional Shaking," *Journal of the Geotechnical Engineering Division*, ASCE, 101(4), 379-398.

Ramsdell, J. V. and G. L. Andrews, 1986, Tornado climatology of the contiguous United States: Prepared by Pacific Northwest Laboratory for the U.S. Nuclear Regulatory Commission, NUREG/CR-4461, PNL-5697.

Rigby, J.K., 1958, Geology of the Stansbury Mountains, Tooele County, Utah: Utah Geological Society Guidebook 13, 168 pp.

Roberts, R.J., Crittenden, M.D., Jr., Tooker, E.W., Morris, H.T., Hose, R.K., and Cheney, T.M., 1965, Pennsylvanian and Permian basins in northwestern Utah, northeastern Nevada and south-central Idaho: Amer. Assoc. Petrol. Geologists Bulletin, vol. 49, pp. 1926-1956.

Robertson, P. K., and Campanella, R. G., 1988, Guidelines for Use, Interpretations, and Application of the Cone Penetration and Piezocone Penetration Test, *Soil Mechanics Series No. 105*, Department of Civil Engineering, University of British Columbia, Vancouver, Canada.

Sack, Dorothy, 1993, Quaternary geologic map of Skull Valley, Tooele County, Utah: Utah Geological Survey Map 150, Scale 1:100,000, 16 p.

Sbar, M.L., and Barazangi, M., 1970, Tectonics of the intermountain seismic belt, western United States, Part I, microearthquake seismicity and composite fault plane solutions: Geological Society of America Abst. with Programs, vol. 2, p. 675.

Schimming, B.B., H.J. Haas, and H.C. Saxe, 1966. Study and Dynamic and Static Envelopes. Journal of Soil Mechanics and Foundation Division, ASCE Vol. 92, No. SM2 (March), pp. 105-24.

Schmertmann, J. H., 1970, "Static cone to compute static settlement over sand," Journal of the Soil Mechanics and Foundations Division, ASCE, 96(SM3), 1011-43.

Schmertmann, J. H., 1978, "Guidelines for cone penetration test, performance and design," US Federal Highway Administration, Washington, D.C., Report FHWA TS-78-209, 145.

Scott, W.E., 1988, Temporal relations of lacustrine and glacial events at Little Cottonwood Canyon and Bells Canyon, Utah, in Machette, M.N. and Currey, D.E., editors: In the footsteps of G.K. Gilbert - Lake Bonneville and neotectonics of the eastern Basin and Range Province, guidebook for field trip twelve, Utah Geological and Mineral Survey Misc. Publ. 88-1, pp. 78-82.

Seed, H. B., and Whitman, R. V., 1970, "Design of Earth Retaining Structures for Dynamic Loads," ASCE Specialty Conference on Lateral Stresses in the Ground and the Design of Earth Retaining Structures, pp 103-147.

Silver, M. and Seed, H. B., 1971, "Volume Changes in Sands During Cyclic Loading," Proceedings of the American Society of Civil Engineers, Journal of the Soil Mechanics and Foundations Division, Vol 97, SM9, September.

Simiu, E., M. J. Changery, and J. J. Filliben, 1979, Extreme wind speeds at 129 stations in the contiguous United States, NBS building science series 118: U.S. Department of Commerce, National Bureau of Standards.

Slemmons, D.B., 1980, Design earthquake magnitudes for the western Great Basin, in Proc. of Conference X, Earthquake hazards along the Wasatch-Sierra Nevada frontal fault zones: U.S. Geological Survey Open-file Report 80-801, pp. 62-85.

Smith, R.B., 1978, Seismicity, crustal structure, and intraplate tectonics of the interior of the western Cordillera, in Smith, R.B., and Eaton, G.P., editors, Cenozoic tectonics and

regional geophysics of the western Cordillera: Geological Society of America Memoir 152, pp. 111-144.

Smith, R.B., and Arabasz, W.J., 1991, Seismicity of the intermountain seismic belt, in Slemmons, D.B., Engdahl, E.R., Zoback, M.D., and Blackwell, D.C., eds., Neotectonics of North America: Geological Society of America, Decade Map Volume 1, pp. 185-228.

Smith, R.B., and Sbar, M.L., 1970, Seismicity and tectonics of the intermountain seismic belt, western United States, Part II, Focal mechanism of major earthquakes: Geological Society of America Abst. with Programs, vol. 2, p. 657.

Smith, R.B., and Sbar, M.L., 1974, Contemporary tectonics and seismicity of the western United States with emphasis on the intermountain seismic belt: Geological Society of America Bulletin, vol. 85, pp. 1205-1218.

Smith, R.B., Nagy, W.C., Julander, D.R., Viveiros, J.J., Baker, C.A., and Gants, D.G., 1989, Geophysical and tectonic framework of the eastern Basin and Range-Colorado Plateau-Rocky Mountain transition, in Pakiser, L.C., and Mooney, W.D., eds., Geophysical framework of the continental United States: Geological Society of America Memoir 172, pp. 205-233.

Stewart, J.H., 1976, Late Precambrian evolution of North America: plate tectonic implication: Geology, vol. 4, pp. 11-15.

Stewart, J.H., 1978, Basin-range structure in western North America: A review, in Smith, R.B. and Eaton, G.P., editors, Cenozoic tectonics and regional geophysics of the western Cordillera: Geological Society of America Memoir 152, pp. 1-31.

Stickney, M.C., and Bartholomew, M.J., 1987, Seismicity and late Quaternary faulting of the northern Basin and Range province, Montana and Idaho: Seismological Society of America Bulletin, vol. 77, pp. 1602-1625.

Stokes, W.L., 1986, Geology of Utah, Utah Museum of Natural History and Utah Geological and Mineral Survey, Salt Lake City, UT, 280 pp.

Stone & Webster Engineering Corporation (SWEC), 1995. Evaluation of H-Piles, Waste Packaging Area (WPA), and Condensate Demineralizer Waste Evaporator Building (CDWEB), Sequoyah Nuclear Power Plant – Units 1 and 2 (FSAR issues). Tennessee Valley Authority, SE-CEB-SWEC. Calculation No. SCG1S505, Revision 0 (April).

Stone & Webster Engineering Corporation (SWEC), 1998, Calculation No. 05996.02-G(C)-14, Revision 0, Static Settlement of the Canister Transfer Building Supported on a Mat Foundation.

Stone & Webster Engineering Corporation (SWEC), 1999a, Calculation No. 05996.02-G(B)-12, Revision 1, Flood Analysis with a Larger Drainage Basin.

Stone & Webster Engineering Corporation (SWEC), 1999b, Calculation No. 05996.02-G(B)-15, Revision 0, Determination of Aquifer Permeability from Constant Head Test and Estimation of Radius of Influence for the Proposed Water Well.

Stone & Webster Engineering Corporation (SWEC), 1999c, Calculation No. 05996.02-G(B)-16, Revision 1, Flood Analysis at 3-mile Long Portion of Rail Spur.

Stone & Webster Engineering Corporation (SWEC), 1999d, Calculation No. 05996.02-G(B)-17, Revision 1, PMF Flood Analysis with Proposed Access Road and Rail Road.

Stone & Webster Engineering Corporation (SWEC), 1999e, Calculation No. 05996.02-G(B)-4, Revision 4, Stability Analyses of Storage Pad.

Stone & Webster Engineering Corporation (SWEC), 1999f, Calculation No. 05996.02-G(B)-3, Revision 3, Estimate Static Settlement of Storage Pads.

Stone & Webster Engineering Corporation (SWEC), 1999g, Calculation No. 05996.02-G(B)-13, Revision 1, Stability Analyses of the Canister Transfer Building Supported on a Mat Foundation.

Stone & Webster Engineering Corporation (SWEC), 1999h, Calculation No. 05996.02-SC-5, Revision 1, Seismic Analysis of Canister Transfer Building.

Stover, C.W. and Coffman, J.L., 1993, Seismicity of the United States, 1568-1989 (Revised): U.S. Geological Survey Professional Paper 1527, 418 pp.

Stover, C.W., Reagor, B.G., and Algermissen, S.T., 1986, Seismicity map of the State of Utah, U.S. Geological Survey Miscellaneous Field Studies Map MF-1856, scale 1:1,000,000.

Terzaghi, K, "Evaluation of Coefficients of Subgrade Reaction," Geotechnique, Vol 5, 1955, pp 297-325.

Terzaghi, K., and Peck, R. B., Soil Mechanics in Engineering Practice, John Wiley & Sons, New York, NY, 1967, pp 347 and 491.

Thom, H. C. S., 1963, Tornado probabilities: Monthly Weather Review 91, pp. 730-736.

Tokimatsu, A. M., and H. B. Seed, 1987, "Evaluation of Settlements in Sands Due to Earthquake Shaking," *Journal of the Geotechnical Engineering Division*, ASCE, 113(8), 861-878.

Tooele County Commission, 1995, Brochure entitled "Tooele County, Utah, Where Land And Sky Embrace."

Tooele, 1995. Tooele County General Plan, November 1995.

Tooker, E.W., 1983, Variations in structural style and correlation of thrust plates in the Sevier foreland thrust belt, Great Salt Lake area, Utah, in Miller, D.M., Todd, V.R., and Howard, K.A. editors, Tectonic and stratigraphic studies in the eastern Great Basin: Geological Society of America Memoir 157, pp. 61-73.

Tooker, E.W., and Roberts, R.J., 1971, Structures related to thrust faults in the Stansbury Mountains, Utah: U.S. Geological Survey Professional Paper 750-B, pp. B1-B12.

U.S. Army Corps of Engineers, 1952, Standard Project Flood Determinations, Civil Engineer Bulletin, No. 52-8, Washington, D.C., 19 pp.

U.S. Army Corps of Engineers, 1990, Office of the Chief of Engineers, Flood hydrograph package, HEC-1, Hydrologic Engineering Center, 283 pp.

U.S. Army Corps of Engineers, 1997, Hydrologic Engineering Center, River analysis system, HEC-RAS, Davis, CA.

U.S. Department of Agriculture, undated, Soil survey of Tooele County, Utah, unpublished maps and data, National Resources Conservation Service, Tooele, UT.

U.S. Department of Commerce, National Oceanic and Atmospheric Administration, 1977, Probable maximum precipitation estimates, Colorado River and Great Basin drainage, Hydrometeorological Report No. 49 (HMR 49), 161 pp.

U.S. Geological Survey, 1994, Methods for estimating magnitude and frequency of floods in the southwestern United States, Open-File Report 93-419, 211 pp.

U.S. Nuclear Regulatory Commission, 1991, Safety Evaluation Report related to the operation of Diablo Canyon Nuclear Power Plant Units 1 and 2, NUREG-0675, Supplement No. 34, June 1991.

U.S. Weather Bureau, 1947, Thunderstorm rainfall. Hydrometeorological Report No. 5, Department of Commerce, Washington, D.C., 330 pp.

Vucetic, M., and R. Dobry, 1991, "Effect of Soil Plasticity on Cyclic Response," Journal of the Geotechnical Engineering Division, ASCE, 117(1), 89-107.

Wells, D.L., and Coppersmith, K.J., 1994, Analysis of empirical relationships among magnitude, rupture length, rupture area, and surface displacement: Seismological Society of America Bulletin, vol. 84, pp. 974-1002.

Wong, I., Olig, S., Green, R., Moriwaki, Y., Abrahamson, N., Baures, D., Silva, W., Somerville, P., Davidson, D., Pilz, J., and Dunne, B., 1995, Seismic hazard analysis of the Magna tailings impoundment, in Lund, W.R., ed., Environmental and engineering geology of the Wasatch Front Region: 1995 Symposium and Field Conference, Utah Geological Association Publication 24, pp. 95-110.

Youngs, R.R., Swan, F.H., III, Power, M.S., Schwartz, D.P., and Green, R.K., 1987, Probabilistic analysis of earthquake ground shaking hazard along the Wasatch Front, Utah, in Gori. P.L. and Hays, W.W., editors, Assessment of regional earthquake hazards and risk along the Wasatch Front, Utah: U.S. Geological Survey Open-File Report 87-585, Vol. 2, pp. M-1-110.

Zoback, M.L., 1983, Structure and Cenozoic tectonism along the Wasatch fault zone, in Miller, D.M., Todd, V.R., and Howard, K.A., editors, Tectonic and stratigraphic studies in the eastern Great Basin: Geological Society of America Memoir 157, pp. 3-27.

Zoback, M.L., and Zoback, M.D., 1989, Tectonic stress field of the continental United States, in Pakiser, L.C., and Mooney, W.D., eds., Geophysical framework of the continental United States: Geological Society of America Memoir 172, pp. 523-539.

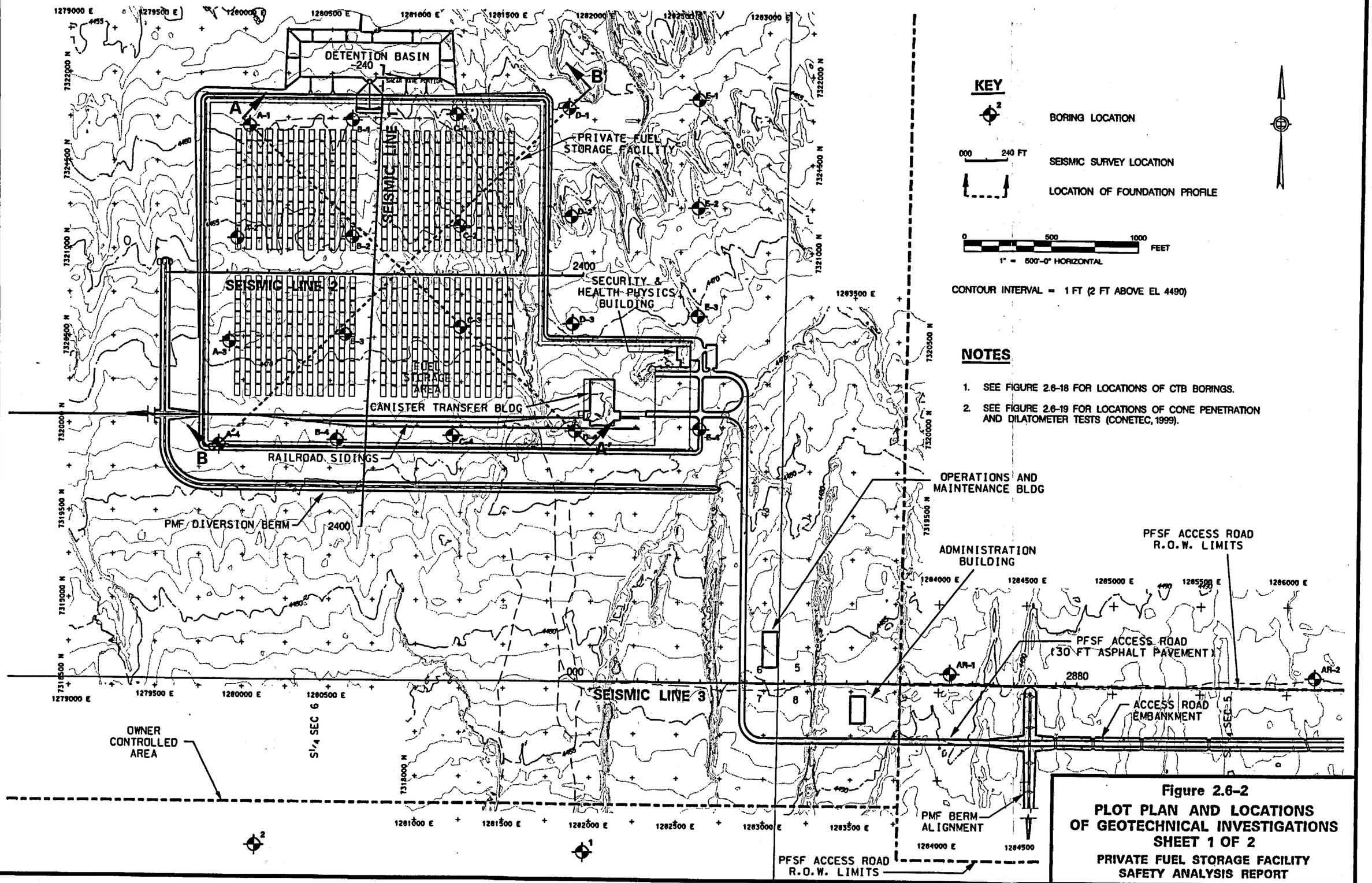

KEY

BORING LOCATION

000 240 FT — SEISMIC SURVEY LOCATION

LOCATION OF FOUNDATION PROFILE

0 500 1000 FEET

1" = 500'-0" HORIZONTAL

CONTOUR INTERVAL = 1 FT (2 FT ABOVE EL 4490)

NOTES

1. SEE FIGURE 2.6-18 FOR LOCATIONS OF CTB BORINGS.
2. SEE FIGURE 2.6-19 FOR LOCATIONS OF CONE PENETRATION AND DILATOMETER TESTS (CONETEC, 1999).

Figure 2.6-2
PLOT PLAN AND LOCATIONS OF GEOTECHNICAL INVESTIGATIONS SHEET 1 OF 2
PRIVATE FUEL STORAGE FACILITY SAFETY ANALYSIS REPORT

g:\05096\gak\b\03\a-3.dgn 08-DEC-1999 16:13

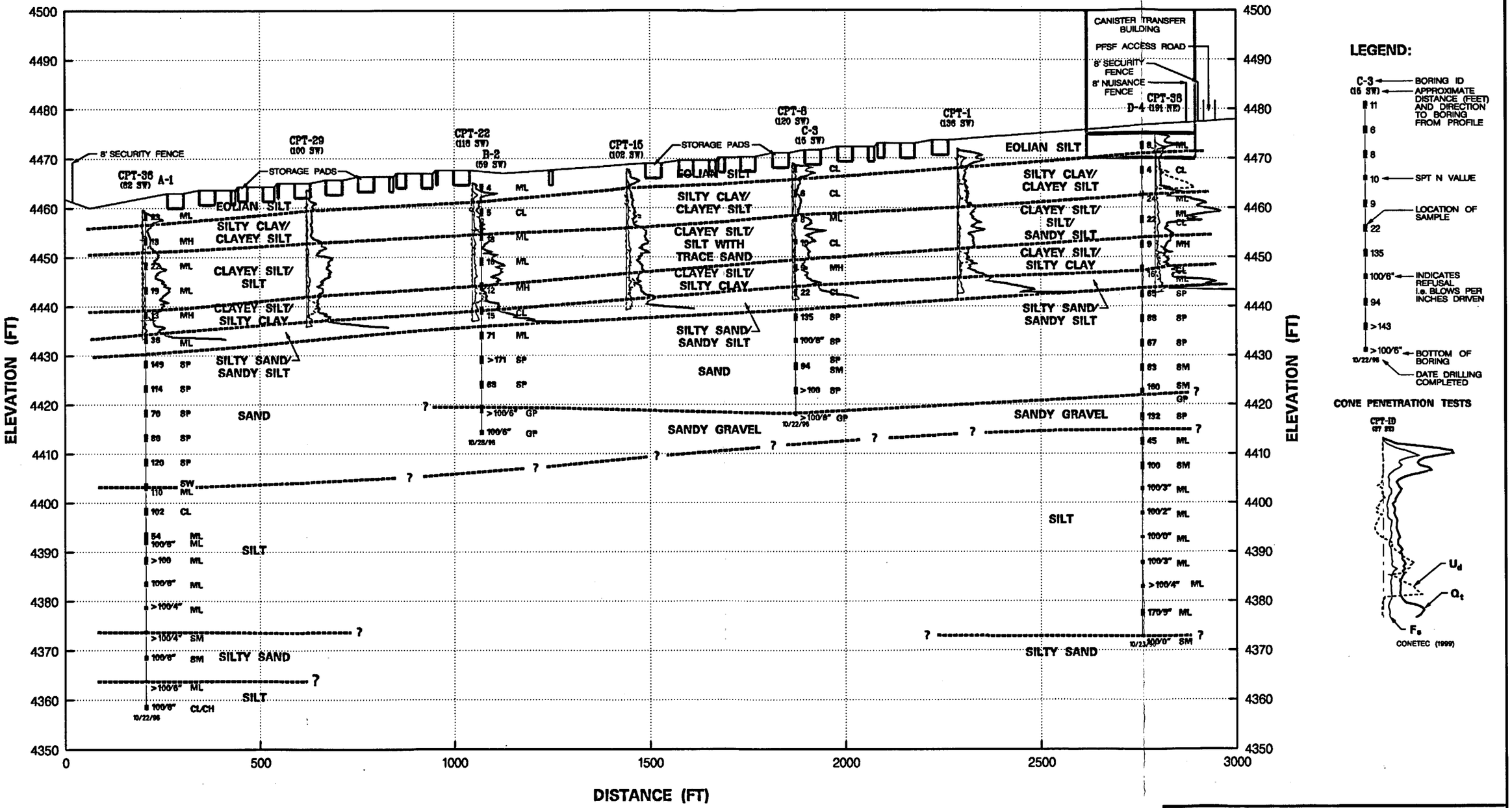

LEGEND:

CONE PENETRATION TESTS

Figure 2.6–5
PAD EMPLACEMENT AREA FOUNDATION PROFILE A–A'
SHEET 1 OF 14
PRIVATE FUEL STORAGE FACILITY SAFETY ANALYSIS REPORT

Revision 8

08-DEC-1999 12:20

g:\05995\gak\b\53\3.dgn

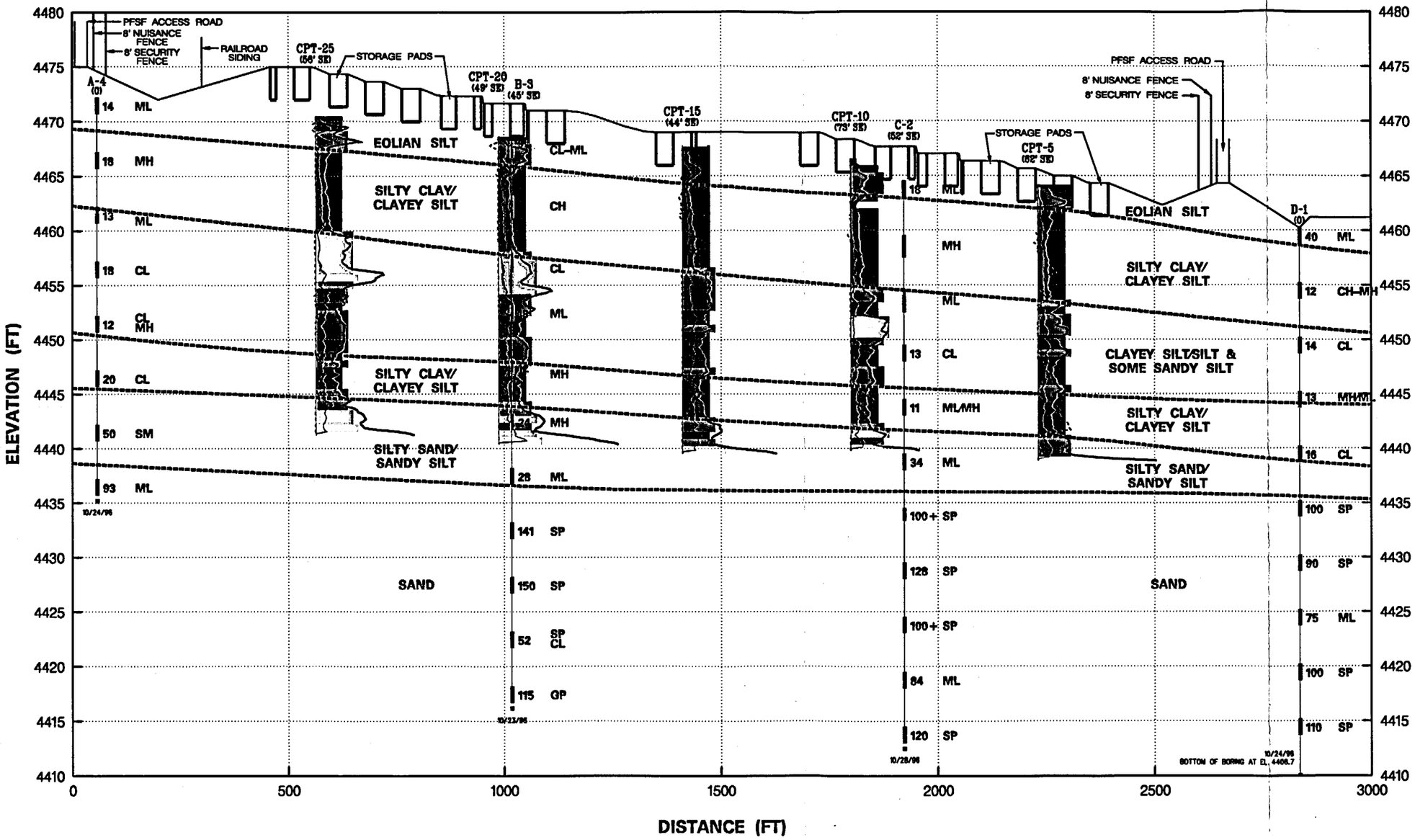

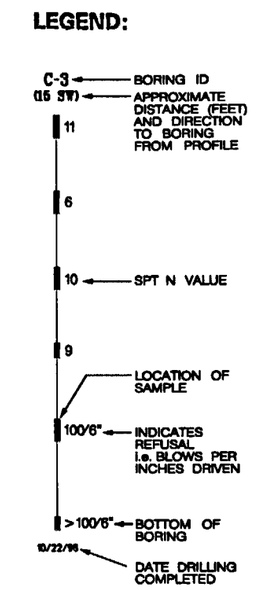

NOTE:
SOIL BEHAVIOR TYPES SHOWN HERE ARE RECALIBRATED AS DISCUSSED IN SECTION 2.6.1.6 OF THE SAR TO MORE ACCURATELY REFLECT SOIL CLASSIFICATIONS DEVELOPED BASED ON THE BORINGS AND LABORATORY TESTS.

HORIZONTAL 0 250 500 FEET
VERTICAL 0 10 20
SCALE IN FEET

Figure 2.6–5
PAD EMPLACEMENT AREA FOUNDATION PROFILE B–B'
SHEET 2 OF 14
PRIVATE FUEL STORAGE FACILITY SAFETY ANALYSIS REPORT

g:\05996\gak\b74\1.dgn 08-DEC-1999 12:20

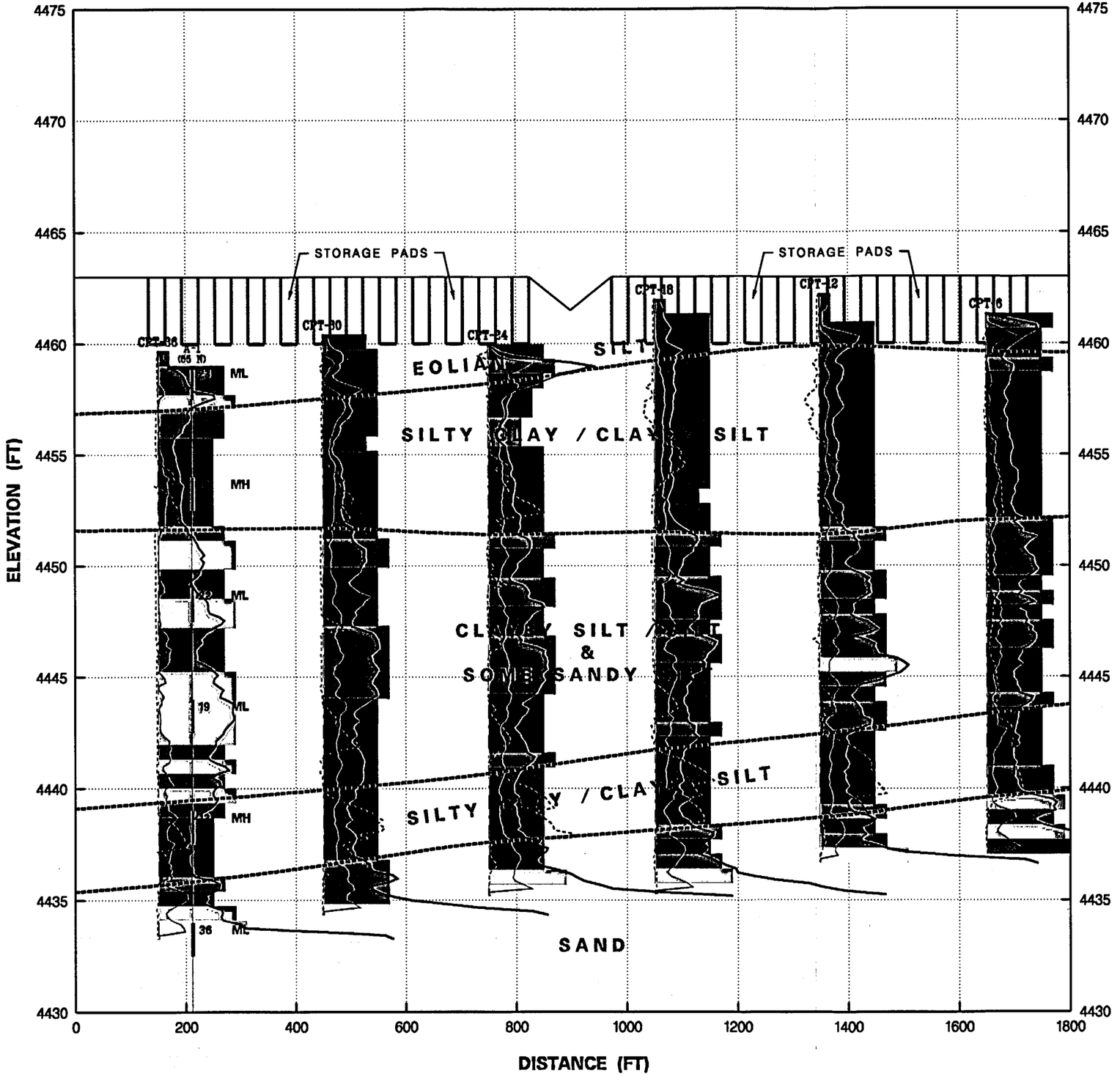

LEGEND:

BORING

B-ID — BORING ID
(25 NW) — APPROXIMATE DISTANCE (FEET) AND DIRECTION TO BORING FROM PROFILE

11
6
8
10 — SPT N VALUE
9 — LOCATION OF SAMPLE
100/6" — INDICATES REFUSAL i.e. BLOWS PER INCHES DRIVEN
94
>143
>100/6"
10/22/96 — BOTTOM OF BORING — DATE DRILLING COMPLETED

CONE PENETRATION TESTS

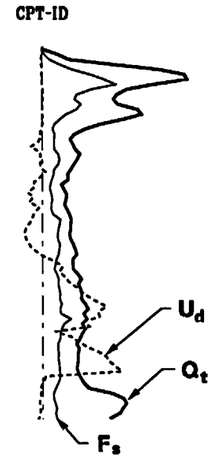

CONETEC (1999)

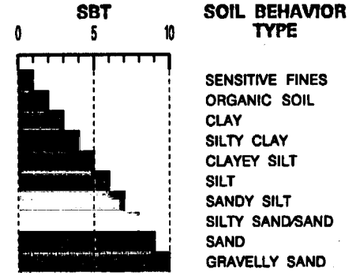

SOIL BEHAVIOR TYPE

SENSITIVE FINES
ORGANIC SOIL
CLAY
SILTY CLAY
CLAYEY SILT
SILT
SANDY SILT
SILTY SAND/SAND
SAND
GRAVELLY SAND

NOTE:

SOIL BEHAVIOR TYPES SHOWN HERE ARE RECALIBRATED AS DISCUSSED IN SECTION 2.6.1.6 OF THE SAR TO MORE ACCURATELY REFLECT SOIL CLASSIFICATIONS DEVELOPED BASED ON THE BORINGS AND LABORATORY TESTS.

HORIZONTAL 0 200 400 FEET
VERTICAL 0 5 10
SCALE IN FEET

Figure 2.6–5
PAD EMPLACEMENT AREA
FOUNDATION PROFILE 1–1'
SHEET 3 OF 14
PRIVATE FUEL STORAGE FACILITY
SAFETY ANALYSIS REPORT

g:\05998\gak\b\40\1.dgn 08-DEC-1999 12:20

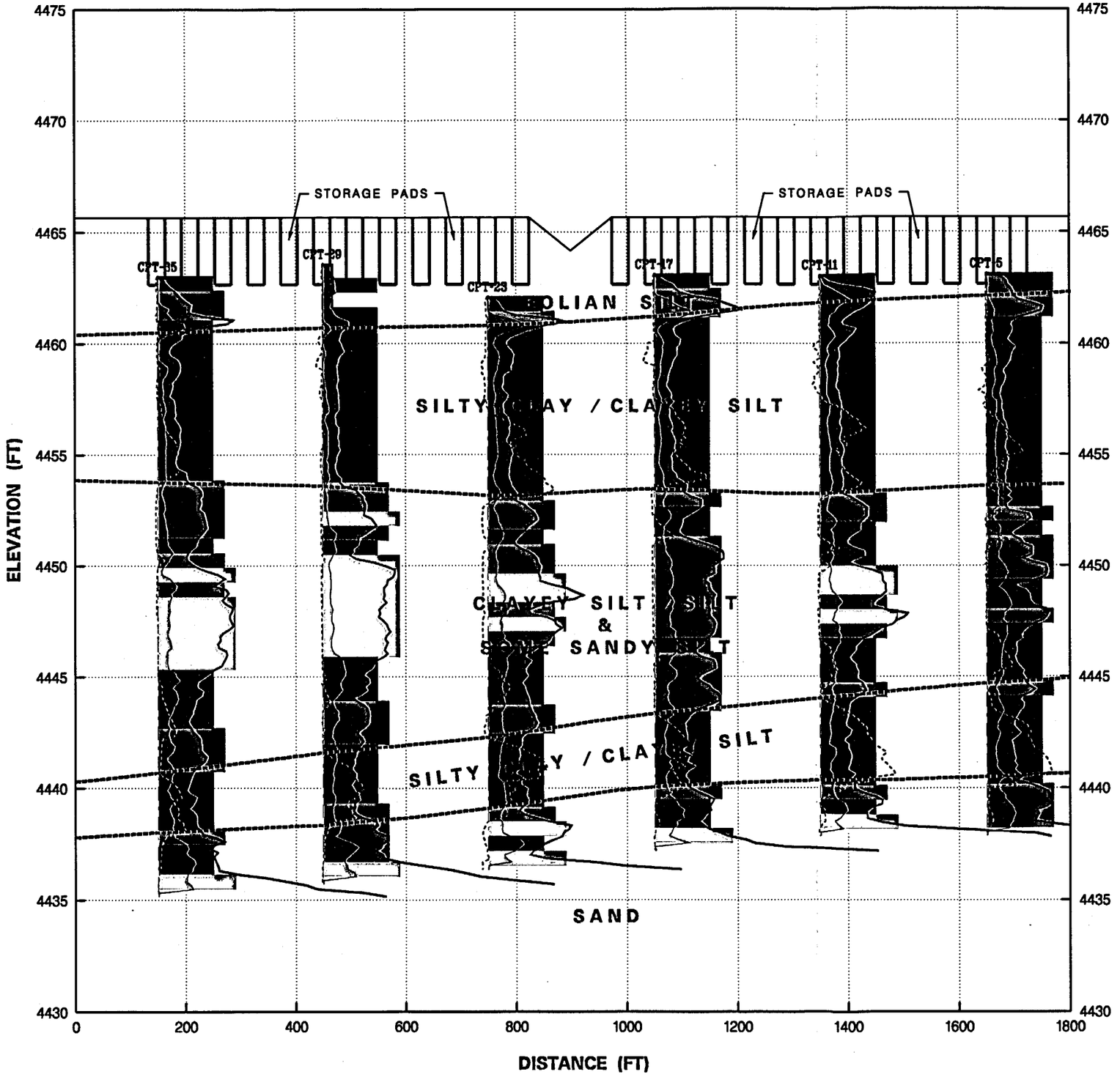

NOTE:

SOIL BEHAVIOR TYPES SHOWN HERE ARE RECALIBRATED AS DISCUSSED IN SECTION 2.6.1.6 OF THE SAR TO MORE ACCURATELY REFLECT SOIL CLASSIFICATIONS DEVELOPED BASED ON THE BORINGS AND LABORATORY TESTS.

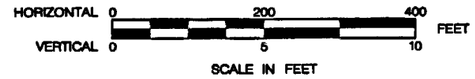

Figure 2.6-5

PAD EMPLACEMENT AREA FOUNDATION PROFILE 2-2'
SHEET 4 OF 14

PRIVATE FUEL STORAGE FACILITY SAFETY ANALYSIS REPORT

g:\05996\gak\b141\1.dgn 08-DEC-1999 12:20

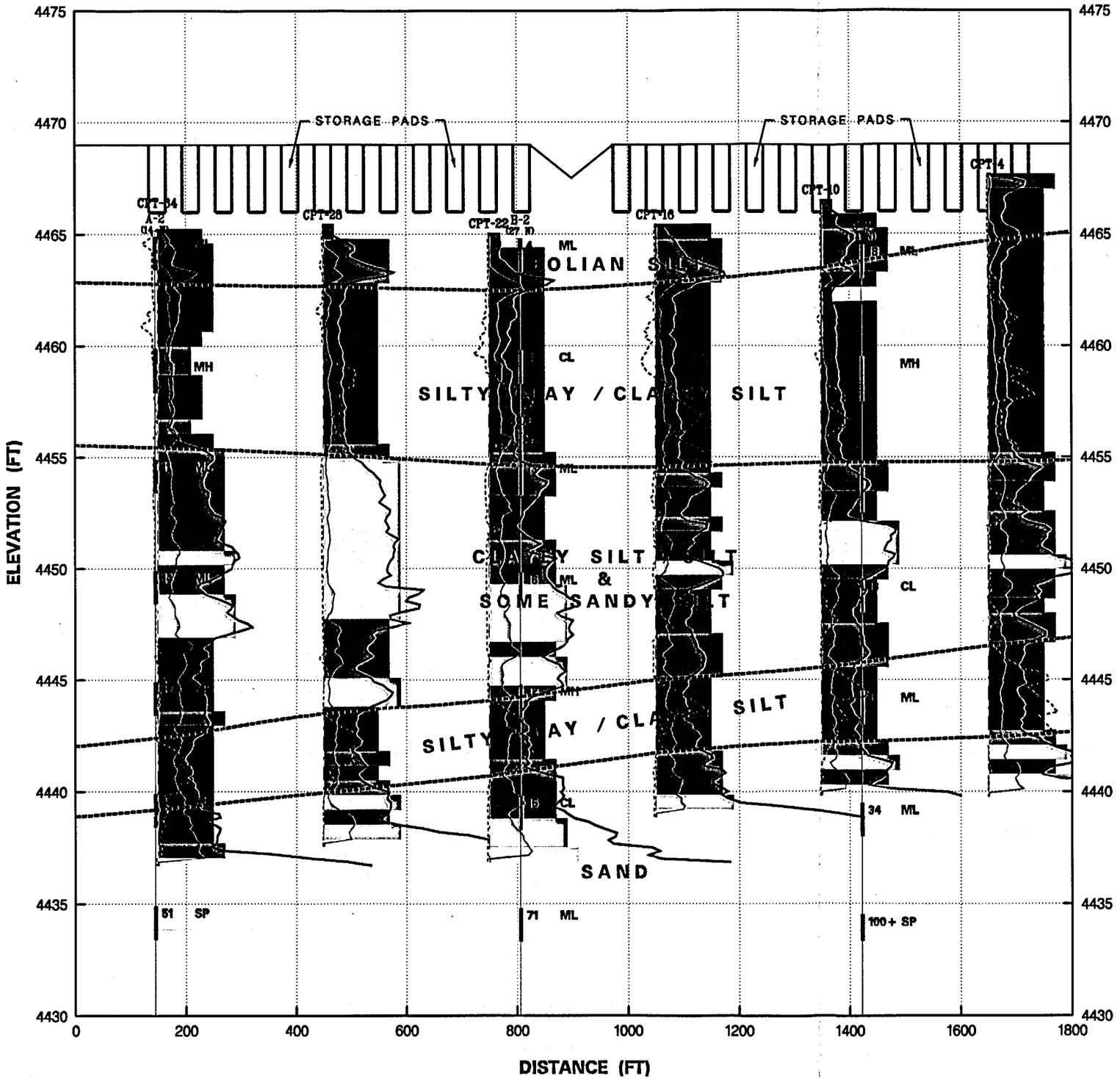

g:\05998\gak\b142\1.dgn 08-DEC-1999 12:20

LEGEND:

BORING

B-ID ← BORING ID
(25 NW) ← APPROXIMATE DISTANCE (FEET) AND DIRECTION TO BORING FROM PROFILE

11
6
8
10 ← SPT N VALUE
9 ← LOCATION OF SAMPLE
100/6" ← INDICATES REFUSAL i.e. BLOWS PER INCHES DRIVEN
94
>143
>100/6"
10/22/98 ← DATE DRILLING COMPLETED
BOTTOM OF BORING

CONE PENETRATION TESTS

CPT-ID

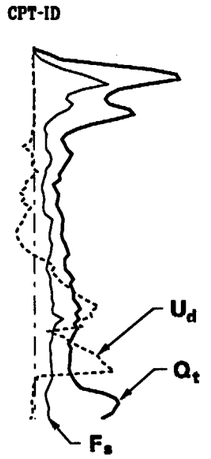

CONETEC (1999)

SBT — **SOIL BEHAVIOR TYPE**

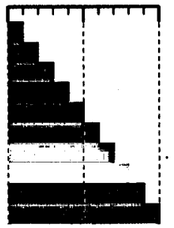

1. SENSITIVE FINES
2. ORGANIC SOIL
3. CLAY
4. SILTY CLAY
5. CLAYEY SILT
6. SILT
7. SANDY SILT
8. SILTY SAND/SAND
9. SAND
10. GRAVELLY SAND

NOTE:

SOIL BEHAVIOR TYPES SHOWN HERE ARE RECALIBRATED AS DISCUSSED IN SECTION 2.6.1.6 OF THE SAR TO MORE ACCURATELY REFLECT SOIL CLASSIFICATIONS DEVELOPED BASED ON THE BORINGS AND LABORATORY TESTS.

HORIZONTAL 0 200 400 FEET
VERTICAL 0 5 10
SCALE IN FEET

Figure 2.6–5
PAD EMPLACEMENT AREA FOUNDATION PROFILE 3–3'
SHEET 5 OF 14
PRIVATE FUEL STORAGE FACILITY SAFETY ANALYSIS REPORT

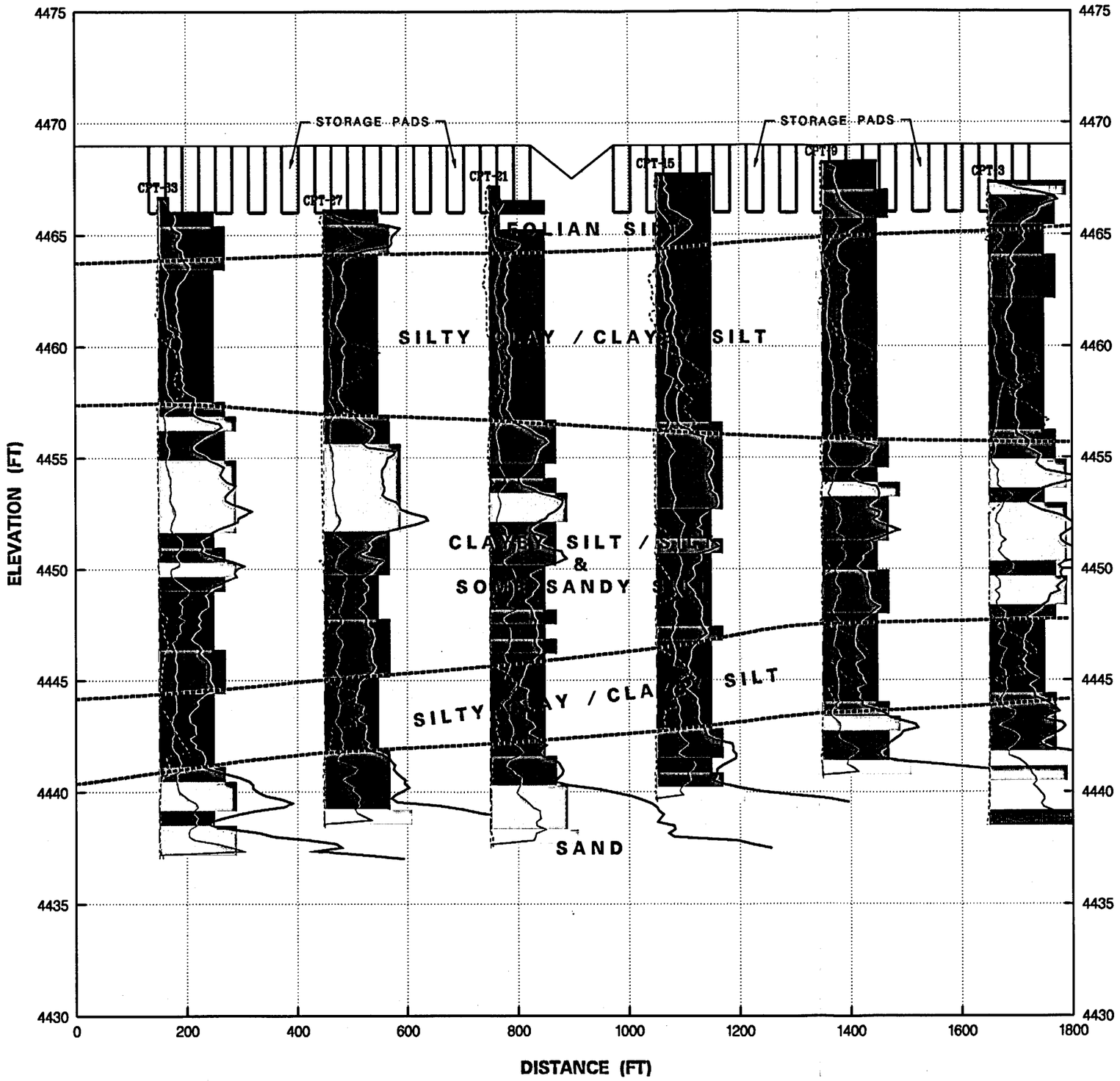

LEGEND:

BORING

B-ID ← BORING ID
(25 NW) ← APPROXIMATE DISTANCE (FEET) AND DIRECTION TO BORING FROM PROFILE

11
6
8
10 ← SPT N VALUE
9 ← LOCATION OF SAMPLE
100/6" ← INDICATES REFUSAL i.e. BLOWS PER INCHES DRIVEN
94
>143
>100/6"
10/22/98 ← DATE DRILLING COMPLETED
BOTTOM OF BORING

CONE PENETRATION TESTS

CPT-ID

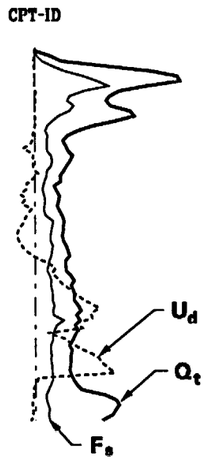

CONETEC (1999)

SBT 0 5 10

SOIL BEHAVIOR TYPE

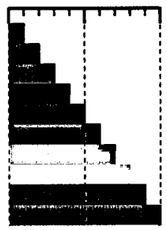

SENSITIVE FINES
ORGANIC SOIL
CLAY
SILTY CLAY
CLAYEY SILT
SILT
SANDY SILT
SILTY SAND/SAND
SAND
GRAVELLY SAND

NOTE:

SOIL BEHAVIOR TYPES SHOWN HERE ARE RECALIBRATED AS DISCUSSED IN SECTION 2.6.1.6 OF THE SAR TO MORE ACCURATELY REFLECT SOIL CLASSIFICATIONS DEVELOPED BASED ON THE BORINGS AND LABORATORY TESTS.

HORIZONTAL 0 200 400 FEET
VERTICAL 0 5 10
SCALE IN FEET

Figure 2.6–5
PAD EMPLACEMENT AREA FOUNDATION PROFILE 4–4′ SHEET 6 OF 14
PRIVATE FUEL STORAGE FACILITY SAFETY ANALYSIS REPORT

g:\05998\gak\b\43\1.dgn 08-DEC-1998 12:20

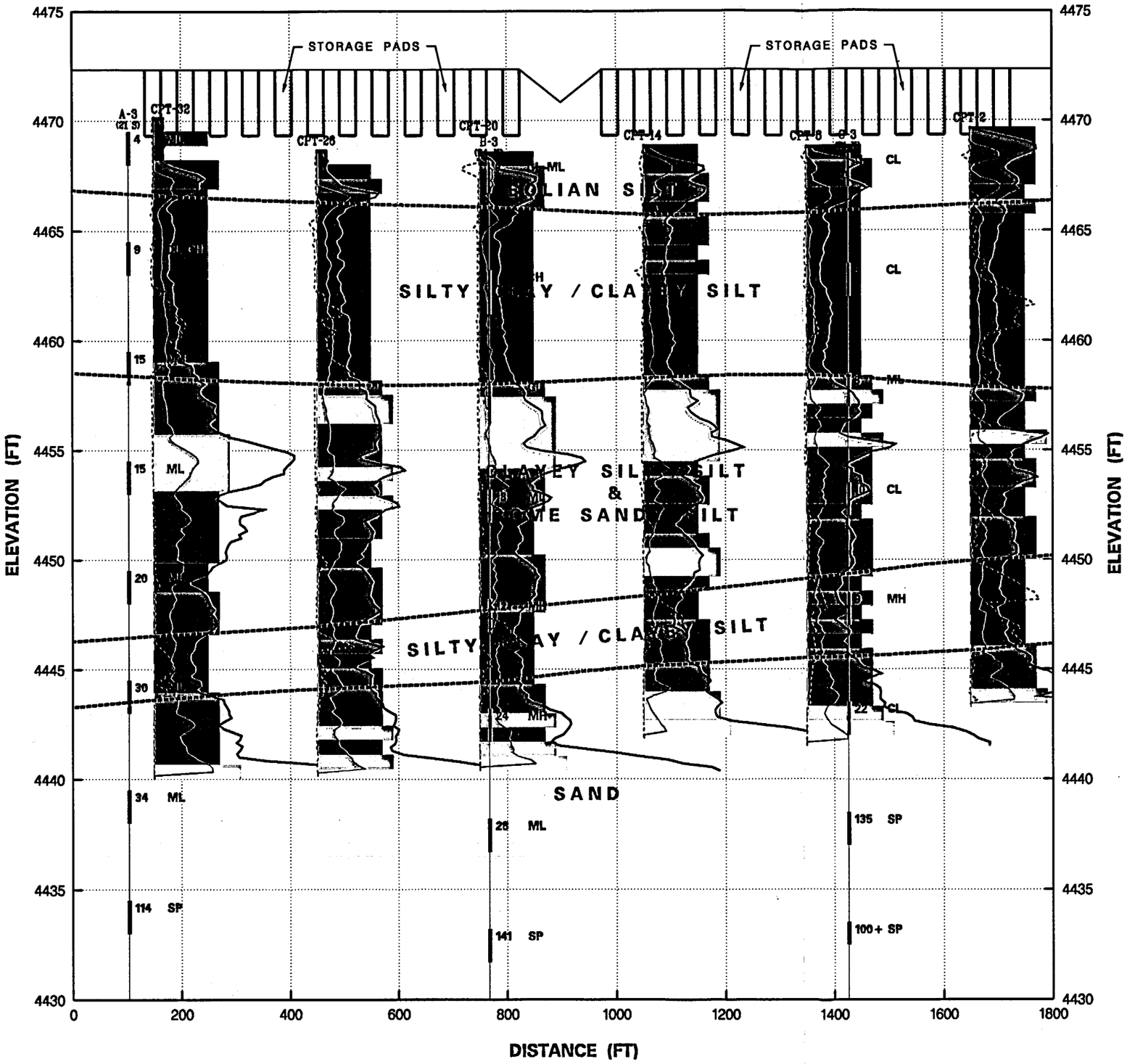

LEGEND:

BORING

B-ID (25 NW) — BORING ID; APPROXIMATE DISTANCE (FEET) AND DIRECTION TO BORING FROM PROFILE

11
6
8
10 — SPT N VALUE
9 — LOCATION OF SAMPLE
100/6" — INDICATES REFUSAL i.e. BLOWS PER INCHES DRIVEN
94
>143
>100/6"
10/22/98 — BOTTOM OF BORING; DATE DRILLING COMPLETED

CONE PENETRATION TESTS

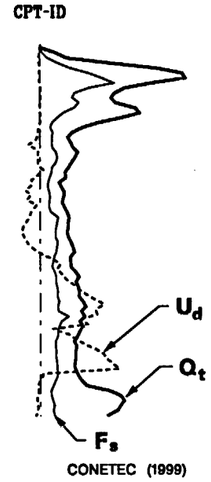

CONETEC (1999)

SOIL BEHAVIOR TYPE

1. SENSITIVE FINES
2. ORGANIC SOIL
3. CLAY
4. SILTY CLAY
5. CLAYEY SILT
6. SILT
7. SANDY SILT
8. SILTY SAND/SAND
9. SAND
10. GRAVELLY SAND

NOTE:

SOIL BEHAVIOR TYPES SHOWN HERE ARE RECALIBRATED AS DISCUSSED IN SECTION 2.6.1.6 OF THE SAR TO MORE ACCURATELY REFLECT SOIL CLASSIFICATIONS DEVELOPED BASED ON THE BORINGS AND LABORATORY TESTS.

HORIZONTAL 0 200 400 FEET
VERTICAL 0 5 10
SCALE IN FEET

Figure 2.6–5
PAD EMPLACEMENT AREA FOUNDATION PROFILE 5–5′
SHEET 7 OF 14
PRIVATE FUEL STORAGE FACILITY SAFETY ANALYSIS REPORT

Revision 8

g:\05596\gak\b\44\1.dgn 08-DEC-1999 12:20

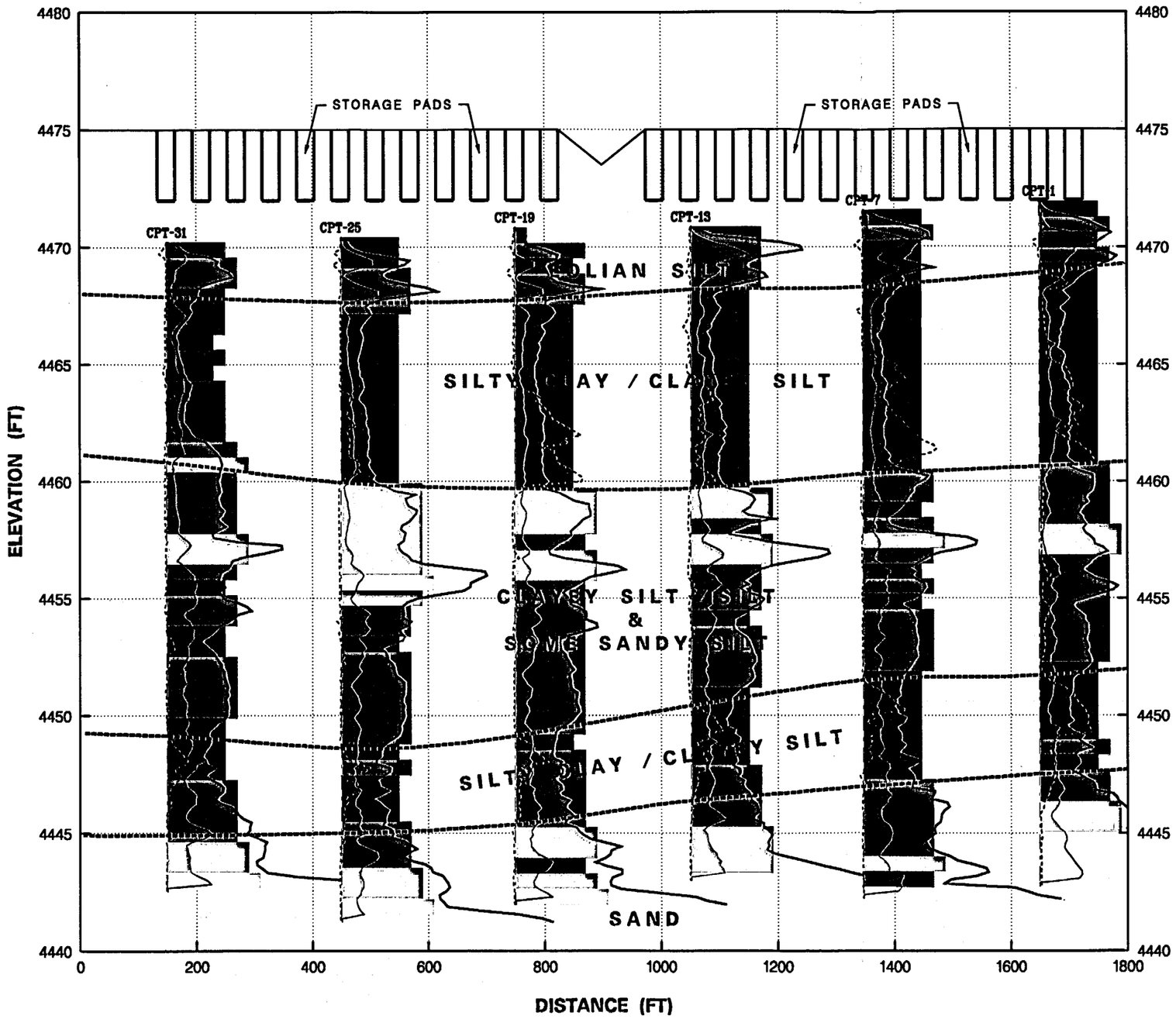

LEGEND:

BORING

B-ID ← BORING ID
(25 NW) ← APPROXIMATE DISTANCE (FEET) AND DIRECTION TO BORING FROM PROFILE

11
6
8
10 ← SPT N VALUE
9 ← LOCATION OF SAMPLE
100/6" ← INDICATES REFUSAL i.e. BLOWS PER INCHES DRIVEN
94
>143
>100/6"
10/22/96 ← BOTTOM OF BORING
DATE DRILLING COMPLETED

CONE PENETRATION TESTS

CPT-ID

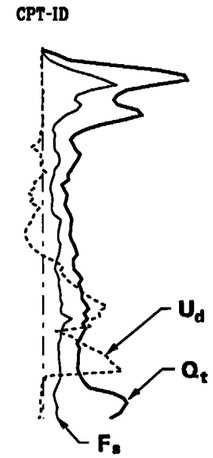

CONETEC (1999)

SBT: 0 5 10

SOIL BEHAVIOR TYPE

1. SENSITIVE FINES
2. ORGANIC SOIL
3. CLAY
4. SILTY CLAY
5. CLAYEY SILT
6. SILT
7. SANDY SILT
8. SILTY SAND/SAND
9. SAND
10. GRAVELLY SAND

NOTE:

SOIL BEHAVIOR TYPES SHOWN HERE ARE RECALIBRATED AS DISCUSSED IN SECTION 2.6.1.6 OF THE SAR TO MORE ACCURATELY REFLECT SOIL CLASSIFICATIONS DEVELOPED BASED ON THE BORINGS AND LABORATORY TESTS.

HORIZONTAL 0 200 400 FEET
VERTICAL 0 5 10
SCALE IN FEET

Figure 2.6–5
PAD EMPLACEMENT AREA FOUNDATION PROFILE 6–6′ SHEET 8 OF 14
PRIVATE FUEL STORAGE FACILITY SAFETY ANALYSIS REPORT

g:\05998\gak\b139\1.dgn 08-DEC-1999 12:20

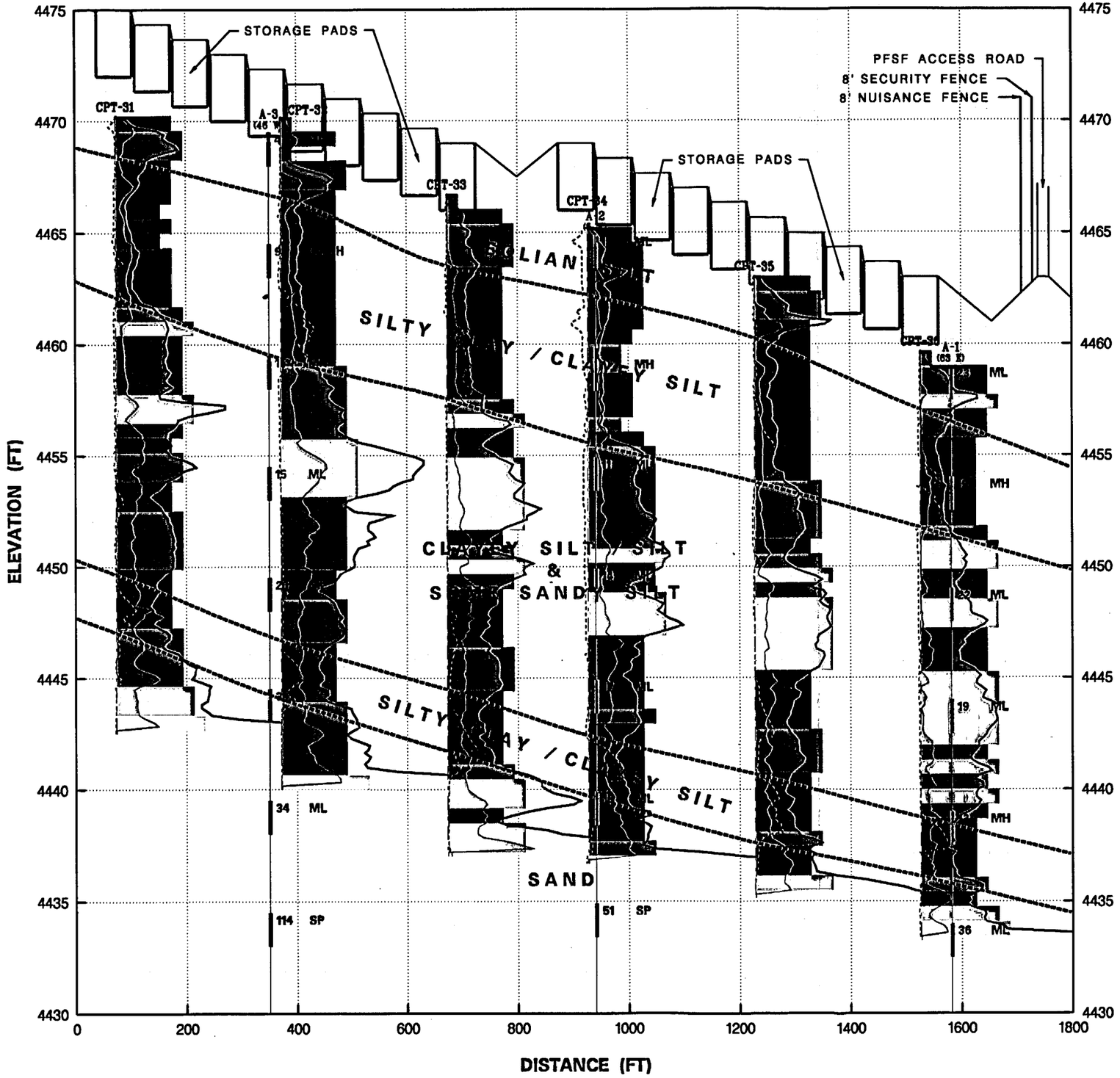

g:\105998\gak\b\45N1.dgn 08-DEC-1999 12:20

LEGEND:

BORING

B-ID ← BORING ID
(25 NW) ← APPROXIMATE DISTANCE (FEET) AND DIRECTION TO BORING FROM PROFILE

11
6
8
10 ← SPT N VALUE
9 ← LOCATION OF SAMPLE
100/6" ← INDICATES REFUSAL i.e. BLOWS PER INCHES DRIVEN
94
>143
>100/6"
10/22/98 ← BOTTOM OF BORING
← DATE DRILLING COMPLETED

CONE PENETRATION TESTS

CPT-ID

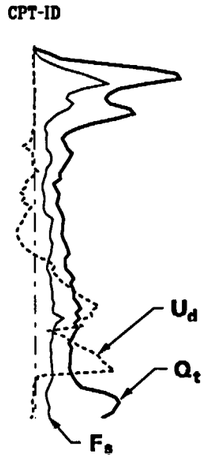

CONETEC (1999)

SBT

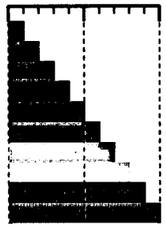

SOIL BEHAVIOR TYPE

SENSITIVE FINES
ORGANIC SOIL
CLAY
SILTY CLAY
CLAYEY SILT
SILT
SANDY SILT
SILTY SAND/SAND
SAND
GRAVELLY SAND

NOTE:

SOIL BEHAVIOR TYPES SHOWN HERE ARE RECALIBRATED AS DISCUSSED IN SECTION 2.6.1.6 OF THE SAR TO MORE ACCURATELY REFLECT SOIL CLASSIFICATIONS DEVELOPED BASED ON THE BORINGS AND LABORATORY TESTS.

HORIZONTAL 0 200 400 FEET
VERTICAL 0 5 10
SCALE IN FEET

Figure 2.6–5
PAD EMPLACEMENT AREA
FOUNDATION PROFILE 7–7'
SHEET 9 OF 14
PRIVATE FUEL STORAGE FACILITY
SAFETY ANALYSIS REPORT

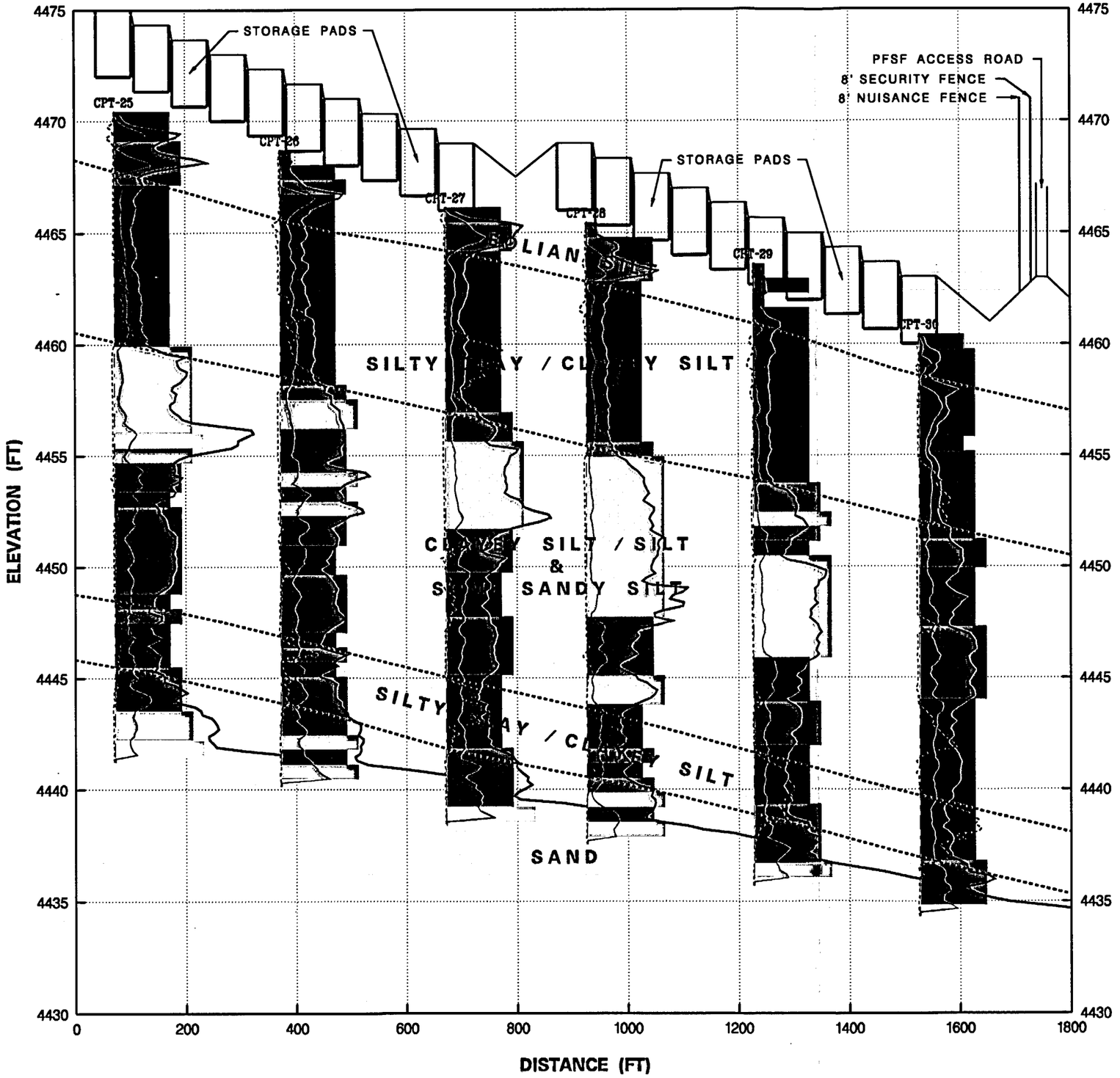

LEGEND:

BORING

B-ID — BORING ID
(25 NW) — APPROXIMATE DISTANCE (FEET) AND DIRECTION TO BORING FROM PROFILE

11
6
8
10 — SPT N VALUE
9 — LOCATION OF SAMPLE
100/6" — INDICATES REFUSAL i.e. BLOWS PER INCHES DRIVEN
94
>143
>100/6"
10/22/96 — BOTTOM OF BORING
DATE DRILLING COMPLETED

CONE PENETRATION TESTS

CPT-ID

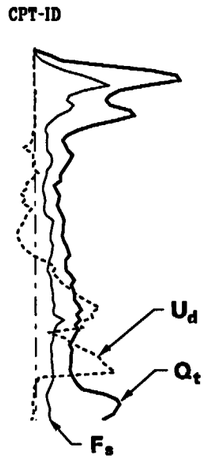

CONETEC (1999)

SBT

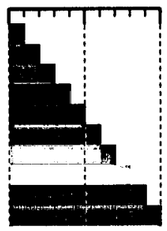

SOIL BEHAVIOR TYPE

SENSITIVE FINES
ORGANIC SOIL
CLAY
SILTY CLAY
CLAYEY SILT
SILT
SANDY SILT
SILTY SAND/SAND
SAND
GRAVELLY SAND

NOTE:

SOIL BEHAVIOR TYPES SHOWN HERE ARE RECALIBRATED AS DISCUSSED IN SECTION 2.6.1.6 OF THE SAR TO MORE ACCURATELY REFLECT SOIL CLASSIFICATIONS DEVELOPED BASED ON THE BORINGS AND LABORATORY TESTS.

HORIZONTAL 0 200 400 FEET
VERTICAL 0 5 10
SCALE IN FEET

Figure 2.6–5
PAD EMPLACEMENT AREA FOUNDATION PROFILE 8–8′
SHEET 10 OF 14
PRIVATE FUEL STORAGE FACILITY SAFETY ANALYSIS REPORT

g:\05998\gsk\b\46\1.dgn 08-DEC-1999 12:20

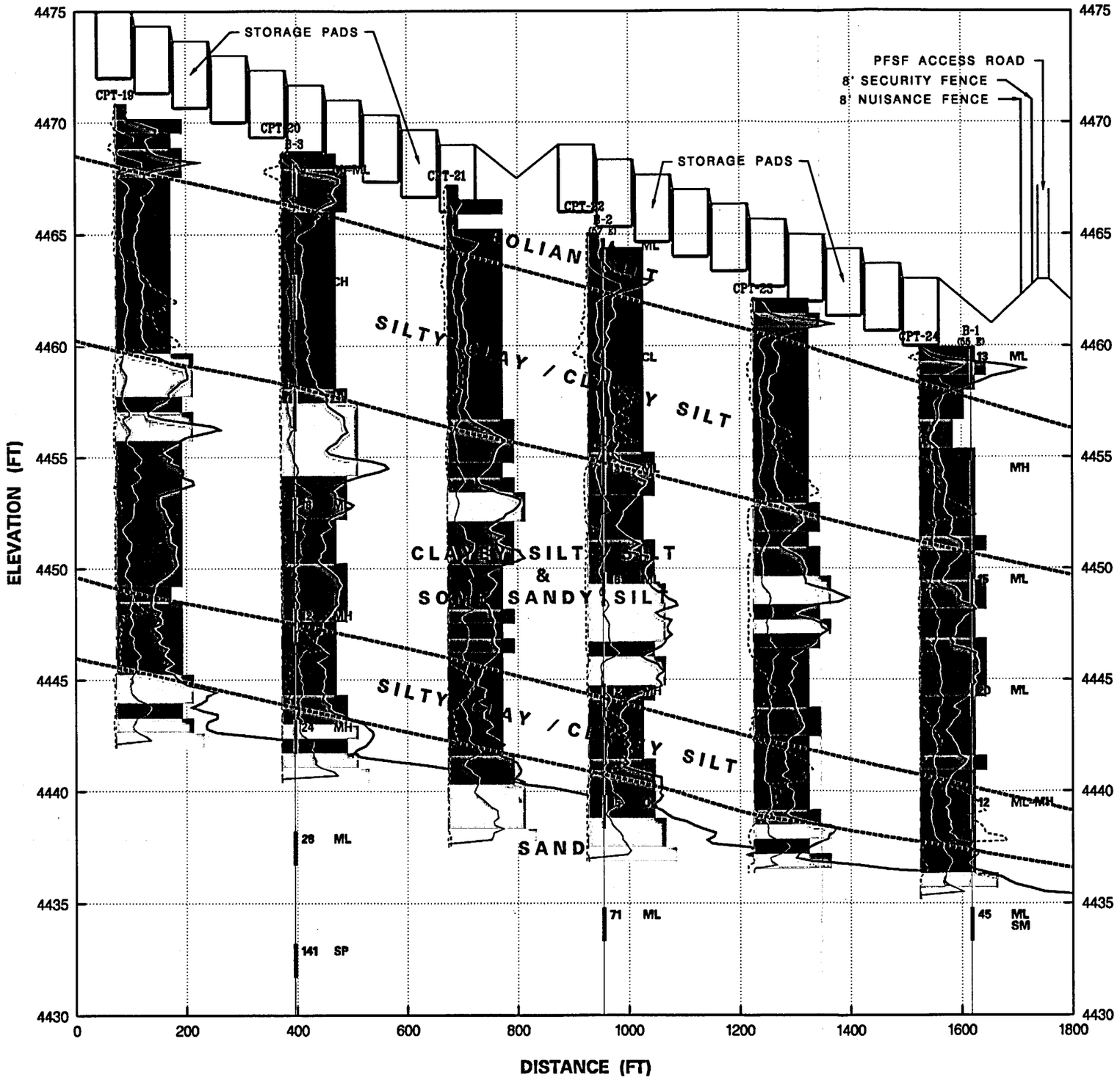

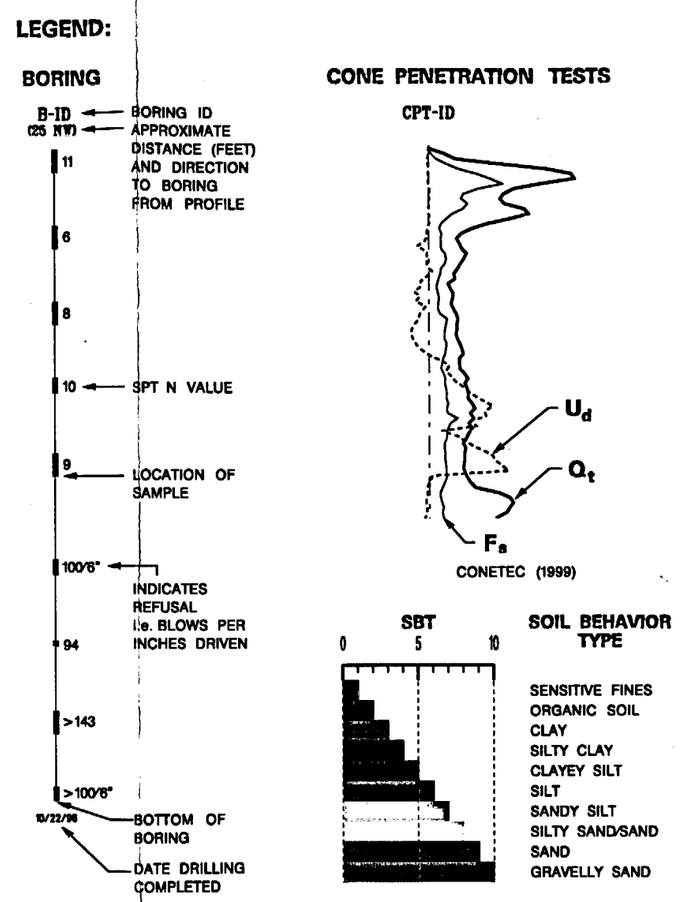

NOTE:

SOIL BEHAVIOR TYPES SHOWN HERE ARE RECALIBRATED AS DISCUSSED IN SECTION 2.6.1.6 OF THE SAR TO MORE ACCURATELY REFLECT SOIL CLASSIFICATIONS DEVELOPED BASED ON THE BORINGS AND LABORATORY TESTS.

HORIZONTAL 0 200 400 FEET
VERTICAL 0 5 10
SCALE IN FEET

Figure 2.6–5
PAD EMPLACEMENT AREA
FOUNDATION PROFILE 9–9'
SHEET 11 OF 14
PRIVATE FUEL STORAGE FACILITY
SAFETY ANALYSIS REPORT

g:\05998\gsk\b\47\1.dgn 08-DEC-1999 12:20

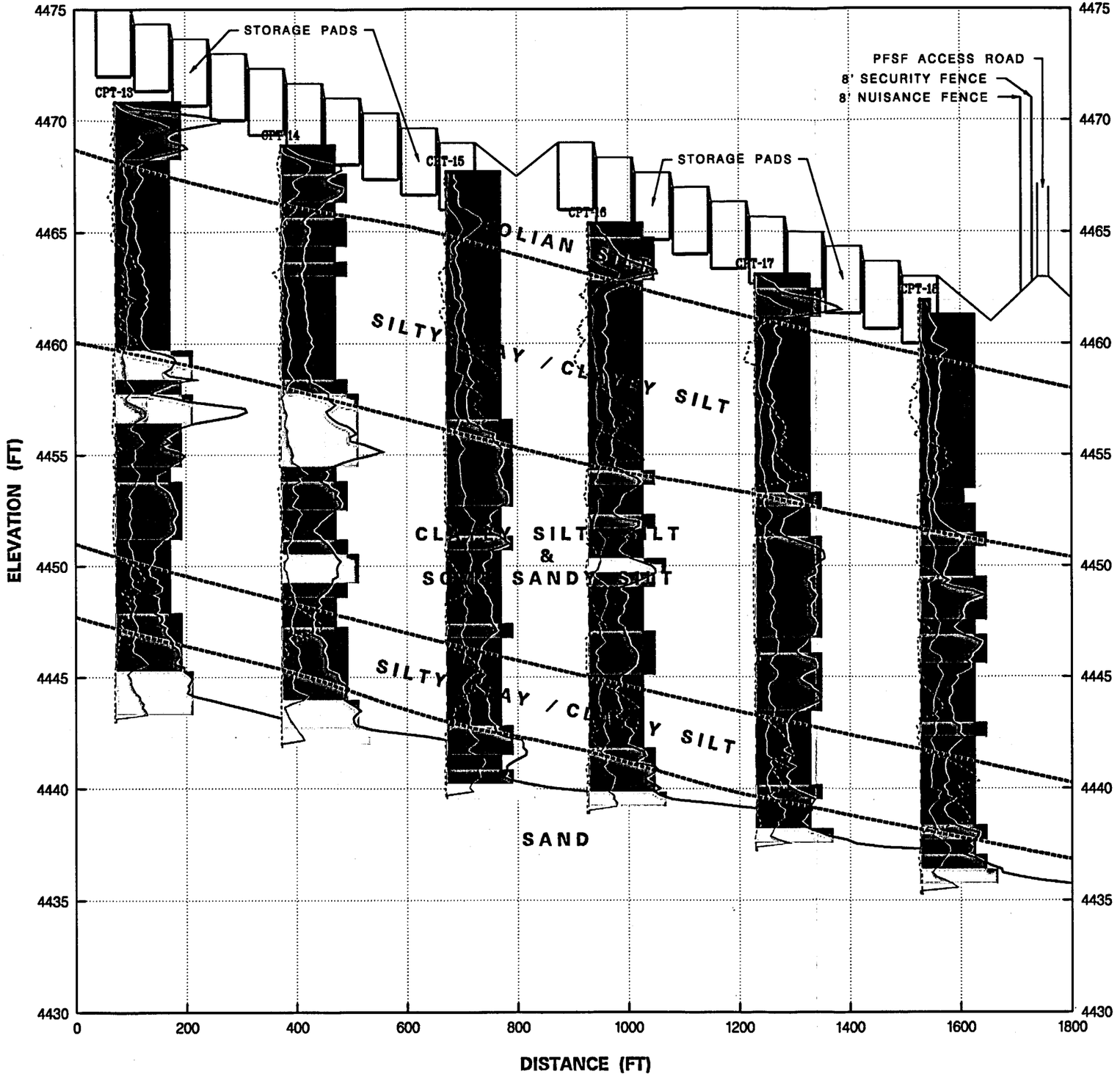

LEGEND:

BORING

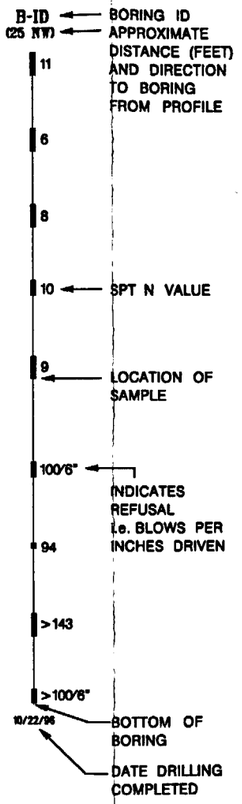

CONE PENETRATION TESTS

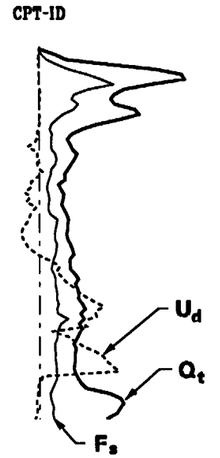

CONETEC (1999)

SBT

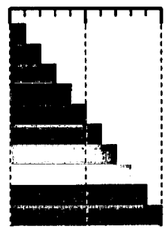

SOIL BEHAVIOR TYPE

SENSITIVE FINES
ORGANIC SOIL
CLAY
SILTY CLAY
CLAYEY SILT
SILT
SANDY SILT
SILTY SAND/SAND
SAND
GRAVELLY SAND

NOTE:

SOIL BEHAVIOR TYPES SHOWN HERE ARE RECALIBRATED AS DISCUSSED IN SECTION 2.6.1.6 OF THE SAR TO MORE ACCURATELY REFLECT SOIL CLASSIFICATIONS DEVELOPED BASED ON THE BORINGS AND LABORATORY TESTS.

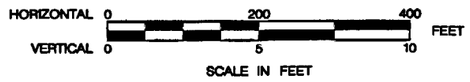

Figure 2.6–5

PAD EMPLACEMENT AREA FOUNDATION PROFILE 10–10′ SHEET 12 OF 14

PRIVATE FUEL STORAGE FACILITY SAFETY ANALYSIS REPORT

g:\05996\gsk\b148v1.dgn 08-DEC-1999 12:20

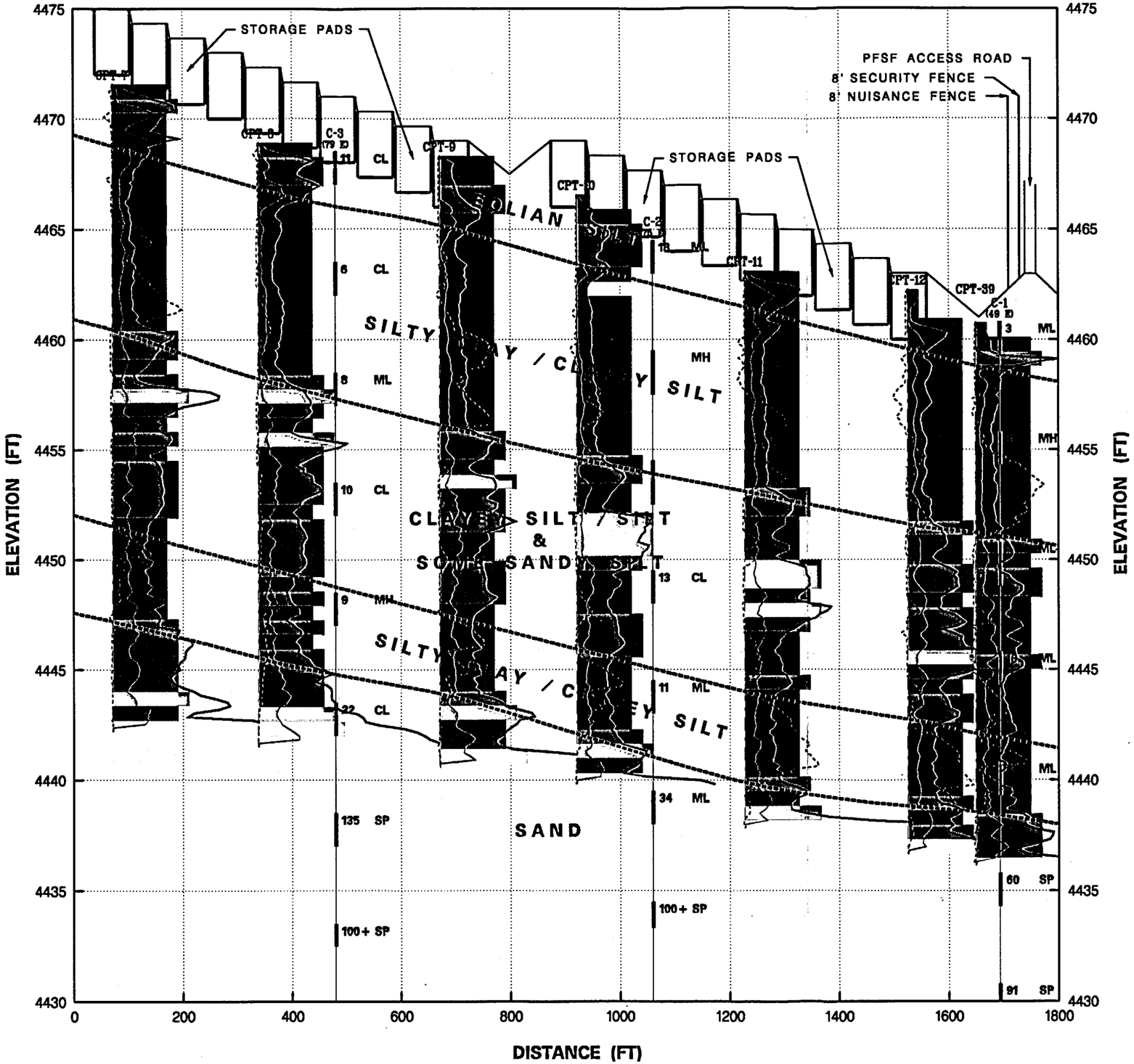

LEGEND:

BORING

B-ID (25 NW) — BORING ID; APPROXIMATE DISTANCE (FEET) AND DIRECTION TO BORING FROM PROFILE

11
6
8
10 — SPT N VALUE
9 — LOCATION OF SAMPLE
100/6" — INDICATES REFUSAL i.e. BLOWS PER INCHES DRIVEN
94
>143
>100/6"
10/22/98 — BOTTOM OF BORING; DATE DRILLING COMPLETED

CONE PENETRATION TESTS

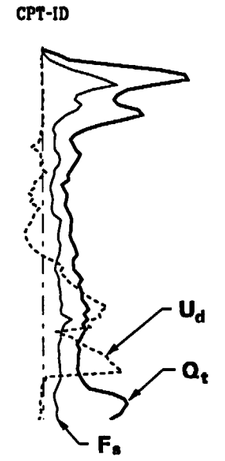

CONETEC (1999)

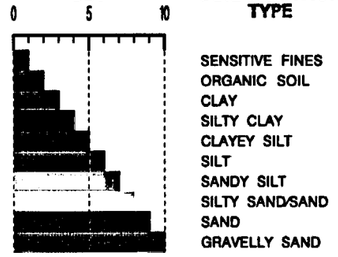

SOIL BEHAVIOR TYPE

SENSITIVE FINES
ORGANIC SOIL
CLAY
SILTY CLAY
CLAYEY SILT
SILT
SANDY SILT
SILTY SAND/SAND
SAND
GRAVELLY SAND

NOTE:

SOIL BEHAVIOR TYPES SHOWN HERE ARE RECALIBRATED AS DISCUSSED IN SECTION 2.6.1.6 OF THE SAR TO MORE ACCURATELY REFLECT SOIL CLASSIFICATIONS DEVELOPED BASED ON THE BORINGS AND LABORATORY TESTS.

HORIZONTAL 0 200 400 FEET
VERTICAL 0 5 10
SCALE IN FEET

Figure 2.6–5
PAD EMPLACEMENT AREA
FOUNDATION PROFILE 11–11'
SHEET 13 OF 14
PRIVATE FUEL STORAGE FACILITY
SAFETY ANALYSIS REPORT

g:\05996\gak\b1491.dgn 08-DEC-1999 12:20

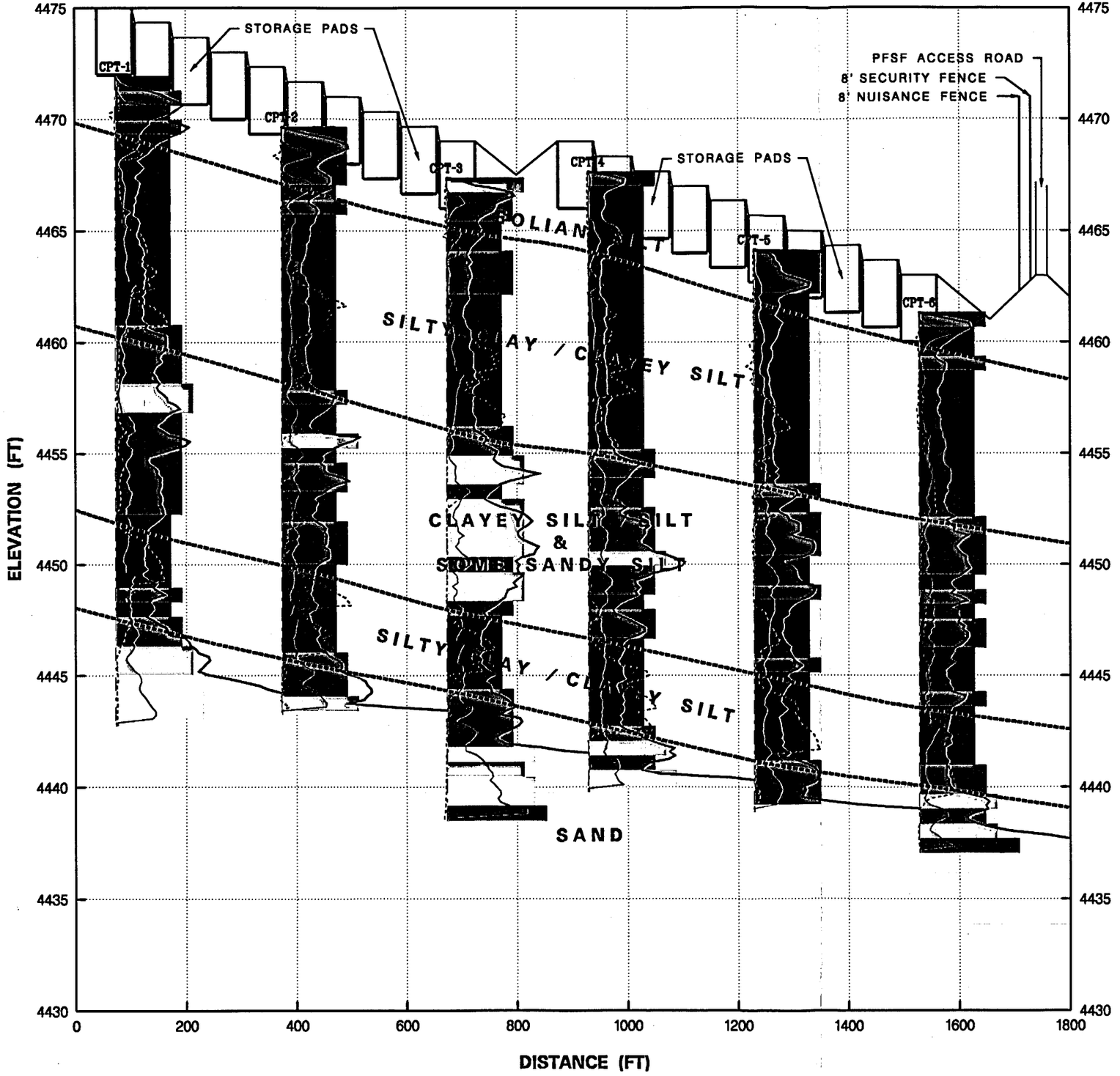

LEGEND:

BORING

B-ID ← BORING ID
(25 NW) ← APPROXIMATE DISTANCE (FEET) AND DIRECTION TO BORING FROM PROFILE

11
6
8
10 ← SPT N VALUE
9 ← LOCATION OF SAMPLE
100/6" ← INDICATES REFUSAL i.e. BLOWS PER INCHES DRIVEN
94
>143
>100/6"
10/22/98 ← BOTTOM OF BORING
← DATE DRILLING COMPLETED

CONE PENETRATION TESTS

CPT-ID

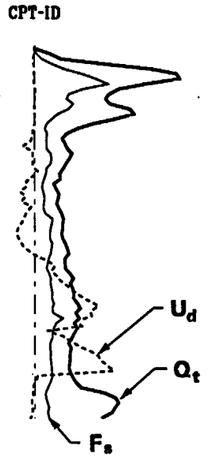

CONETEC (1999)

SBT (0, 5, 10)

SOIL BEHAVIOR TYPE

SENSITIVE FINES
ORGANIC SOIL
CLAY
SILTY CLAY
CLAYEY SILT
SILT
SANDY SILT
SILTY SAND/SAND
SAND
GRAVELLY SAND

NOTE:

SOIL BEHAVIOR TYPES SHOWN HERE ARE RECALIBRATED AS DISCUSSED IN SECTION 2.6.1.6 OF THE SAR TO MORE ACCURATELY REFLECT SOIL CLASSIFICATIONS DEVELOPED BASED ON THE BORINGS AND LABORATORY TESTS.

HORIZONTAL 0 200 400 FEET
VERTICAL 0 5 10
SCALE IN FEET

Figure 2.6–5
PAD EMPLACEMENT AREA
FOUNDATION PROFILE 12–12'
SHEET 14 OF 14
PRIVATE FUEL STORAGE FACILITY
SAFETY ANALYSIS REPORT

g:\05996\gak\b1501.dgn 08-DEC-1999 12:20

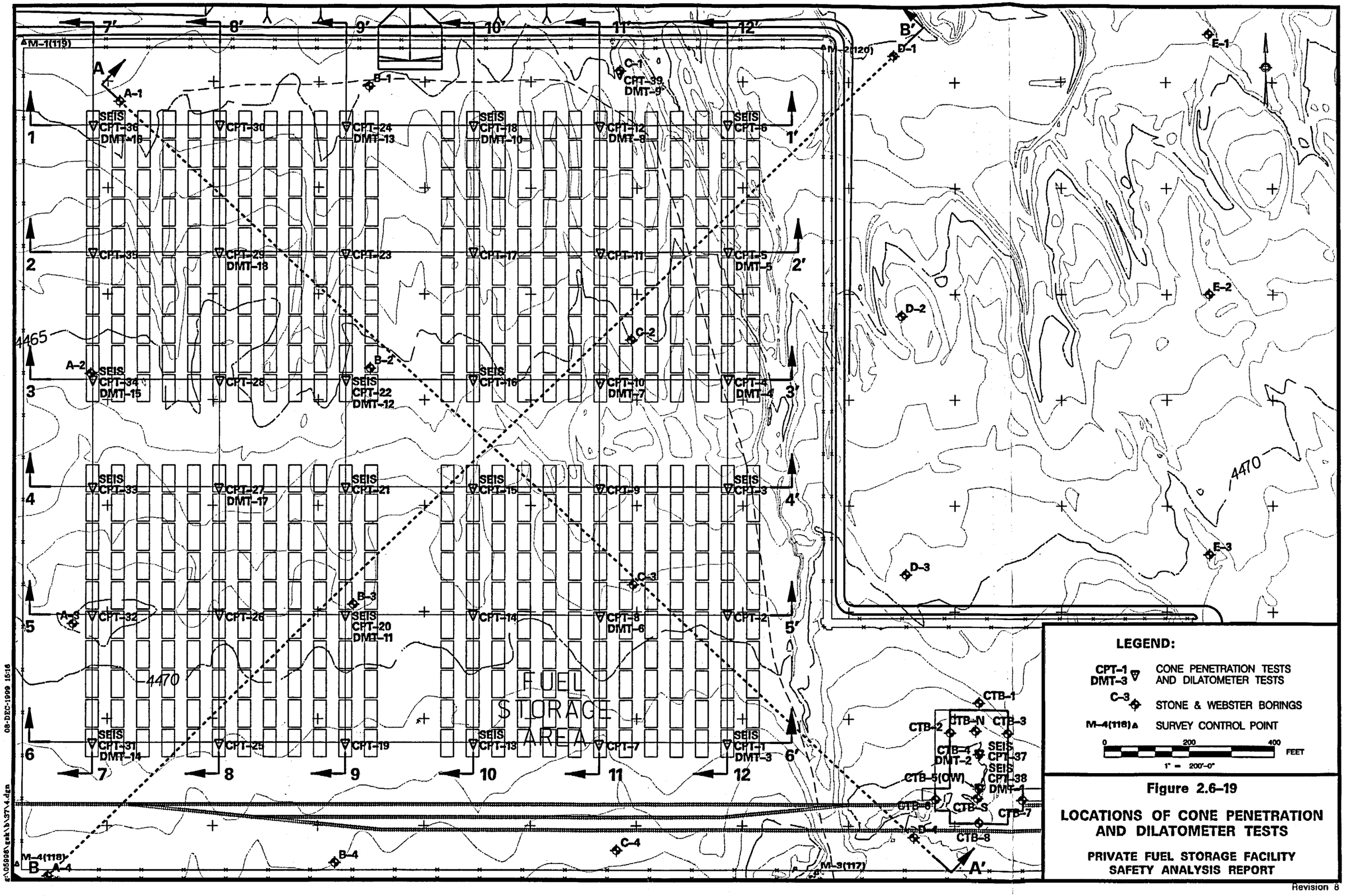

Figure 2.6-19

LOCATIONS OF CONE PENETRATION AND DILATOMETER TESTS

PRIVATE FUEL STORAGE FACILITY
SAFETY ANALYSIS REPORT

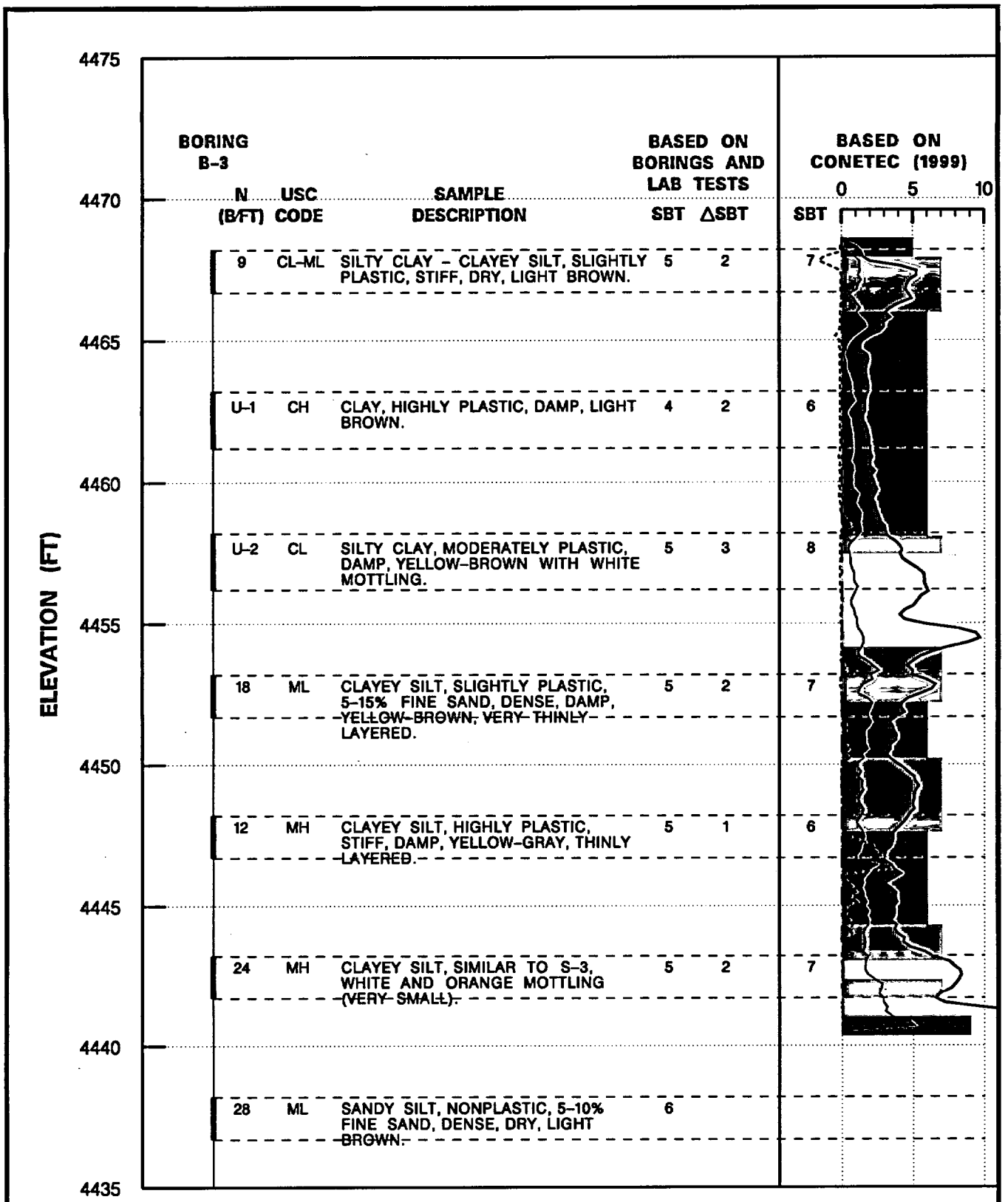

08-DEC-1999 15:45

g:\05986\gak\a\75\0.dgn

Figure 2.6-30

COMPARISON OF SOIL CLASSIFICATION BETWEEN BORING B-3 AND CPT-20 SHEET 1 OF 6

PRIVATE FUEL STORAGE FACILITY SAFETY ANALYSIS REPORT

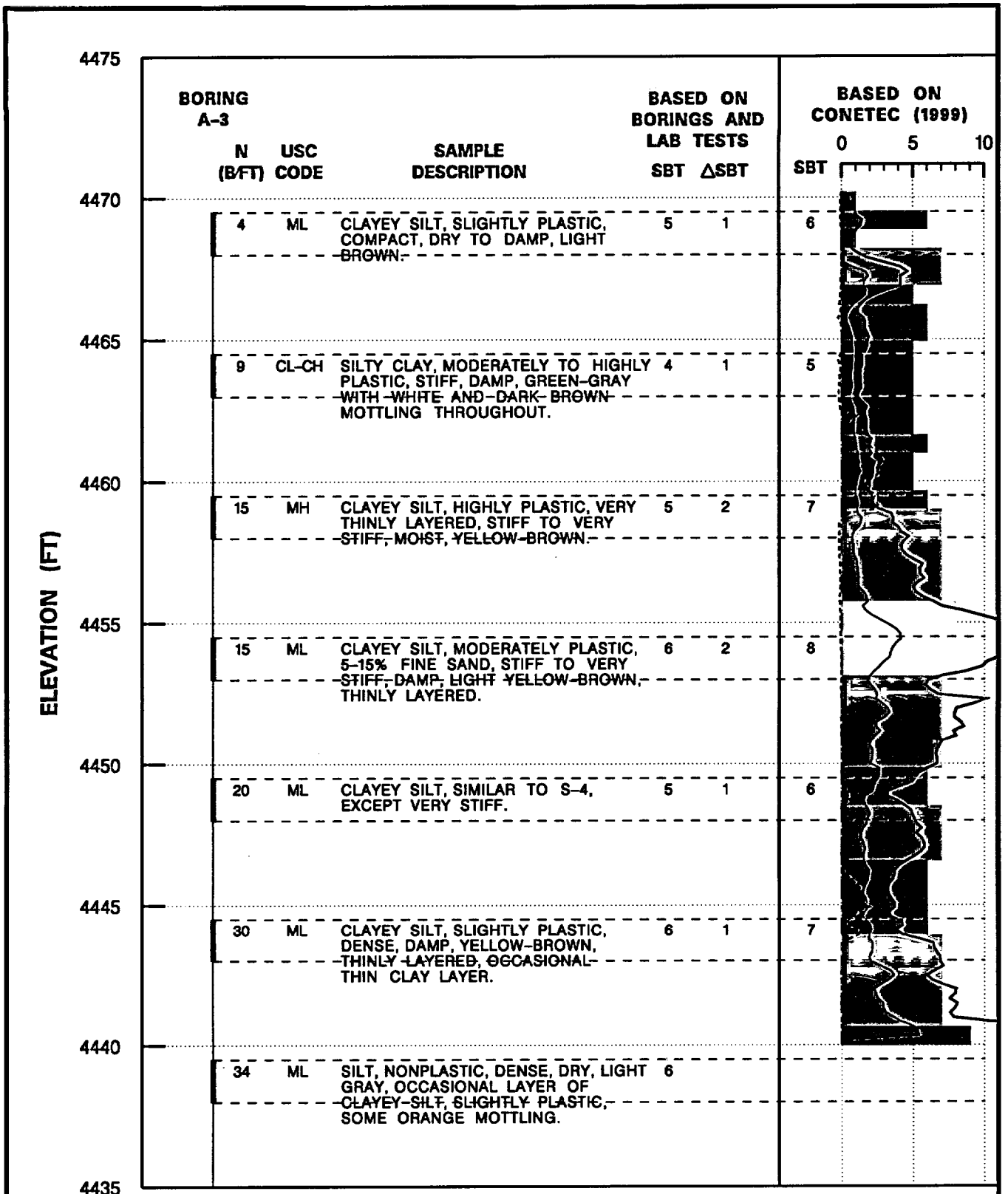

08-DEC-1999 15:45

g:\05996\gsk\a\76\0.dgn

Figure 2.6-30

COMPARISON OF SOIL CLASSIFICATION BETWEEN BORING A-3 AND CPT-32
SHEET 2 OF 6

PRIVATE FUEL STORAGE FACILITY
SAFETY ANALYSIS REPORT

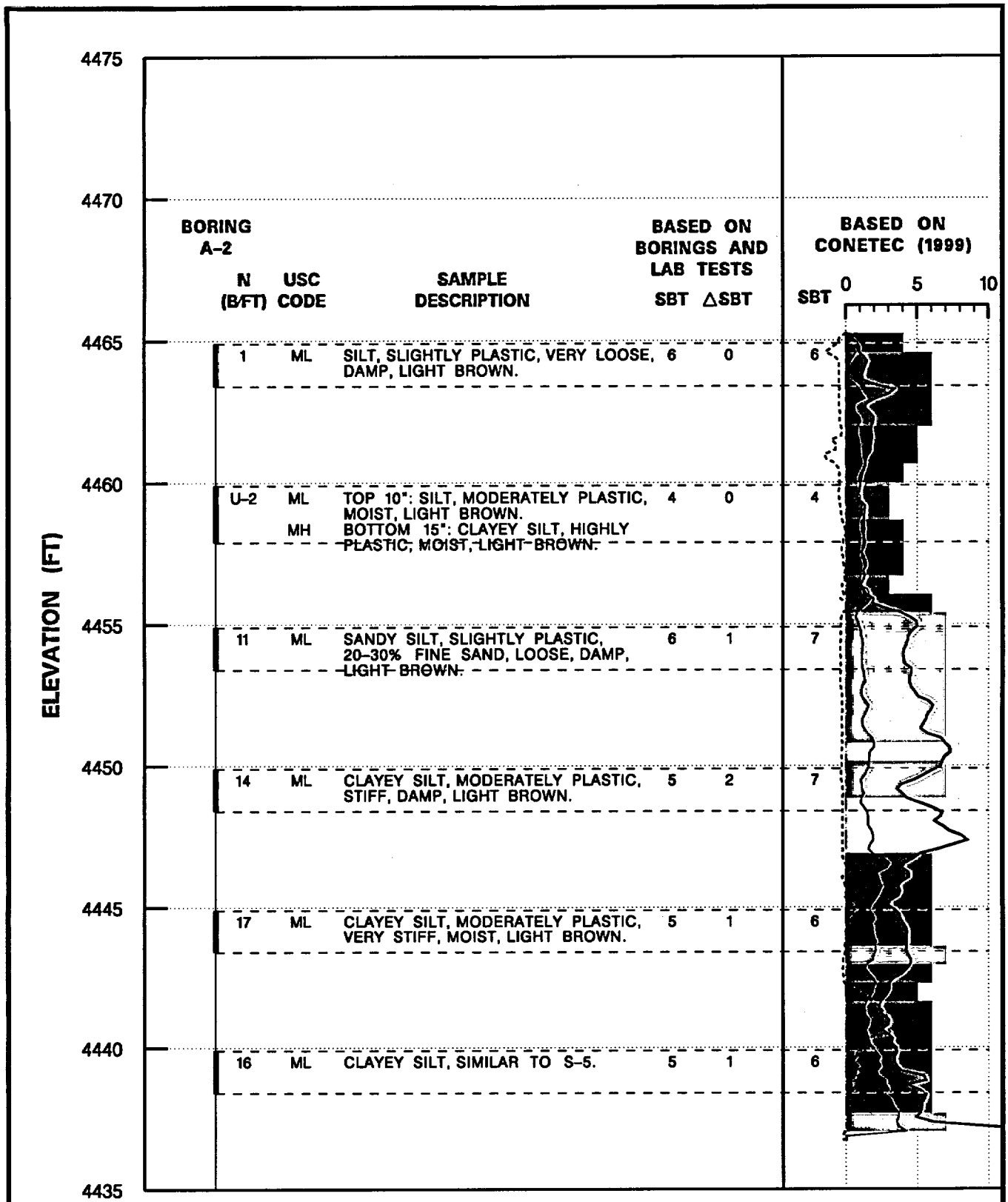

08-DEC-1999 15:45

g:\05996\gsk\a\77\0.dgn

Figure 2.6-30

COMPARISON OF SOIL CLASSIFICATION BETWEEN BORING A-2 AND CPT-34
SHEET 3 OF 6

PRIVATE FUEL STORAGE FACILITY
SAFETY ANALYSIS REPORT

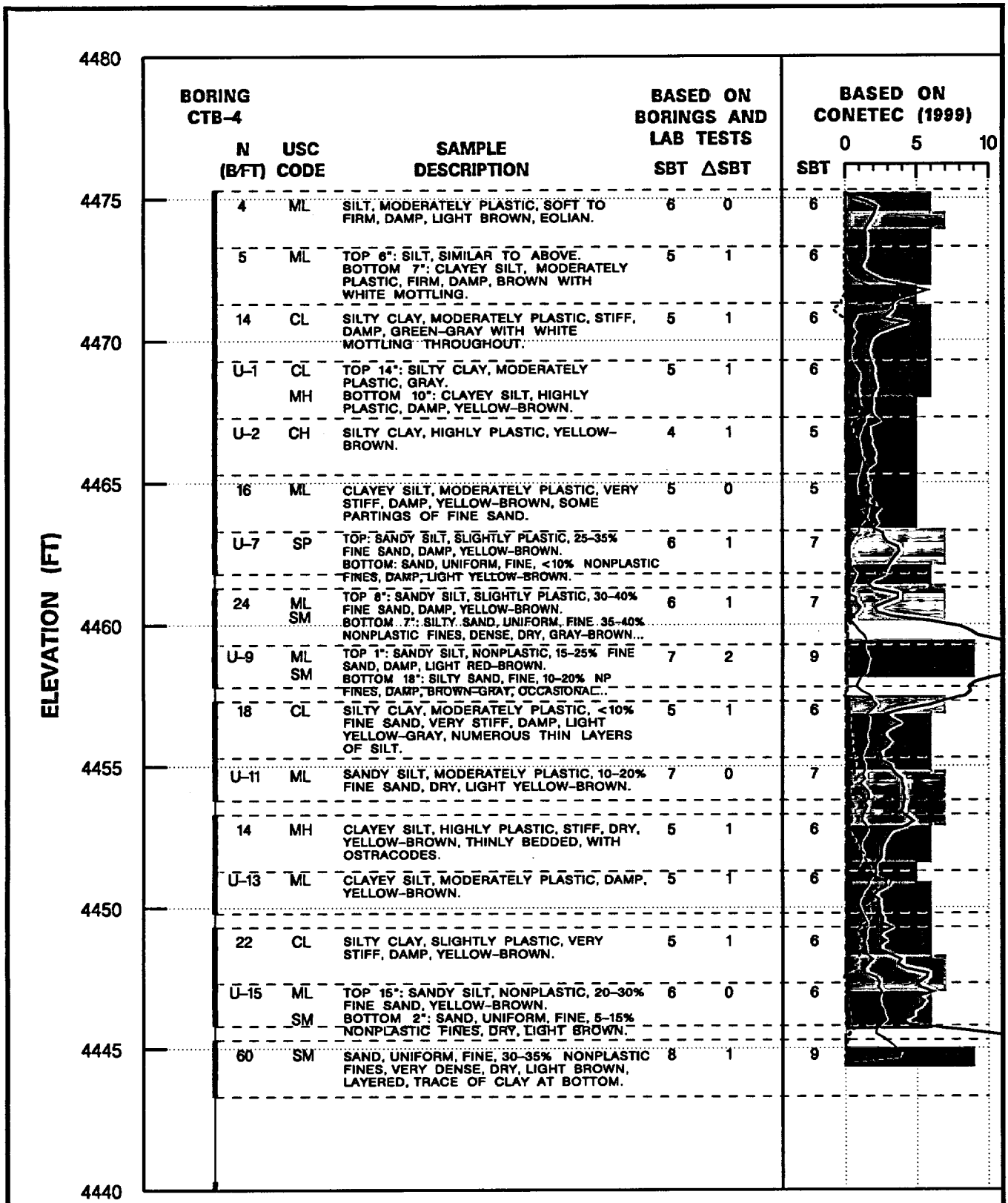

08-DEC-1999 15:45

g:\05996\gsk\a\78\0.dgn

Figure 2.6-30

COMPARISON OF SOIL CLASSIFICATION BETWEEN BORING CTB-4 AND CPT-37 SHEET 4 OF 6

PRIVATE FUEL STORAGE FACILITY SAFETY ANALYSIS REPORT

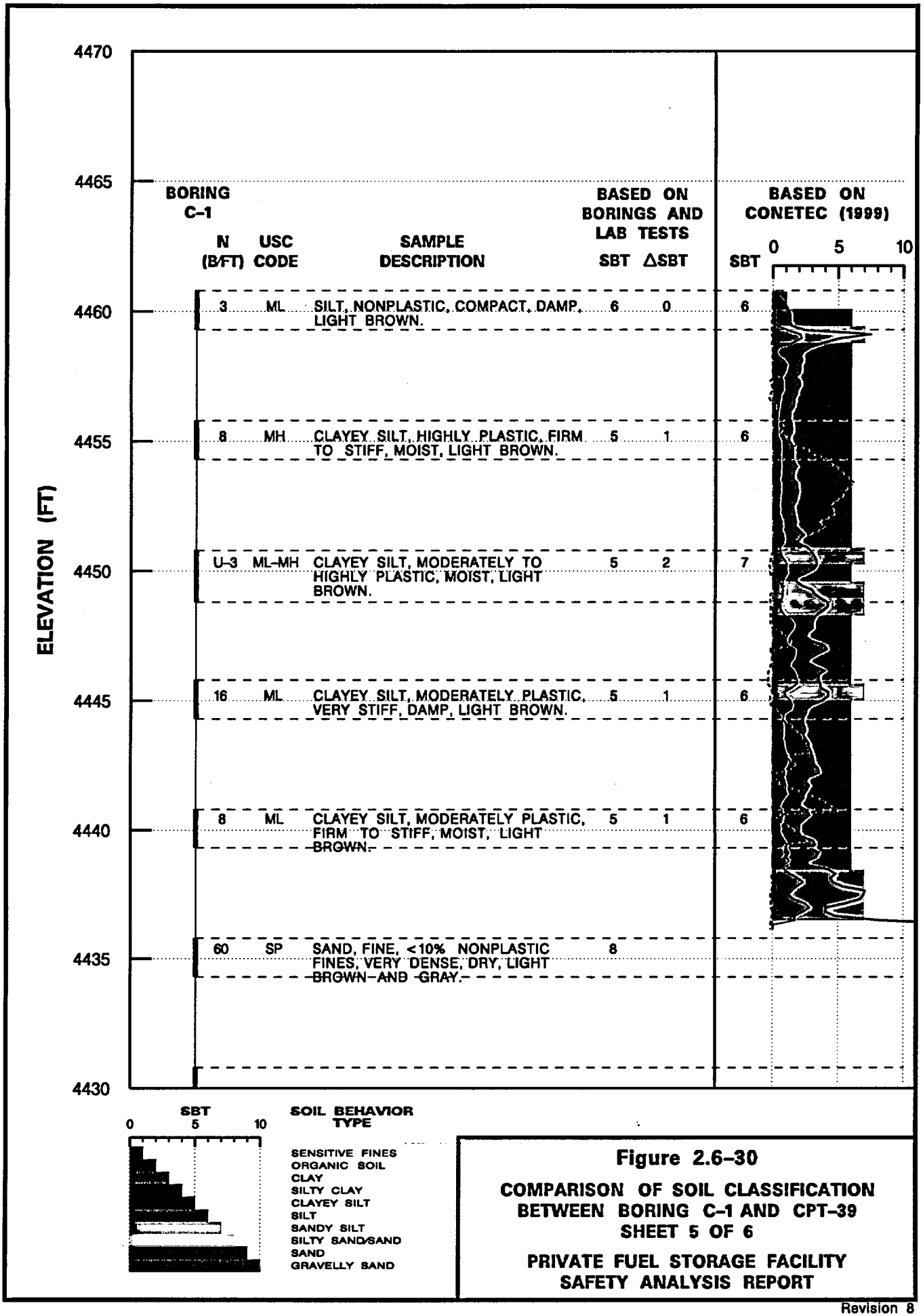

08-DEC-1999 15:45

g:\05998\gak\a\79\0.dgn

Figure 2.6-30

COMPARISON OF SOIL CLASSIFICATION BETWEEN BORING C-1 AND CPT-39 SHEET 5 OF 6

PRIVATE FUEL STORAGE FACILITY SAFETY ANALYSIS REPORT

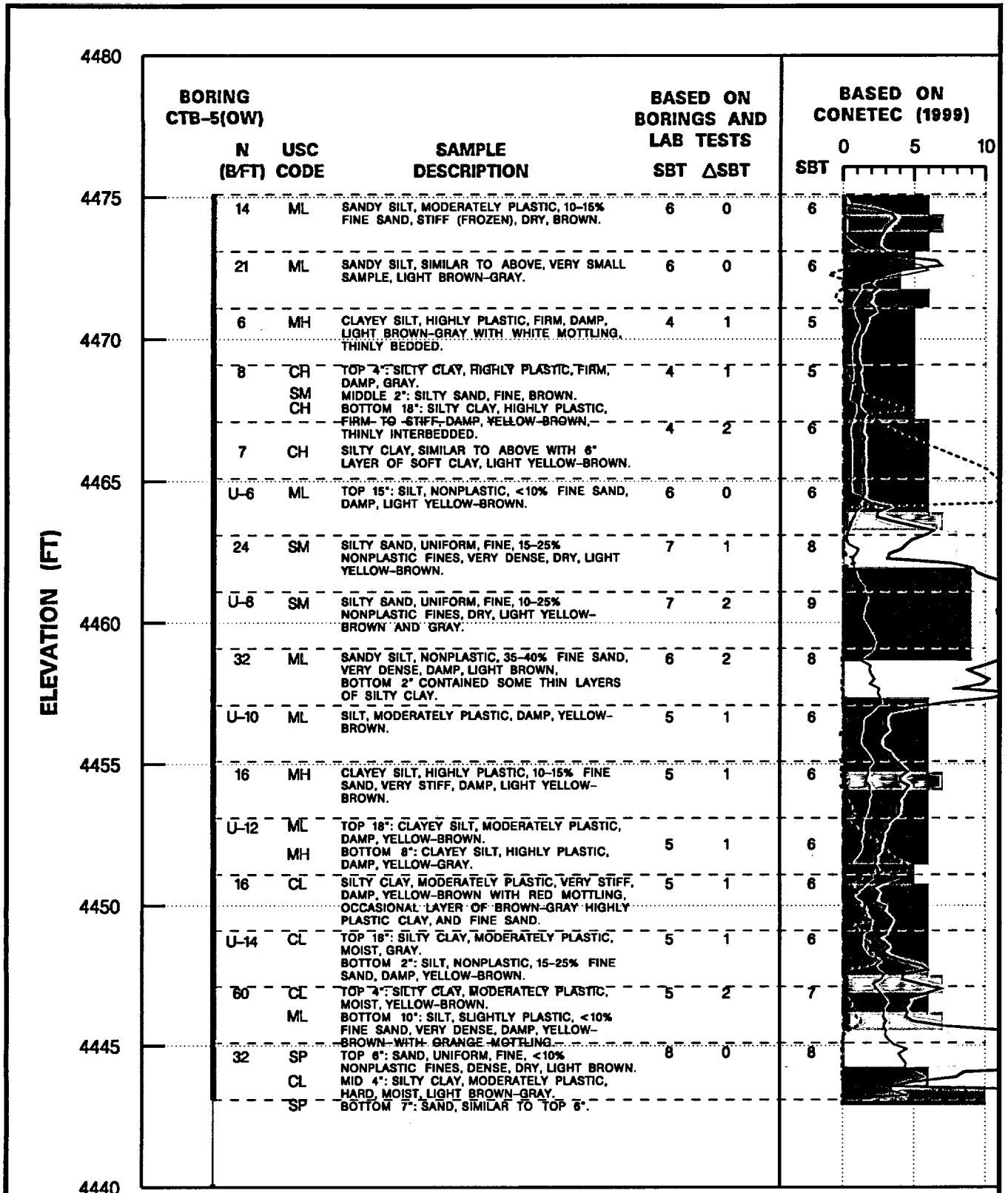

Figure 2.6-30

COMPARISON OF SOIL CLASSIFICATION BETWEEN BORING CTB-5(OW) AND CPT-38 SHEET 6 OF 6

PRIVATE FUEL STORAGE FACILITY SAFETY ANALYSIS REPORT

g:\05996\gsk\a\80\0.dgn 08-DEC-1999 15:45

APPENDIX 2A

ATTACHMENT 8

SUPPLEMENTAL GEOTECHNICAL LABORATORY TESTING NOVEMBER 1999

SWEC Project No. 05996.02

SUPPLEMENTAL GEOTECHNICAL LABORATORY TESTING NOVEMBER 1999

Prepared for:
Private Fuel Storage, LLC
Private Fuel Storage Facility
Skull Valley, Utah

QUALITY ASSURANCE CATEGORY I
STONE & WEBSTER ENGINEERING CORPORATION
BOSTON, MASSACHUSETTS

STONE & WEBSTER